Understanding glucose uptake in breast cancer cells

By

Joshua A. Martin

A dissertation submitted in partial fulfillment of

the requirements for the degree of

Doctor of Philosophy
(Cancer Biology)

at the

UNIVERSITY OF WISCONSIN-MADISON

2019

Date of final oral examination: 11/14/2019

The dissertation is approved by the following members of the Final Oral Committee:

Caroline M. Alexander, Professor, Department of Oncology
William Sugden, Professor, Department of Oncology
Paul Lambert, Professor, Department of Oncology
Deric Wheeler, Professor, Department of Human Oncology
Elaine Alarid, Professor, Department of Oncology

TABLE OF CONTENTS

LIST OF FIGURES AND TABLES

Chapter I

Chapter II

Chapter III

ACKNOWLEDGEMENTS

I am truly thankful to the many people who have supported me throughout the completion of my thesis. I will always be grateful for your kindness and support.

Dr. Caroline Alexander, my mentor and thesis advisor. I have always admired your drive and passion as a scientist, it was these traits that inspired me to pursue my thesis in your lab. Thank you for supporting me and advocating on my behalf early in my graduate studies when I was facing a challenging transition between labs. I am a better scientist because of you and your ability to get me to challenge my own perceived limitations. I will forever be indebted to you, thank you.

The past and present Alexander lab members. Emily, thank you for taking me under your wing when I first joined the lab and I always enjoyed your sense of humor, you helped make work fun. To the many undergraduate students I have had to privilege to mentor, thank you for help in pursuit of challenging projects.

Thank you Saja, for your support from nearly my very first day in graduate school. You were always available to answer my questions and provide support when I needed it most. I will never forget your advice and encouragement when preparing for my preliminary exam. Thank you for your skillful editing of my thesis and your willingness to help, even many years removed from lab.

Thank you Dr. Ildiko Kasza. I am thankful for the opportunity to work alongside you all these years. I appreciate your friendship and the example you set for me as a scientist and colleague.

My committee members Dr. Bill Sugden, Dr. Paul Lambert, Dr. Deric Wheeler, Dr. Dudley Lamming and Dr. Elaine Alarid. Thank you for your guidance, support and encouragement during the completion of my thesis.

Thank you to my friends inside and outside of the Cancer Biology program. Special thanks to Thejas, Mailee and Will. I will always appreciate the friendships we have built over the last seven years and could not imagine what things would have been like without you all.

My family. Thanks to my Mom and Dad, your support and love has helped me become the person I am. My siblings, you all are my best friends and I appreciate your support. Thank you for your unending support and encouragement to pursue my passions. None of this would have been possible without you.

To Siera Garcia, thank you for everything you have done for me. The are no words to express what you mean to me. Thank you for all the thoughtful and caring things you have done for me to help me get to this moment. I will never forget the surprise pizza delivery for me after a long walk home from a late night in lab so I would have something ready to eat. Thank you for traveling from Chicago all of those weekends while I was

unable to get away. Thank you for moving to Madison and being my in-person support. I don’t know how I would have made it through this without you.

ABSTRACT

Understanding glucose uptake in breast cancer cells

JOSHUA A. MARTIN

Under the direction of Dr. Caroline Alexander

at the University of Wisconsin – Madison

Considerable evidence suggests that cancer cells rely disproportionately on glucose uptake for growth, creating a therapeutic opportunity for “starving” cancer cells. Our data implicated a cell surface receptor called LDL receptor related protein-5 (LRP5) in glucose uptake in mammary epithelial cells. Thus, this thesis aimed to interrogate the mechanisms underlying the uptake of glucose into normal and transformed mammary epithelial cells. Firstly, we characterized the expression of the principal family of hexose transporters (GLUT) in breast epithelial cells. We confirmed that glucose uptake was key to the survival of breast cancer cells. While GLUT1 has been shown to be a dominant GLUT, crucial for HER2-induced breast tumor initiation, we found considerable residual glucose uptake upon pharmacologic inhibition. In search of potentially redundant GLUTs, we focused on the co-expressed GLUT, GLUT8. Other studies initially pursued GLUT8 as an alternative transporter to the insulin-activated GLUT, GLUT4, but found that it was inessential to mammalian development, and rarely, if ever, present at the cell surface. *In silico* analysis showed that several GLUTs are transcribed as different mRNA isomers. For GLUT8, we observed three alternatively spliced isomers and found that only two are competent to produce stable proteins, one a relatively minor species. The dominant isomer in cancer cells does not produce a protein, suggesting that cancer cells have

little/no GLUT8 function. More interesting, we revealed that the full-length GLUT8 protein is cleaved to produce a C-terminal peptide, and we speculate that this reaction is typical of metabolic sensors. To test this hypothesis, we aim to find partners for the GLUT8 protein, and to identify cell types that show regulated GLUT8 cleavage. Furthermore, we have shown that knockdown of GLUT8 with shRNA, and other shRNA species, induces senescence in breast cancer cells, but have not fully established the molecular basis for this reaction. This will be important to understanding results from any knockdown experiment, and possibly to understanding senescence of breast tumors *in vivo*. In summary, we have revealed that the GLUT family is likely to have additional roles besides regulated ectopic glucose uptake and suggest a novel role for the enigmatic GLUT8 transporter.

ABBREVIATIONS

2-DG	2-Deoxyglucose
AMPK	5'-AMP Activated Protein Kinase
AP2	Adapter Protein Complex 2
ATP	Adenosine Triphosphate
CRISPR	Clustered Regularly Interspaced Short Palindromic Repeats
DKK1	Dickkopf Wnt Signaling Pathway Inhibitor 1
DOX	Doxycycline
EGF	Epidermal Growth Factor
ErbB2	ErbB2 Receptor Tyrosine Kinase 2
EDTA	Ethylenediaminetetraacetic Acid
FGF	Fibroblast Growth Factor
FZD	Frizzled
GLUT	Glucose Transporter
HMIT	H+/myo-inositol cotransporter
HBM	High Bone Mass
HER2	Human Epidermal Growth Factor Receptor 2
HPRT	Hypoxanthine-guanine Phosphoribosyltransferase
IP	Immunoprecipitation
IRGT	Insulin Responsive Glucose Transporter
LRP	Low Density Lipoprotein Receptor-Related Protein
mTORC1/2	Mammalian Target of Rapamycin Complex 1/2
MEC	Mammary Epithelial Cells
MRC	Maximal Respiratory Capacity
miRNA	microRNA
MAPK	Mitogen-Activated Protein Kinase
MEF	Mouse Embryonic Fibroblast
MMTV	Mouse Mammary Tumor Virus
NAMPT	Nicotinamide Phosphoribosyltransferase
OPPG	Osteoporosis Pseudoglioma
OXPHOS	Oxidative Phosphorylation
OCR	Oxygen Consumption Rate
PPARα	Peroxisome Proliferator-activated Receptor
PTEN	Phosphatase and Tensin Homolog
PyMT	Polyoma Middle T Antigen
PORCN	Porcupine
pre-miRNA	Precursor microRNA
pri-miRNA	Primary microRNA
AKT	Protein Kinase B
PKC	Protein Kinase C

ROS	Reactive Oxygen Species
RLU	Relative Luminescence Units
RNAi	RNA Interference
RISC	RNA-induced Silencing Complex
SOST	Sclerostin
SFRP	Secreted Frizzled-Related Protein
shRNA	Small Hairpin RNA
siRNA	Small Interfering RNA
SDS-PAGE	Sodium dodecyl sulfate polyacrylamide gel electrophoresis
SGLT	Sodium-Glucose Transport Proteins
SLC	Solute Carrier Protein
SNX27	Sorting Nexin 27
SRC	Spare Respiratory Capacity
SREBP	Sterol Regulatory Element Binding Protein
TXNIP	Thioredoxin Interacting Protein
TPM	Transcripts Per Kilobase Million
TM	Transmembrane Domain
UTR	Untranslated Region
VSP26	Vacuolar Sorting Protein 26
WCL	Whole Cell Lysate

Chapter I

Introduction

Overview of glucose metabolism and uptake

Rapidly dividing cells rely on increased import of nutrients to provide sufficient amounts of ATP and biosynthetic precursors needed to support production of new cells. The Warburg effect, first described by Otto Warburg, is the process of aerobic glycolysis as it occurs in cancer cells. Specifically, cancer cells often increase the conversion of glucose to pyruvate and ultimately lactate, which is then secreted from the cell [1]. Warburg initially identified this phenomenon following a direct comparison of metabolic processes between cancer cells and normal cells, and he attributed the observed phenotype to dysfunctional mitochondria in cancer cells. It has since become known that aerobic glycolysis is in fact common in normal proliferating cells as well as cancer cells, and is not the result of defective mitochondria but is rather an adaptive strategy adopted by cancer cells to increase output of biosynthetic precursors derived from glycolysis and related pathways [2].

Glucose uptake is mediated by two families of solute transporters, the SLC2 and SLC5 family of transporters. The SLC5 family are sodium glucose cotransporters (SGLTs) that utilize a sodium gradient to transport glucose against its concentration gradient [3]. The SLC2 family of glucose transporters (GLUTs) comprise a family of 14 proteins that manage the energy-independent movement of glucose across the cell membrane. All GLUTs contain 12 membrane spanning domains with cytoplasmic amino and carboxy termini [4, 5]. GLUTs are sorted into 3 classes according to their topography and protein sequence. Class I GLUTs, comprising GLUT1-4 and GLUT14 are characterized by a large extracellular loop between transmembrane domains 1 and 2. Class II GLUTs, GLUT5, 7, 9, and 11, also have a large extracellular loop between transmembrane

domains 1 and 2. The third class of GLUTs are made up of GLUTs 6, 8, 10, 12, and 13. Class III GLUTs, lack the large extracellular loop after transmembrane domain 1 found in class I and II GLUTs, and instead have a large extracellular loop between transmembrane domains 9 and 10. GLUT13 is known as H+/myo-inositol cotransporter (HMIT) and has only one known substrate, myo-inositol. GLUT13 activity is regulated by changes in intracellular pH. GLUT expression is varied in tissues throughout the body (Table 1 & Chapter 3, Figure 1). Glucose is not the only substrate transported by GLUTs. Although some GLUTs are reported to only transport a single substrate type, other GLUTs have broader transport capabilities. GLUTs also vary in their affinity (K_m) for their substrate which reflects their biological roles within different tissue. For example, GLUT3 is a high affinity transporter (K_m = 1.4mM) that is mainly expressed in the brain, which requires efficient glucose uptake under normal physiological conditions (Table 1). GLUT2, however, is a low affinity transporter (K_m = 17mM) and is expressed in the small intestine and pancreas where transport activity is required only when high amounts of glucose are present.

Regulation of GLUT localization and activity

Most of our understanding of GLUT regulation and trafficking originates from studies of class I GLUTs. Two class I transporters, GLUT1 and GLUT4, were the first among the family to be identified and described. GLUT1, initially called the erythrocyte transporter, was first cloned from human liver carcinoma (HEPG2) cells and erythrocytes [6, 7]. Since then, studies have shown that GLUT1 is ubiquitously expressed in most tissues and is often over-expressed in cancer cells. GLUT4, initially referred to as insulin responsive glucose transporter (IRGT), was first cloned from muscle and adipose tissue

through work aimed at identifying the source of insulin-induced glucose uptake in those tissues [8, 9]. GLUT4 was identified as the transporter whose cellular localization undergoes a dramatic and rapid shift from intracellular vesicles to the plasma membrane in response to insulin secreted by the pancreas due to high circulating glucose levels. The mobilization of GLUT4 drives the import of glucose into tissues like fat and muscle.

The trafficking of GLUTs is a coordinated process that balances the core metabolic needs of the cell. Recent work has begun to describe the underlying mechanics of GLUT trafficking and cell surface presentation of class I GLUTs. Basal level glucose uptake is maintained via GLUT1-retromer recycling from endosomes back to the cell surface, and disturbing the retromer driven recycling causes mis-sorting of GLUT1 into lysosomal vesicles [10-12]. Disruption of retromer complex components, sorting nexin 27 (SNX27) or vacuolar sorting protein 26 (VSP26), decreases cell surface expression of GLUT1 subsequently leading to a decrease in glucose uptake [11]. Under metabolic and oncogenic stress, autophagy facilitates GLUT1-retromer recycling to the cell surface thereby coordinating intracellular degradation and glucose uptake [10]. Retromer-mediated recycling of GLUT1 to the cell surface is also disrupted by phosphatase and tensin homolog (PTEN) in a phosphatase-independent manner through a physical interaction with SNX27, which serves to direct GLUT1 trafficking to lysosomes [12].

Controlling the flow of glucose into the cell in response to growth stimuli and metabolic stress requires constant adjustments to the number of GLUT molecules on the cell surface. The protein Thioredoxin interacting protein (TXNIP) serves as a regulatory hub directing the internalization of class I glucose transporters from the cell surface. The inhibitory interaction of the TXNIP is controlled by the activity of 5’-AMP activated protein

kinase (AMPK) and protein kinase B (AKT) [13, 14]. AMPK activation under energy stress results in phosphorylation and degradation TXNIP, which in turn results in a decreased rate of GLUT1 internalization [13]. Growth factors also induce acute glucose uptake through AKT-dependent TXNIP phosphorylation and degradation, which disrupts TXNIP association with multiple class I GLUTs [14]. Direct phosphorylation of GLUT1 at S226 by PKC also induces an increase in GLUT1 cell surface expression and glucose uptake [15]. Additionally, the tumor suppressor p53 has been shown to be a repressor of glucose uptake[16]. Loss of wild-type or expression of mutant p53 increases GLUT1 cell surface presentation resulting in enhanced glucose uptake in cancer cell lines without altering total GLUT1 expression. The activity c-Myc and mutant KRAS have been shown to increase total GLUT1 expression in cell lines, with mutant KRAS providing a growth advantage in experimental low-glucose conditions. [17, 18].

It is not known whether the regulatory mechanisms above function similarly on class II and class III GLUTs. Given the topological similarities between class I and class II GLUTs, it is possible that they are regulated by similar mechanisms. The sequence motifs that define the GLUT/TXNIP association have not been defined. The retromer-associated motif of GLUT1 is located in the last four amino acids of the C-terminal domain. GLUT1 lacks the natural di-leucine motifs that drive endocytosis and are found in other GLUTs (discussed below). However, a disordered region in the C-terminus of GLUT1 has been identified and missense mutations in this region can introduce di-leucine patterns that lead to aberrant internalization through adaptor protein 2 (AP2) complex and disruption in basal glucose uptake [19]. GLUT4, a primarily intracellular residing GLUT

contains multiple targeting motifs, including a di-leucine motif in the C-terminal tail, that are essential for steady-state internalization of GLUT4 [20-22].

The intracellular sequestration of GLUT8 has been tied to the presence of a di-leucine motif in the N-terminus cytoplasmic domain. Multiple studies have shown that GLUT8 maintains an exclusively intracellular distribution in human embryonic kidney cells (293T), fibroblast-like cells (COS-7), neuroblastoma cells, and rat adipose cells [23-29]. Mutating the di-leucine motif of GLUT8 causes abnormal plasma membrane accumulation [27]. Altering residues upstream of the di-leucine motif of GLUT8 also results in plasma membrane localization. The di-leucine motif is bound by the β2 subunit of the AP2 complex, and inhibition of AP2 complex proteins phenocopies the plasma membrane accumulation that occurs when the di-leucine motif is mutated [26, 30]. Mutation of the N-terminal di-leucine motif of GLUT6 also disrupts its normally cytoplasmic accumulation and like GLUT8, GLUT6 is not responsive to insulin exposure [27]. The stimulus for GLUT8 translocation, if one exists, has not yet been identified.

GLUT structure and function

The crystal structures for GLUT1 and GLUT3 have been resolved, providing insight into the mechanism of substrate transport [31, 32]. These structures have contributed to the development of a model describing the mechanism underlying GLUTs-mediated substrate transport. The model involves a progression through 4 conformational states: outward open, ligand-bound occluded, inward open, and ligand-free occluded [31]. In the outward open state, the substrate binding site is exposed to the extracellular milieu. High concentrations of substrate favor binding to the GLUT. Bound substrate generates a conformational change that results in the predicted formation of a hydrogen bond between

transmembrane domains on the extracellular face. The GLUT then cycles to the ligand-bound occluded state. The extracellular domains are now in close proximity and generate an extracellular gate, closing off the binding site to the extracellular exposure. The transporter will then shift to the inward open state exposing the substrate site to the low concentration intracellular environment which favors substrate release. Loss of the substrate shifts the transporter to the ligand-free occluded position and the intracellular loops form an intracellular bridge. This bridge is thought to pull the intracellular face of the transporter together opening up the substrate binding site to the extracellular side.

Point mutations, both natural and artificial, in the GLUT coding sequence have been found to have mostly detrimental effects on the function of the transporter. 42 different disease-causing mutations in GLUT1 have been identified that result in either glut1 deficiency syndrome or epilepsy [31]. Disease-causing mutations in GLUT2 have also been identified resulting in Fanconi-Bickel syndrome [33].

GLUT inhibitors

Inhibition of glucose metabolism at the level of transport is of active interest due to the established association between GLUTs and metabolic diseases such as cancer and obesity. However, the development of an isoform-specific GLUT inhibitor has been challenging with multiple candidate compounds demonstrating non-specific activity. WZB117 was first described as a GLUT1 specific inhibitor that demonstrated anti-cancer activity *in vitro* and *in vivo* [34-36]. However, WZB117 was later found to have broader anti-GLUT activity, targeting other GLUT isoforms including a notably higher inhibitory activity against GLUT4 [37]. Another candidate inhibitor, STF-31, was shown to disrupt GLUT1 activity in renal cell carcinoma xenografts [38]. However, a follow-up study

revealed that STF-31 also inhibits the enzyme nicotinamide phosphoribosyltransferase (NAMPT) [39]. Additionally, both Fasentin and Phloretin have broad inhibitory activity against multiple GLUTs [5, 40]. The candidate GLUT inhibitor BAY-876 demonstrates preference for GLUT1 over other class I GLUTs 2, 3, and 4 [41]. Designing and screening drugs to target specific GLUT isoforms has been challenging, but to aid in the discovery of GLUT-specific inhibitors, GLUT1 has been crystallized while bound to 3 different inhibitors shedding light on how these drugs interact with GLUT1 [42]. In the future, studies like this can inform design of inhibitors so that more targeted isoform-specific drugs can be developed.

Other chemical inhibitors of glucose uptake have been identified. These inhibitors were not initially designed to target GLUT specifically but were found to have secondary GLUT inhibiting activity. HIV protease inhibitors were found to inhibit multiple class 1 GLUTs after patients using these inhibitors developed insulin resistance [43]. Cytochalasin B blocks actin filament polymerization but also binds to the intracellular face of GLUT1 and has been shown to have broad GLUT isoform Inhibition activity [42]. 2-deoxyglucose is a non-metabolizable glucose analog that competes with glucose for transport through GLUTs and indirectly blocks uptake through inhibition of hexokinase activity [44].

GLUT8 phenotypes *in vivo*

The search that identified GLUT8 began when the phenotypes of GLUT4 knockout mice were described. GLUT4-null mice, although viable, had decrease longevity but displayed a near normal capacity to clear blood glucose without any significant changes in expression of other known GLUTs at the time [45]. This led to a search for a GLUT that

may be responsive to insulin, and GLUT8 was cloned. However, as mentioned earlier, GLUT8 activity is not insulin-regulated [46]. GLUT8 expression varies between tissues throughout the body but is most highly expressed in the testis, liver, brain, heart, skeletal muscle, and adipose tissue [25, 29, 46]. GLUT8 knockout mouse models have very subtle phenotypes. One of the first phenotypes identified following GLUT8 knockout was a significant decrease (17-22%) in the number of expected (25%) homozygous knockout animals [47, 48]. This led to an examination of the spermatozoa which revealed that GLUT8 knockout spermatozoa had reduced motility and abnormal mitochondrial morphology, but 2-deoxyglucose uptake was not affected [48]**.** No other significant physical phenotypes were identified. One location of prominent GLUT8 expression is within regions of the brain, which led to the examination of the effect of GLUT8 on behavioral and neuronal phenotypes. GLUT8 knockout mice displayed slight but statistically significant increase in hyperactive behavior and had increased defecation compared to the wild-type cohort [49]. While on a normal diet, GLUT8 knockout mice do not display any abnormal metabolic phenotypes as measured by normal serum glucose, insulin, triglycerides, and free fatty acids [47, 48]. Knockout mice on a high fat diet had lower body fat compared to wild-type counterparts [50]. On a high fructose diet, female GLUT8 knockout mice are resistant to fatty liver development [51].

GLUT expression in breast cancer

Enhancing nutrient uptake is an important priority for rapidly proliferating cells. There is evidence that GLUT1 expression is crucial to mammary tumor growth and development *in vivo*. Anderson and colleagues implicated GLUT1 in two phases of HER-2-induced tumorigenesis [36, 52]. They showed that knockdown of GLUT1 expression in

a Her2/ErbB2 tumor cell line decreased proliferation and tumor growth *in vivo*. The authors also knocked out expression of GLUT1 in polyoma virus middle T-transformed mouse mammary epithelial cells, which also resulted in decreased tumor growth (35%) *in vivo.* While modulation of GLUT1 expression does alter previously formed tumors, the effects of GLUT1 loss on tumorigenesis are more dramatic. Wellberg et al., utilized a mouse model that expressed an activated version of Her2 and cre recombinase in the mammary gland in mice with $GLUT1^{+/+}$, $GLUT1^{flox/+}$, or $GLUT1^{flox/flox}$. Loss of just one GLUT1 allele was sufficient to virtually eliminate Her2-induced tumors as both $GLUT1^{flox/+}$ and $GLUT1^{flox/flox}$ mice remained essentially tumor-free for over 500 days, while $GLUT1^{+/+}$ mice were 100% tumor positive at 200 days [36]. The authors did report a lack of cre expression in the nucleus of mammary epithelial cells of GLUT1 floxed mice, which suggests that cells with tumorigenic potential were somehow eliminated from the otherwise normal mammary gland.

Other GLUT proteins have also been implicated in breast cancer malignancy. Bissell and colleagues examined the effects of extracellular glucose in an *in vitro* 3-d culture model of tumor malignancy [53]. In this model, suppression of activated signaling pathways causes a phenotypic reversion of malignant cells to form polarized acini-like nonmalignant cells. Extracellular glucose was the limiting factor for malignancy. Thus, upon exposure to higher extracellular glucose concentrations, GLUT3 expression increased leading to a parallel loss of polarization of cells in 3-d culture. Suppression of GLUT3 expression by siRNA was sufficient to revert the malignant cells back to a polarized state even when cultured in the presence of high extracellular glucose concentrations.

To date, examination of the expression of GLUT1 in primary breast tumors has yielded mixed results. The percentage of GLUT1-positive breast tumors varies greatly depending on the study, and not all breast tumors stain positive for GLUT1 expression [54-60]. However, of the tumors that do express GLUT1, there is a significant association with a basal-like molecular phenotype, higher histological score, and Ki67-positive staining [57-60]. GLUT1 expression in invasive ductal carcinoma was significantly correlated with worse overall survival and disease-free survival [57].

The functional significance of GLUT8 expression in breast cancer specifically and cancer generally has not been widely explored. Knockdown studies have been performed on GLUT8 in the HEPG2 hepatocellular carcinoma cell line without any noticeable phenotype [51, 61]. One study found GLUT8 expressed along with GLUT4 and GLUT11 in multiple myeloma cell lines [62]. Knockdown of GLUT8 expression in three multiple myeloma cell lines in that study caused cell death and growth inhibition.

LRP5 and the Wnt pathway

The low-density lipoprotein receptor-related protein 5 (LRP5) is a membrane receptor most widely known as a coreceptor for the Wnt signaling pathway but has recently been discovered to regulate glycolysis and glucose uptake. As a Wnt pathway receptor, LRP5 and the related protein LRP6, activate canonical Wnt signaling through the function of the canonical Wnt effector ß-catenin. LRP5 is a type I, single pass transmembrane receptor 1615 amino acids in length. LRP5, like LRP6, has intracellular domains that contain five PPPS/TP motifs which may be phosphorylated to activate canonical Wnt signaling kinases [63]. It was determined that the difference in the capacity

of LRP5 and LRP6 to transduce a canonical Wnt signal is attributed to a region in the cytoplasmic domain of the receptors [63].

The Wnt pathway has important regulatory functions during embryonic development and in the maintenance of adult somatic stem cells. Wnt signaling is crucial to normal mammary gland development [64, 65]. Furthermore, mutation of Wnt pathway components is known to be oncogenic, particularly in the colon [66, 67]. In breast cancer, mutations of Wnt signaling components are rare, however there is evidence of active Wnt signaling (represented by nuclear localization of ß-catenin) in patients with basal-like/triple negative tumors [68, 69]. Studies in breast cancer cell lines have identified a functional role for the Wnt pathway. Expression of the Wnt inhibitor sFRP1 in the breast cancer cell line MDA-MB-231 caused a decrease in proliferation *in vitro* and in xenograft tumor growth *in vivo* [70].

The two Wnt coreceptors, LRP5 and LRP6, are often thought to be interchangeable since they share approximately 71% amino acid homology and are both capable of transducing a canonical Wnt signal. However, studies on these receptors have revealed non-overlapping functions. *In* vivo, homozygous deletion of each of the LRP receptors individually results in unique phenotypes. Thus, *Lrp6-/-* mice die at birth, with dramatic developmental defects, while *Lrp5-/-* mice are viable but have decreased bone mass and exhibit metabolic defects such as hypercholesterolemia and impaired glucose tolerance [71-74]. Primary mammary epithelial cells (MECs) isolated from *Lrp5-/-* mice lack stem cell activity, demonstrated by the inability to regenerate a ductal tree when inoculated into a cleared mammary fat pad [75] despite expression of LRP6, which is often viewed as the more efficient Wnt receptor [63]. The expression of LRP5 has

oncogenic implications as well. Thus, transgenic mice over-expressing Wnt1 in the mammary gland develop breast tumors within six months [76]. However, Lrp5-/- mice are resistant to Wnt1-induced tumorigenesis [75]. Collectively, these studies demonstrate that LRP5 expression sensitizes mice to Wnt1-induced tumor development, and that LRP5 and LRP6 serve unique, non-redundant functions in the mammary gland.

Wnt signaling through LRP5 is an important regulator of bone biology. Loss-of-function mutations in the LRP5 ecto-domain are associated with the rare syndrome osteoporosis pseudoglioma (OPPG) characterized by loss of bone mass and susceptibility to fractures [77]. Gain-of-function mutations in the ecto-domain of LRP5 have been discovered to be responsible for high bone mass (HBM) [78-80]. *In vivo* studies have identified analogous mutations that recapitulate the human disorders, OPPG and HBM [71, 81, 82]. *In vitro,* the corresponding LRP5 mutations alter the efficiency of binding to the secreted inhibitors DKK1 and SOST, causing resistance to inhibition of canonical activity through ß-catenin [83, 84]. While another study found LRP5 contributes to osteoblast differentiation by increasing aerobic glycolysis, independent of ß-catenin and canonical Wnt signaling [85]. Taken together, these studies suggest the mutations found in OPPG and HBM could be altering LRP5 function in both a Wnt-dependent and -independent manner. Recent work has contributed to an increased understanding of the contribution of the canonical Wnt pathway to regulation of cell metabolism [86]. One study specifically showed that LRP5 non-canonically increases aerobic glycolysis (Warburg effect) during the process of differentiation of bone marrow stromal cells to osteoblasts through a mammalian target of rapamycin complex 2 (mTORC2)-dependent mechanism [85].

RNAi biogenesis and regulation of gene expression

Possessing the ability to modulate the amount of a gene product has enhanced our understanding of how genes influence normal physiology and disease. RNA interference (RNAi), by either small interfering RNA (siRNA) or short hairpin RNA (shRNA), has been extensively used for post-transcriptional gene silencing to functionally test gene products. Unfortunately, unintended off-target effects can sometimes account for the phenotypes identified by RNAi and complicate the interpretation of data generated from its use. RNAi has been co-opted for experimental use from endogenous RNAi and utilize the same biogenesis pathways as naturally occurring RNAi. Endogenous RNAi regulate gene expression through the expression of endogenous non-coding RNA called microRNA (miRNA) (Figure 1). The first miRNA, lin-4, was discovered in 1993 and was shown to be crucial to the regulation of developmental timing in *C. elegans* [87]. Shortly afterward, another miRNA, let-7, was discovered, and eventually multiple orthologs were also discovered in humans and other species. miRNA transcripts are produced by RNA polymerase II from either stand-alone genes or from introns of protein-coding genes [87]. The initial miRNA, known as the primary-miRNA (pri-miRNA), which may be more than 1kb in length, is cleaved in the nucleus by the endonuclease Drosha to form a 50-60 nucleotide long precursor-miRNA (pre-miRNA). The pre-miRNA is then exported from the nucleus via Exportin-5 ahead of final maturation steps which occur in the cytoplasm [88]. The pre-miRNA is further processed to an approximately 22 nucleotide double-stranded RNA by the endonuclease Dicer. The double-stranded RNA is then incorporated into the RNA-induced silencing complex (RISC), and the passenger strand of the RNA is cleaved or unwound from the guide strand which remains in complex with RISC [89]. The active

RISC complex then binds to complementary mRNA sequences to either block translation of the mRNA or cause the degradation of the target transcript [90].

Exogenous RNAi species have been important experimental tools for studying gene function. Both siRNA and shRNA rely upon portions of the endogenous RNAi biogenesis machinery for their maturation and function [91]. Both methods utilize Dicer and the collection of proteins that comprise the RISC complex, however only shRNAs, which rely upon transcription in the nucleus, utilize Drosha and Exportin-5 for their trimming and export.

The occurrence of off-target effects has been documented with the use of these tools. There are three types of off-target effects, the first of which is sequence-dependent targeting of unintended genes [92]. It has now been determined that the non-specific gene targeting is not totally dependent on overall identity of the siRNA but rather through exact matches of hexamer and heptamer siRNA sequences to the 3'UTR of off-target genes [93]. The second type of off-target effect is through activation of innate immunity by recognition of foreign RNA [94]. The third type of off-target effect is the result of saturation of endogenous RNAi components such as Exportin-5 [95]. Expression of exogenous RNAi has been shown to alter the function of endogenous RNAi.

Aim of the Thesis

Since the observations made by Otto Warburg back in 1954, exploring the metabolic changes occurring in cancer cells has been an active area of research. As cancer cells acquire activating mutations in oncogenes that drive their proliferation, they acquire the ability to take in and utilize nutrients such as glucose to satisfy the core requirements of rapidly proliferating cells. Given the role of GLUT transporters as the

proximal step in glucose metabolism, it is important to understand the processes that influence their expression and activity. In recent years, details regarding the function and regulation of GLUT1 have become clearer in the context of cancer and transformation. The purpose of this thesis was to explore the role of lesser known GLUTs, and to investigate whether expression of multiple GLUTs serves redundant functions in breast cancer cells.

REFERENCES

1. Warburg, O., *On the origin of cancer cells.* Science, 1956. **123**(3191): p. 309-14.

2. Vander Heiden, M.G. and R.J. DeBerardinis, *Understanding the Intersections between Metabolism and Cancer Biology.* Cell, 2017. **168**(4): p. 657-669.

3. McCracken, A.N. and A.L. Edinger, *Nutrient transporters: the Achilles' heel of anabolism.* Trends Endocrinol Metab, 2013. **24**(4): p. 200-8.

4. Barron, C.C., et al., *Facilitative glucose transporters: Implications for cancer detection, prognosis and treatment.* Metabolism, 2016. **65**(2): p. 124-39.

5. Augustin, R., *The protein family of glucose transport facilitators: It's not only about glucose after all.* IUBMB Life, 2010. **62**(5): p. 315-33.

6. Mueckler, M., et al., *Sequence and structure of a human glucose transporter.* Science, 1985. **229**(4717): p. 941-5.

7. Mueckler, M. and B. Thorens, *The SLC2 (GLUT) family of membrane transporters.* Mol Aspects Med, 2013. **34**(2-3): p. 121-38.

8. James, D.E., et al., *Insulin-regulatable tissues express a unique insulin-sensitive glucose transport protein.* Nature, 1988. **333**(6169): p. 183-5.

9. Piper, R.C., L.J. Hess, and D.E. James, *Differential sorting of two glucose transporters expressed in insulin-sensitive cells.* Am J Physiol, 1991. **260**(3 Pt 1): p. C570-80.

10. Roy, S., et al., *Autophagy-Dependent Shuttling of TBC1D5 Controls Plasma Membrane Translocation of GLUT1 and Glucose Uptake.* Mol Cell, 2017. **67**(1): p. 84-95 e5.

11. Steinberg, F., et al., *A global analysis of SNX27-retromer assembly and cargo specificity reveals a function in glucose and metal ion transport.* Nat Cell Biol, 2013. **15**(5): p. 461-71.

12. Shinde, S.R. and S. Maddika, *PTEN Regulates Glucose Transporter Recycling by Impairing SNX27 Retromer Assembly.* Cell Rep, 2017. **21**(6): p. 1655-1666.

13. Wu, N., et al., *AMPK-dependent degradation of TXNIP upon energy stress leads to enhanced glucose uptake via GLUT1.* Mol Cell, 2013. **49**(6): p. 1167-75.

14. Waldhart, A.N., et al., *Phosphorylation of TXNIP by AKT Mediates Acute Influx of Glucose in Response to Insulin.* Cell Rep, 2017. **19**(10): p. 2005-2013.

15. Lee, E.E., et al., *A Protein Kinase C Phosphorylation Motif in GLUT1 Affects Glucose Transport and is Mutated in GLUT1 Deficiency Syndrome.* Mol Cell, 2015. **58**(5): p. 845-53.

16. Zhang, C., et al., *Tumour-associated mutant p53 drives the Warburg effect.* Nat Commun, 2013. **4**: p. 2935.

17. Yun, J., et al., *Glucose deprivation contributes to the development of KRAS pathway mutations in tumor cells.* Science, 2009. **325**(5947): p. 1555-9.

18. Osthus, R.C., et al., *Deregulation of glucose transporter 1 and glycolytic gene expression by c-Myc.* J Biol Chem, 2000. **275**(29): p. 21797-800.

19. Meyer, K., et al., *Mutations in Disordered Regions Can Cause Disease by Creating Dileucine Motifs.* Cell, 2018. **175**(1): p. 239-253 e17.

20. Al-Hasani, H., et al., *Roles of the N- and C-termini of GLUT4 in endocytosis.* J Cell Sci, 2002. **115**(Pt 1): p. 131-40.

21. Kandror, K.V. and P.F. Pilch, *The sugar is sIRVed: sorting Glut4 and its fellow travelers.* Traffic, 2011. **12**(6): p. 665-71.

22. Song, X.M., R.C. Hresko, and M. Mueckler, *Identification of amino acid residues within the C terminus of the Glut4 glucose transporter that are essential for insulin-stimulated redistribution to the plasma membrane.* J Biol Chem, 2008. **283**(18): p. 12571-85.

23. Aerni-Flessner, L.B., M.C. Otu, and K.H. Moley, *The amino acids upstream of NH(2)-terminal dileucine motif play a role in regulating the intracellular sorting of the Class III transporters GLUT8 and GLUT12.* Mol Membr Biol, 2011. **28**(1): p. 30-41.

24. Augustin, R., J. Riley, and K.H. Moley, *GLUT8 contains a [DE]XXXL[LI] sorting motif and localizes to a late endosomal/lysosomal compartment.* Traffic, 2005. **6**(12): p. 1196-212.

25. Carayannopoulos, M.O., et al., *GLUT8 is a glucose transporter responsible for insulin-stimulated glucose uptake in the blastocyst.* Proc Natl Acad Sci U S A, 2000. **97**(13): p. 7313-8.

26. Diril, M.K., et al., *Lysosomal localization of GLUT8 in the testis--the EXXXLL motif of GLUT8 is sufficient for its intracellular sorting via AP1- and AP2-mediated interaction.* FEBS J, 2009. **276**(14): p. 3729-43.

27. Lisinski, I., et al., *Targeting of GLUT6 (formerly GLUT9) and GLUT8 in rat adipose cells.* Biochem J, 2001. **358**(Pt 2): p. 517-22.

28. Shin, B.C., R.A. McKnight, and S.U. Devaskar, *Glucose transporter GLUT8 translocation in neurons is not insulin responsive.* J Neurosci Res, 2004. **75**(6): p. 835-44.

29. Ibberson, M., M. Uldry, and B. Thorens, *GLUTX1, a novel mammalian glucose transporter expressed in the central nervous system and insulin-sensitive tissues.* J Biol Chem, 2000. **275**(7): p. 4607-12.

30. Schmidt, U., et al., *Endocytosis of the glucose transporter GLUT8 is mediated by interaction of a dileucine motif with the beta2-adaptin subunit of the AP-2 adaptor complex.* J Cell Sci, 2006. **119**(Pt 11): p. 2321-31.

31. Deng, D., et al., *Crystal structure of the human glucose transporter GLUT1.* Nature, 2014. **510**(7503): p. 121-5.

32. Deng, D., et al., *Molecular basis of ligand recognition and transport by glucose transporters.* Nature, 2015. **526**(7573): p. 391-6.

33. Santer, R., et al., *Mutations in GLUT2, the gene for the liver-type glucose transporter, in patients with Fanconi-Bickel syndrome.* Nat Genet, 1997. **17**(3): p. 324-6.

34. Liu, Y., et al., *A small-molecule inhibitor of glucose transporter 1 downregulates glycolysis, induces cell-cycle arrest, and inhibits cancer cell growth in vitro and in vivo.* Mol Cancer Ther, 2012. **11**(8): p. 1672-82.

35. Liu, Y., et al., *Small compound inhibitors of basal glucose transport inhibit cell proliferation and induce apoptosis in cancer cells via glucose-deprivation-like mechanisms.* Cancer Lett, 2010. **298**(2): p. 176-85.

36. Wellberg, E.A., et al., *The glucose transporter GLUT1 is required for ErbB2-induced mammary tumorigenesis.* Breast Cancer Res, 2016. **18**(1): p. 131.

37. Ojelabi, O.A., et al., *WZB117 (2-Fluoro-6-(m-hydroxybenzoyloxy) Phenyl m-Hydroxybenzoate) Inhibits GLUT1-mediated Sugar Transport by Binding Reversibly at the Exofacial Sugar Binding Site.* J Biol Chem, 2016. **291**(52): p. 26762-26772.

38. Chan, D.A., et al., *Targeting GLUT1 and the Warburg effect in renal cell carcinoma by chemical synthetic lethality.* Sci Transl Med, 2011. **3**(94): p. 94ra70.

39. Adams, D.J., et al., *NAMPT is the cellular target of STF-31-like small-molecule probes.* ACS Chem Biol, 2014. **9**(10): p. 2247-54.

40. Wood, T.E., et al., *A novel inhibitor of glucose uptake sensitizes cells to FAS-induced cell death.* Mol Cancer Ther, 2008. **7**(11): p. 3546-55.

41. Siebeneicher, H., et al., *Identification and Optimization of the First Highly Selective GLUT1 Inhibitor BAY-876.* ChemMedChem, 2016. **11**(20): p. 2261-2271.

42. Kapoor, K., et al., *Mechanism of inhibition of human glucose transporter GLUT1 is conserved between cytochalasin B and phenylalanine amides.* Proc Natl Acad Sci U S A, 2016. **113**(17): p. 4711-6.

43. Hresko, R.C. and P.W. Hruz, *HIV protease inhibitors act as competitive inhibitors of the cytoplasmic glucose binding site of GLUTs with differing affinities for GLUT1 and GLUT4.* PLoS One, 2011. **6**(9): p. e25237.

44. Aft, R.L., F.W. Zhang, and D. Gius, *Evaluation of 2-deoxy-D-glucose as a chemotherapeutic agent: mechanism of cell death.* Br J Cancer, 2002. **87**(7): p. 805-12.

45. Katz, E.B., et al., *Cardiac and adipose tissue abnormalities but not diabetes in mice deficient in GLUT4.* Nature, 1995. **377**(6545): p. 151-5.

46. Doege, H., et al., *GLUT8, a novel member of the sugar transport facilitator family with glucose transport activity.* J Biol Chem, 2000. **275**(21): p. 16275-80.

47. Membrez, M., et al., *GLUT8 is dispensable for embryonic development but influences hippocampal neurogenesis and heart function.* Mol Cell Biol, 2006. **26**(11): p. 4268-76.

48. Gawlik, V., et al., *Targeted disruption of Slc2a8 (GLUT8) reduces motility and mitochondrial potential of spermatozoa.* Mol Membr Biol, 2008. **25**(3): p. 224-35.

49. Schmidt, S., et al., *Deletion of glucose transporter GLUT8 in mice increases locomotor activity.* Behav Genet, 2008. **38**(4): p. 396-406.

50. Adastra, K.L., et al., *Slc2a8 deficiency in mice results in reproductive and growth impairments.* Biol Reprod, 2012. **87**(2): p. 49.

51. Debosch, B.J., et al., *Glucose transporter 8 (GLUT8) mediates fructose-induced de novo lipogenesis and macrosteatosis.* J Biol Chem, 2014. **289**(16): p. 10989-98.

52. Young, C.D., et al., *Modulation of glucose transporter 1 (GLUT1) expression levels alters mouse mammary tumor cell growth in vitro and in vivo.* PLoS One, 2011. **6**(8): p. e23205.

53. Onodera, Y., J.M. Nam, and M.J. Bissell, *Increased sugar uptake promotes oncogenesis via EPAC/RAP1 and O-GlcNAc pathways.* J Clin Invest, 2014. **124**(1): p. 367-84.

54. Binder, C., et al., *Deregulated simultaneous expression of multiple glucose transporter isoforms in malignant cells and tissues.* Anticancer Res, 1997. **17**(6D): p. 4299-304.

55. Brown, R.S. and R.L. Wahl, *Overexpression of Glut-1 glucose transporter in human breast cancer. An immunohistochemical study.* Cancer, 1993. **72**(10): p. 2979-85.

56. Godoy, A., et al., *Differential subcellular distribution of glucose transporters GLUT1-6 and GLUT9 in human cancer: ultrastructural localization of GLUT1 and GLUT5 in breast tumor tissues.* J Cell Physiol, 2006. **207**(3): p. 614-27.

57. Jang, S.M., et al., *The Glycolytic Phenotype is Correlated with Aggressiveness and Poor Prognosis in Invasive Ductal Carcinomas.* J Breast Cancer, 2012. **15**(2): p. 172-80.

58. Younes, M., et al., *GLUT1 expression in human breast carcinoma: correlation with known prognostic markers.* Anticancer Res, 1995. **15**(6B): p. 2895-8.

59. Pinheiro, C., et al., *GLUT1 and CAIX expression profiles in breast cancer correlate with adverse prognostic factors and MCT1 overexpression.* Histol Histopathol, 2011. **26**(10): p. 1279-86.

60. Hussein, Y.R., et al., *Glut-1 Expression Correlates with Basal-like Breast Cancer.* Transl Oncol, 2011. **4**(6): p. 321-7.

61. Mayer, A.L., et al., *SLC2A8 (GLUT8) is a mammalian trehalose transporter required for trehalose-induced autophagy.* Sci Rep, 2016. **6**: p. 38586.

62. McBrayer, S.K., et al., *Multiple myeloma exhibits novel dependence on GLUT4, GLUT8, and GLUT11: implications for glucose transporter-directed therapy.* Blood, 2012. **119**(20): p. 4686-97.

63. MacDonald, B.T., et al., *Dissecting molecular differences between Wnt coreceptors LRP5 and LRP6.* PLoS One, 2011. **6**(8): p. e23537.

64. Andl, T., et al., *WNT signals are required for the initiation of hair follicle development.* Dev Cell, 2002. **2**(5): p. 643-53.

65. van Genderen, C., et al., *Development of several organs that require inductive epithelial-mesenchymal interactions is impaired in LEF-1-deficient mice.* Genes Dev, 1994. **8**(22): p. 2691-703.

66. Clevers, H. and R. Nusse, *Wnt/beta-catenin signaling and disease.* Cell, 2012. **149**(6): p. 1192-205.

67. Polakis, P., *Wnt signaling in cancer.* Cold Spring Harb Perspect Biol, 2012. **4**(5).

68. Geyer, F.C., et al., *beta-Catenin pathway activation in breast cancer is associated with triple-negative phenotype but not with CTNNB1 mutation.* Mod Pathol, 2011. **24**(2): p. 209-31.

69. Khramtsov, A.I., et al., *Wnt/beta-catenin pathway activation is enriched in basal-like breast cancers and predicts poor outcome.* Am J Pathol, 2010. **176**(6): p. 2911-20.

70. Matsuda, Y., et al., *WNT signaling enhances breast cancer cell motility and blockade of the WNT pathway by sFRP1 suppresses MDA-MB-231 xenograft growth.* Breast Cancer Res, 2009. **11**(3): p. R32.

71. Cui, Y., et al., *Lrp5 functions in bone to regulate bone mass.* Nat Med, 2011. **17**(6): p. 684-91.

72. Fujino, T., et al., *Low-density lipoprotein receptor-related protein 5 (LRP5) is essential for normal cholesterol metabolism and glucose-induced insulin secretion.* Proc Natl Acad Sci U S A, 2003. **100**(1): p. 229-34.

73. Magoori, K., et al., *Severe hypercholesterolemia, impaired fat tolerance, and advanced atherosclerosis in mice lacking both low density lipoprotein receptor-related protein 5 and apolipoprotein E.* J Biol Chem, 2003. **278**(13): p. 11331-6.

74. Pinson, K.I., et al., *An LDL-receptor-related protein mediates Wnt signalling in mice.* Nature, 2000. **407**(6803): p. 535-8.

75. Lindvall, C., et al., *The Wnt signaling receptor Lrp5 is required for mammary ductal stem cell activity and Wnt1-induced tumorigenesis.* J Biol Chem, 2006. **281**(46): p. 35081-7.

76. Tsukamoto, A.S., et al., *Expression of the int-1 gene in transgenic mice is associated with mammary gland hyperplasia and adenocarcinomas in male and female mice.* Cell, 1988. **55**(4): p. 619-25.

77. Gong, Y., et al., *LDL receptor-related protein 5 (LRP5) affects bone accrual and eye development.* Cell, 2001. **107**(4): p. 513-23.

78. Boyden, L.M., et al., *High bone density due to a mutation in LDL-receptor-related protein 5.* N Engl J Med, 2002. **346**(20): p. 1513-21.

79. Little, R.D., et al., *A mutation in the LDL receptor-related protein 5 gene results in the autosomal dominant high-bone-mass trait.* Am J Hum Genet, 2002. **70**(1): p. 11-9.

80. Van Wesenbeeck, L., et al., *Six novel missense mutations in the LDL receptor-related protein 5 (LRP5) gene in different conditions with an increased bone density.* Am J Hum Genet, 2003. **72**(3): p. 763-71.

81. Holmen, S.L., et al., *Decreased BMD and limb deformities in mice carrying mutations in both Lrp5 and Lrp6.* J Bone Miner Res, 2004. **19**(12): p. 2033-40.

82. Kato, M., et al., *Cbfa1-independent decrease in osteoblast proliferation, osteopenia, and persistent embryonic eye vascularization in mice deficient in Lrp5, a Wnt coreceptor.* J Cell Biol, 2002. **157**(2): p. 303-14.

83. Ai, M., et al., *Reduced affinity to and inhibition by DKK1 form a common mechanism by which high bone mass-associated missense mutations in LRP5 affect canonical Wnt signaling.* Mol Cell Biol, 2005. **25**(12): p. 4946-55.

84. Semenov, M.V. and X. He, *LRP5 mutations linked to high bone mass diseases cause reduced LRP5 binding and inhibition by SOST.* J Biol Chem, 2006. **281**(50): p. 38276-84.

85. Esen, E., et al., *WNT-LRP5 signaling induces Warburg effect through mTORC2 activation during osteoblast differentiation.* Cell Metab, 2013. **17**(5): p. 745-55.

86. Sherwood, V., *WNT signaling: an emerging mediator of cancer cell metabolism?* Mol Cell Biol, 2015. **35**(1): p. 2-10.

87. Bartel, D.P., *MicroRNAs: genomics, biogenesis, mechanism, and function.* Cell, 2004. **116**(2): p. 281-97.

88. Yi, R., et al., *Exportin-5 mediates the nuclear export of pre-microRNAs and short hairpin RNAs.* Genes Dev, 2003. **17**(24): p. 3011-6.

89. Kim, V.N., J. Han, and M.C. Siomi, *Biogenesis of small RNAs in animals.* Nat Rev Mol Cell Biol, 2009. **10**(2): p. 126-39.

90. Tolia, N.H. and L. Joshua-Tor, *Slicer and the argonautes.* Nat Chem Biol, 2007. **3**(1): p. 36-43.

91. Jackson, A.L. and P.S. Linsley, *Recognizing and avoiding siRNA off-target effects for target identification and therapeutic application.* Nat Rev Drug Discov, 2010. **9**(1): p. 57-67.

92. Jackson, A.L., et al., *Expression profiling reveals off-target gene regulation by RNAi.* Nat Biotechnol, 2003. **21**(6): p. 635-7.

93. Birmingham, A., et al., *3′ UTR seed matches, but not overall identity, are associated with RNAi off-targets.* Nature Methods, 2006. **3**(3): p. 199-204.

94. Robbins, M., A. Judge, and I. MacLachlan, *siRNA and innate immunity.* Oligonucleotides, 2009. **19**(2): p. 89-102.

95. Yi, R., et al., *Overexpression of exportin 5 enhances RNA interference mediated by short hairpin RNAs and microRNAs.* RNA, 2005. **11**(2): p. 220-6.

Table 1

Transporter	Km	Tissues
GLUT1 (SLC2A1)	Glucose (Km 3 mM)	Ubiquitous
GLUT2 (SLC2A2)	Glucose (Km 17 mM) Fructose (Km 76 mM)	Kidney, small intestine, liver, pancreas
GLUT3 (SLC2A3)	Glucose (Km 1.4 mM)	Brain, Testis
GLUT4 (SLC2A4)	Glucose (Km 5 mM)	Muscle, fat, liver, heart
GLUT6 (SLC2A6)	Glucose	Spleen, brain, leukocytes
GLUT8 (SLC2A8)	Glucose (Km 2 mM) Fructose	Testis, brain, adrenal gland, liver, spleen, fat, lung
GLUT10 (SLC2A10)	Glucose (Km 0.3 mM)	Heart, lung, brain, liver, muscle, pancreas, placenta, kidney
GLUT12 (SLC2A12)	Glucose	Muscle, heart, fat, small intestine, prostate, placenta
GLUT14 (SLC2A14)	Unknown	Testis

Adapted from Barron et al., 2016 [4]

Figure 1

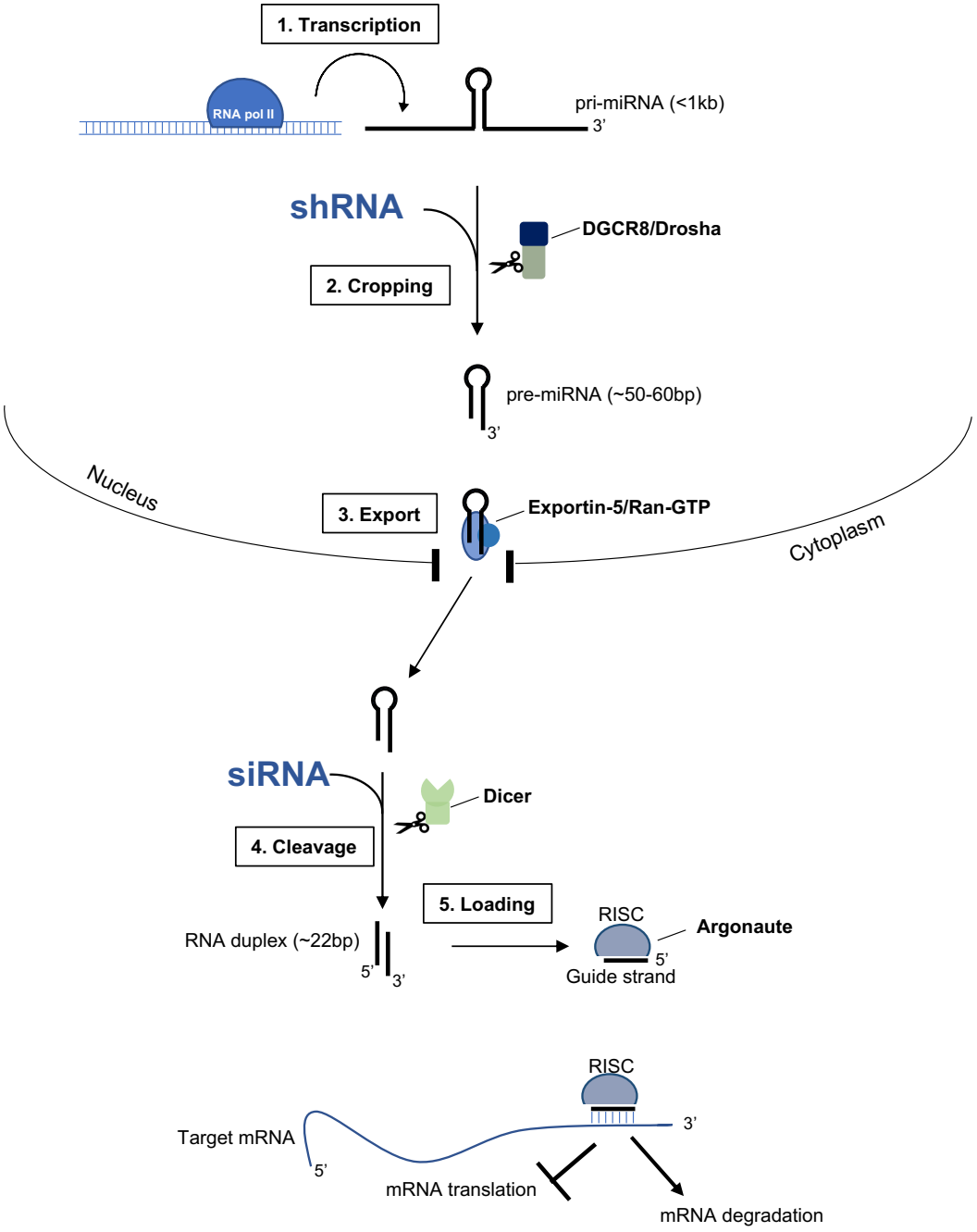
1. Transcription
RNA pol II
pri-miRNA (<1kb)
3'
shRNA
DGCR8/Drosha
2. Cropping
pre-miRNA (~50-60bp)
3'
Nucleus
3. Export
Exportin-5/Ran-GTP
Cytoplasm
siRNA
Dicer
4. Cleavage
5. Loading
RISC
Argonaute
RNA duplex (~22bp)
5'
3'
5'
Guide strand
RISC
Target mRNA
3'
5'
mRNA translation
mRNA degradation

Figure 1. Diagram depicting the RNAi biogenesis pathway and post-transcriptional gene silencing of target mRNA. 1. RNA pol II generates the primary miRNA (pri-miRNA) transcript containing the miRNA stem-loop. **2.** The endonuclease Drosha crops the stem-loop with the help of the RNA-binding protein DGCR8 thereby generating precursor miRNA (pre-miRNA). shRNA processing begins at step 2, utilizing the Drosha/DGCR8 complex and proceeds like pre-miRNA. **3.** The pre-miRNA is exported from the nucleus using Exportin-5. **4.** The cytoplasmic pre-miRNA is now trimmed by the endonuclease Dicer, removing the loop and leaving the RNA duplex containing complementary passenger and guide strands. siRNA biogenesis through the RNAi pathway begins at step 4. **5.** The guide strand of the RNA duplex then complexes with Argonaute and the passenger strands are unwound from the duplex and degraded. The guide strand and Argonaute complex form the RNA-Induced Silencing Complex (RISC). **6.** The guide strand will target the RISC complex to complementary sequences in the mRNA leading to translation inhibition or mRNA degradation.

Chapter II

Lrp5 serves a Wnt-independent role in glucose uptake and growth for mammary epithelial cells

This Chapter has been accepted for publication:

Emily N. Chin, Joshua A. Martin, Saja A. Fakhraldeen, Soyoung Kim and Caroline M. Alexander

Contributions: Figure 1 were performed by S. K. Figures 3, 6, and 8 were performed by E. C. Figures 2, 4 and 7 performed in collaboration with E. C. and J. M. Figure 5 performed by J. M.

ABSTRACT

Lrp5 is typically described as a Wnt signaling receptor, albeit a less effective Wnt signaling receptor than the better studied sister isoform, Lrp6. Here we show that Lrp5 is only a minor player in the response to Wnt3a-type ligands in mammary epithelial cells; instead Lrp5 is required for glucose uptake, and glucose uptake regulates the growth rate of mammary epithelial cells in culture. Thus, loss of Lrp5 leads to profound growth suppression, whether growth is induced by serum or by specific growth factors, and this inhibition is not due to loss of Wnt signaling. Depletion of Lrp5 decreases glucose uptake, lactate secretion and oxygen consumption rates; inhibition of glucose consumption phenocopies loss of Lrp5 function. Both Lrp5 knockdown and low external glucose induce mitochondrial stress, revealed as the accumulation of reactive oxygen species (ROS) and the activation of the ROS-sensitive checkpoint, p38α. In contrast, loss of function for Lrp6 reduces Wnt responsiveness but has little impact on growth. This highlights the distinct functions for these two Lrp receptors, and an important Wnt-ligand independent role of Lrp5 in glucose uptake in mammary epithelial cells.

INTRODUCTION

All somatic stem cells tested to date rely on Wnt signaling to maintain their pluripotentiality [1]. From the point of view of regenerative medicine, this requirement has some disadvantages, since Wnt signaling can also be highly oncogenic [2]. If the molecular regulation of Wnt signaling is better understood, it may be possible to tease apart the positive from the negative aspects of the pathway.

Our study focuses on the signals generated at the cell surface by the Low density lipoprotein receptor-Related Protein (LRP)-5 and LRP-6 Wnt signaling receptors. Cell surface presentation of Lrp species is considered to be the limiting factor for Wnt signal generation [3]. Mammary epithelial cells *in vitro* and *in vivo* grow and divide in response to ectopic Wnt signals. Thus over-expression of Wnt1 or Wnt10B in mouse mammary glands leads to ductal hyperplasia, inducing cell division for both luminal and basal cells that together comprise the mammary ducts [4]. Basal stem cells accumulate as a fraction of the total population [5], and solitary adenocarcinomas arise with a median latency of 7 months, comprising both mammary epithelial cell lineages [6]. Thus, as for intestinal cell populations [2], Wnt signaling is a robust growth signal for mammary epithelial cells, and acts as an oncogenic stimulus with relatively lower efficiency.

We have previously shown that Lrp5 is required to sustain the basal stem cell activity in mammary gland, and also for breast tumor development in response to Wnt1 [5, 7, 8]. This was a surprising result, since Lrp5 and Lrp6 are co-expressed by basal mammary epithelial cells, and Lrp6 is known to be a more effective transducer of Wnt ligand activation [9, 10]. Lrp5 and Lrp6 share 73% and 64% protein sequence identity in their extracellular and intracellular domains, respectively [11].

Almost all the information we know about the canonical Wnt cell surface signaling complex is based on the analysis of Lrp6, which forms a ternary complex with Frizzled (Fzd) receptors and a Wnt ligand (for experimental purposes, this is usually the soluble Wnt ligand, Wnt3A) [2].

There are clues that the primary function of Lrp5 might be different from Lrp6 *in vivo*. For example, reduced Lrp5 activity has been implicated in metabolic changes in mice and humans, though the molecular explanation for these changes has typically been associated with a canonical Wnt signaling function. For example, Lrp5 was cloned as a candidate gene from the IDDM4 locus, linked to genetic susceptibility to diabetes [12]. *Lrp5-/-* mice are leaner and show higher expression of key enzymes required for fatty acid β-oxidation [13]. So far, the only Lrp5 activity not linked to Wnt receptor activity is the binding of ApoE by Lrp5. This is a functional interaction, it's loss leading to hypercholesterolemia, impaired fat tolerance and atherosclerosis in *lrp5-/-* mice [14, 15]. More specifically, humans with syndromes associated with altered bone density have been shown to have mutations in Lrp5. Gain and loss-of-function Lrp5 alleles show alterations of osteoblast differentiation that correlate with altered glucose uptake [16-18]. Our study was designed to address the hypothesis that Lrp5 and Lrp6 have non-redundant activities in mammary epithelial cells, by knocking their expression down separately and testing their relative impact on Wnt signaling and other aspects of cell regulation. We discovered that Lrp5 controls growth of mammary epithelial cells, but not because of its role in Wnt signaling. We show instead that Lrp5 is important for normal glucose uptake, and that decreased glucose uptake accounts for the phenotype of cells absent Lrp5 function.

RESULTS

HC11 cells were derived from COMMA-D1 cells, the ancestor of most of the mouse mammary epithelial cell lines in use today [19, 20]. Originally described as a non-tumorigenic cell line, HC11 cells respond to pro-differentiation protocols with milk secretion and morphologic lumen formation. However, this cell line has drifted with passage to become tumorigenic. We re-derived a non-tumorigenic cell strain from an isolate of HC11 cells kindly provided by Nancy Hynes; thus using flow cytometry, we separated epithelial cells (expressing the epithelial cell adhesion molecule, EpCAM, and mammary epithelial cytokeratins, keratin-8 or keratin-5; K8, K5; Fig. 1A) from non-epithelial cells, which showed a typical epithelial-mesenchymal transition (loss of keratin expression (Fig. 1A), acquisition of vimentin expression and a transcriptional profile typical of EMT; data not shown). Vimentin-positive cells have been observed in COMMA1D cultures before and cloned out at limiting dilution [21]. We confirmed that both alleles of p53 were mutant (C138W, Δ123-130), as described by Nancy Hynes and colleagues [22]. Upon passage, the epithelial phenotype of these EpCAM-positive cells (EP cells) was stable (Fig. 1B,C). Furthermore, we assayed the tumorigenicity of EP and EpCAM-negative cells (EN cells) by transfer to mammary fat pads and found that this activity partitioned to the EN cell fraction. EP cells are therefore a non-tumorigenic epithelial mouse epithelial cell line with predominantly luminal characteristics, and a minor stable subpopulation expressing some basal epithelial cell markers.

Mammary epithelial cells (EP) are predictably responsive to a number of specific growth factor ligands (EGF, FGF and insulin; Fig. 2A), including recombinant Wnt3a. To determine the role of Lrp5 in Wnt-induced growth and Wnt-induced transactivation, Lrp5

and Lrp6 were each knocked down with shRNA lentiviral expression vectors (Fig. 2B), resulting in 60-80% knockdown of each at the protein level (Fig. 2C). Given that these proteins oligomerize [23, 24], we tested their relative stability in the absence of the other, and found no compensatory changes in Lrp6 amount in the absence of Lrp5, and vice versa.

Surprisingly, Lrp5 knockdown cells showed a dramatically decreased growth rate, at all serum levels screened. Cells were counted after 48 hours of growth in 0.5 – 10% FBS (Fig. 2D). Thus, for cells growing in 1% serum, the number of Lrp5KD cells was reduced by 60%.

To evaluate whether Lrp5 was important to growth induced by specific types of growth factors, EP cells were incubated with serum (2% FBS in basal media), rWnt3a, Egf, Fgf or insulin for 48 hours (Fig. 2E). Surprisingly, although Lrp5 KD cells responded to each growth factor, including rWnt3a, overall cell number was much reduced compared to controls. Using two independent shRNA sequences targeting Lrp5, we confirmed the dramatic growth suppression (Fig. 2G), which correlated with the degree of Lrp5 knockdown (Fig. 2F). Interestingly, although Wnt ligands induce growth of EP mammary epithelial cells, canonical Wnt signaling via Lrp6 does not appear to be the driver (Fig. 2E), since there is no effect on growth when Lrp6 is reduced.

Based on the generality of the growth suppression we observed in Lrp5 knockdown cells, it appeared unlikely that Lrp5 regulated growth by a specific, Wnt-dependent mechanism. However, we considered the possibility that endogenous Wnt signaling could be responsible for maintaining growth of these cells and for promoting growth and survival under all these different growth conditions. Indeed, our analysis of mRNAs

expressed by these cells shows significant expression of several Wnt signaling components [5], and at least one breast tumor cell line has been shown to be Wnt-dependent for growth and motility, relying on autocrine Wnt signaling [25]. To evaluate the effect of each Lrp species on basal and induced Wnt signaling, the relative activation of Lrp receptors (assayed using anti-phospho-serine 1490 Lrp antibody) was evaluated for control cells (plko), Lrp6KD and Lrp5KD, and was found to be low/undetectable in the absence of exogenous ligand addition (Fig. 3A). Lrp6KD cells showed a 50% reduction in Lrp activation 60 minutes after treatment with rWnt3a, whereas Lrp5 KD cells showed little change. We also tested the basal (Fig. 3B) and inducible (Fig. 3C) expression of a canonical Wnt reporter (TOPFLASH) in Lrp5KD and Lrp6KD cells, and found that although knockdown of Lrp5 species reduced Wnt signaling by over 50%, knockdown of the minority Lrp6 had a much higher impact. We conclude that despite the fact that Lrp5 comprises the majority of Lrp species in these cells (Fig. 3D)[26], Lrp5 is indeed a much less potent transducer of Wnt signals [9].

Autocrine signaling depends on the production of myrisotoylated Wnt ligands, and this process is sensitive to inhibitors of specific acylases [27-30]. Thus, LGK974 is a PORCN inhibitor that specifically inhibits Wnt ligand production. If autocrine Wnt ligands maintain growth of EP cells *in vitro*, growth will be inhibited by LGK974. To test the efficacy and specificity of LGK974 for inhibiting Wnt-dependent responses, we compared TOPFLASH reporter expression after transfection of Wnt3a or addition of recombinant Wnt3a protein (Fig. 3E). As anticipated, this inhibitor effectively reduced TOPFLASH expression by >90% in cells synthesizing their own Wnt ligands, whereas it had little effect on the response to recombinant Wnt3a. However, LGK974 had no effect on EP cell

growth (Fig. 3F), leading us to conclude that Wnt signaling does not drive growth of these cells (at any of the tested serum concentrations). In sum, the loss of growth observed in Lrp5-deficient cells does not appear to be mediated by canonical Wnt signaling complexes.

A recent study showed that Lrp5 affects glucose uptake in osteoblast cells [18]. Therefore, we evaluated glucose uptake by EP mammary epithelial cells, and found it was reduced by at least 30% by knockdown of Lrp5 (Fig. 4A). Insulin is known to increase glucose uptake by various cell-specific mechanisms; for EP cells, insulin increased glucose uptake by 20%. Lrp5 KD also reduced glucose uptake induced by insulin and Wnt3a. Indeed, the impact of Lrp5 KD on growth directly mirrored relative glucose uptake, whether basal, or induced by specific growth factors.

To determine whether glucose disposition was affected in Lrp5KD cells, we measured lactate efflux under basal and induced culture conditions (Fig. 4B). Lower glucose amounts taken up by Lrp5KD cells were reflected in lower lactate amounts secreted, suggesting there is no dramatic redirection of glycolysis in these cells. If there is less glucose imported and oxidized in mitochondria, oxygen consumption is predicted to decrease. Metabolic analysis of O2 consumption confirmed that cells are less metabolically active, consuming less oxygen (OCR), and also confirming the decreased extracellular acidification (ECAR) characteristic of secreted lactate (Fig. 4C). We confirmed the specificity of the shRNA knockdown by rescuing glucose uptake in Lrp5KD cells with expression of human Lrp5 protein (Fig. 4D, E). We found that over-expression of Lrp5 alone was not sufficient to increase glucose uptake for these cells, and conclude

that the amount of Lrp5 present in EP cells does not solely determine their rate of glucose uptake.

Although we showed that Wnt-induced transactivation is not likely to be implicated in this pathway, other studies have suggested that there are transcriptional targets of Wnt signaling that could affect glucose uptake rates, including IRS1 [31]. Therefore, to test whether a gain of function for canonical Wnt signaling is sufficient to increase glucose uptake, constitutively active βcatenin (CA-βcat) was expressed in EP cells, effectively inducing the TOPFLASH reporter (Fig. 4F). (Interestingly, Wnt-dependent transactivation was significantly suppressed in Lrp5KD cells.) However, the expression of CA-βcat did not increase glucose uptake by mammary epithelial cells, and did not rescue glucose uptake in Lrp5KD cells (Fig. 4G), ruling out a significant role for βcatenin/TCF-induced transcriptional responses.

The rate of glucose uptake by cells is determined by the number, activation status and type of hexose (GLUT) transporters expressed on the cell surface [32]. We incubated EP cells in media with various glucose concentrations, and showed that the growth rate of EP cells decreased below glucose concentrations of 176 mg/L (1 mM) (Fig. 4H). Thus, glucose availability limits growth of EP cells below this threshold concentration. (Note the glucose concentration of regular RPMI 1640 cell culture media is 2g/L or 11.1 mM). Lrp5 knockdown cells did not grow in response to increasing glucose in media (Fig. 4H).

To investigate whether Lrp5 could be regulating the transcription of GLUT mRNA species, we measured their expression in Lrp5 KD cells, alongside two glucose-restriction conditions, low (22 mg/L) glucose media and rapamycin treatment (Fig. 4I). In common with the breast cancer cell lines reported by Anderson and colleagues [33], we found that

mRNAs for GLUT1 and GLUT8 predominate in EP cells (Fig. 4I). All three glucose restriction conditions, rapamycin-treated, low media glucose and Lrp5 KD suppressed mRNA expression for GLUT1 (by approximately 25%), suggesting that this transcriptional response is a component of a compensatory reaction, rather than indicating a specific role of Lrp5-mediated transactivation. We also assayed mRNAs for proteins implicated as important for glucose uptake or metabolism in general by other studies, and found these were not affected by Lrp5 knockdown (HK1/2, LDHA/B, PKM1/M2, PDK1-3, IRS1-4; data not shown).

If low glucose uptake by Lrp5 KD cells is sufficient to explain why cells grow more slowly, we predict that the Lrp5 KD phenotype will be mimicked by reducing the glucose concentration in growth media. When EP cells strains were moved to low glucose media (22 mg/L or 0.12 mM, present in 2% serum), the growth of control cell strains was slowed to approximately the same degree as Lrp5KD cells (Fig. 4J). The addition of the non-metabolized glucose variant, 2-deoxyglucose (2DG) also mimicked the slow-growth phenotype of Lrp5KD cells (Fig. 4K). Together, these data lead us to conclude that these cells are highly dependent on Lrp5-regulated glucose uptake for their growth.

Typically, cancer cells consume more glucose than normal cells [34] (secreting partially oxidized glucose as lactate, as per the “Warburg” effect). We therefore tested whether the breast cancer cell line, MDA-MB-231, showed Lrp5-regulated glucose uptake (Fig. 5). We confirmed that these breast cancer cells showed profound growth inhibition in response to the selective GLUT1 inhibitor, WZB117 [35] (Fig. 5B). Reducing the level of Lrp5 mRNA by 70% with shRNA lentiviral expression constructs reduced cell number by 30%. Furthermore, MDA-MB-231 cells showed a 30% decrease in glucose uptake in

response to the specific GLUT1 inhibitor, WZB117 (Fig. 5C), and a similar decrease in glucose uptake for Lrp5 KD cells, but only when glutamine was omitted from culture media (Fig. 5D). MDA-MB-231 cells are highly glutamine-dependent [34], so Lrp5-regulated glucose uptake may only become growth limiting when glutamine is absent. Lrp5 is expressed by all the breast cancer and non-tumorigenic breast epithelial cells that we tested, and interestingly, there are significant differences in the number and size of bands identified on high resolution Western blots (Fig. 5E), implying regulation of Lrp5 by post-translational modification. (Note that we could not detect an alternatively spliced Lrp5 variant described as characteristic of breast cancer cell lines [36]; data not shown).

A well-characterized response to energetic stress is the activation of AMPK. Indeed, this molecule is considered to be one of the principal brakes on cell growth in conditions of limiting nutrients [37]. We measured ATP concentrations for these cell strains in basal culture conditions and found that Lrp5 KD cells were not statistically different from control cells (Fig. 6A). Not surprisingly then, activation of AMPK was not increased in Lrp5KD cells (Fig. 6B). The activation of other signaling pathways known to determine growth rate were also unchanged (LKB, ERK), including the JNK pathway, known to be a non-canonical Wnt signaling output. However, there was a significant increase in activation of the stress checkpoint protein, p38α/MAPK14, in Lrp5KD cells, but not Lrp6KD cells. Activation of p38α was also observed in control cells cultured in low glucose (Fig. 6C).

Mitochondrial stress, associated with dysregulation of the electron transport chain (ETC) is a source of reactive oxygen species (ROS), which in turn stimulates the activation of the stress checkpoint p38α [38, 39]. Indeed, inhibition of glucose uptake is

typically sufficient to stress the ETC and increase the steady state levels of ROS [39]; we confirmed that 2DG-treated EP cells showed increased ROS (Fig. 6D). Similarly, EP cells growing in low glucose, or Lrp5KD EP cells, also show 2-3x elevated ROS levels (Fig. 6E). Therefore, the loss of glucose uptake observed in Lrp5KD cells is sufficient to account for increased ROS levels, p38α activation and cell growth inhibition.

Given the importance of mTOR signaling as a regulator of cell growth and glucose uptake [40], we tested whether the mTORC1 inhibitor, rapamycin, would reduce glucose uptake in EP cells, and phenocopy other aspects of Lrp5KD cells. Rapamycin abrogated the activation of mTOR signaling targets that impact translation, including S6 kinase, S6 and (less so) 4E-BP1 (Fig. 7A). Inhibiting mTOR signaling effectively inhibited glucose uptake (Fig. 7B). To provide a comparison, cells were also treated with inhibitors of various aspects of metabolism, including the bi-guanide drug, phenformin (by analogy to metformin, likely target is mitochondrial GPDH;[41]), rotenone (classic Complex 1 inhibitor), and UO126 (ERK inhibitor). Interestingly, and in contrast to rapamycin, these inhibitors tended to promote glucose uptake (Fig. 7B). Rapamycin reduced growth (Fig. 7C), glucose uptake (Fig. 7D) and lactate efflux (Fig. 7E), to a similar degree as the knockdown of Lrp5. Rapamycin also replicated other aspects of the Lrp5KD phenotype, inducing ROS and p38α activation (Fig. 7F, G).

mTORC2 is frequently implicated as a key component in glucose sensing and uptake, as opposed to mTORC1, which detects and reacts to amino acids [42]. Since rapamycin inhibits both mTORC1 and mTORC2, depending on time-course of exposure, cell type and drug dose, we asked whether a specific ablation of mTORC2 function could phenocopy Lrp5 knockdown in mammary epithelial cells. RICTOR is an mTORC2-

specific subunit (as opposed to mTORC1) [43]; approximately 50% knockdown significantly inhibited the phosphorylation of (S473) Akt, a known target of mTORC2. Like Lrp5 knockdown, RICTOR knockdown inhibited glucose uptake and EP cell growth (Fig. 7H-K).

We tested whether other mTOR signaling outputs were inhibited in the absence of Lrp5, and found reduced activation of S6, S6kinase and 4EBP (Fig. 8A). S6 is a highly conserved mTOR target, which is also a metabolic regulator in yeast [44]. Interestingly, there was no impact of decreased Lrp5 on the activation of Akt (S473 or T308), or on other signaling hubs (such as ERK; Fig. 6B). Thus, Lrp5 knockdown cells show some phenotypes in common with loss of function for mTORC2 (reduced glucose uptake and growth), and others that are not shared, including reduced pS473-Akt. One phenotype of Lrp5 knockdown cells that may be a unique signature is that the total extractable amount of the translation-associated protein, S6, is much less (Fig. 8A and B), despite expression of S6 (and S6 kinase) mRNAs at wild type levels (Fig. 8C). Much decreased extractable S6 was also observed in primary mammary epithelial cells, isolated from *lrp5-/-* mammary glands (Fig. 8D). Studies of S6 function have focused on a non-phosphorylatable knock-in form ($rpS6^{P-/-}$); therefore, the predicted cause and effects of absent S6 are not well understood.

DISCUSSION

This study has revealed that Lrp5 is a minor player in the response to Wnt3a-type ligands; instead Lrp5 serves to regulate glucose uptake in mammary epithelial cells. This is key, since glucose uptake determines the rate of mammary epithelial cell growth *in vitro*. Decreased glucose uptake inhibits the growth of mammary epithelial cells in general, whether growth is induced by serum or by specific growth factors (including Fgf, Egf), or by Wnt ligands. In contrast, loss of function for Lrp6, the dominant Wnt responder, leads to a predictable loss of Wnt-reporter activity, but little change in growth rate. It has been shown before that Lrp5 is not optimized for stimulating βcatenin/TCF signaling [9]; the carboxy-terminal domain is not easily activated. Our results suggest that Lrp5 structure and function may be optimized to perform a different function.

Since Lrp5 and Lrp6 proteins heteromerize [23, 24, 26], there is great potential for a coordinated response to Wnt ligands that includes an Lrp6-dependent βcatenin/TCF transcriptional response, together with an Lrp5-dependent glucose metabolic response. Our previous studies have shown that canonical Wnt signaling, and therefore mammary stem cell activity, is constrained to cells expressing both Lrp5 and Lrp6 [26, 45, 46]. Thus, all normal mammary stem cells express both Lrp species, and presumably both Lrp-associated activities. The heteromerization of Lrp5 and Lrp6 may explain why Wnt signaling outputs often include metabolic endpoints. For example, Inoki et al [47] reported the indirect activation of mTOR signaling downstream of Wnt signaling breast tumor cell lines. The growth of these cells was inhibited by rapamycin, *in vitro* and *in vivo*. For our study, loss of function for Lrp6 induced a gain of function for some signaling and metabolic parameters, suggesting that Lrp6 has suppressor activity. Thus, ERK and mTOR

signaling increased (Fig. 4B, 6A), oxygen consumption and ATP amounts increased (Fig. 3C, 4A), lactate efflux declined (Fig. 3B), and cells became less stressed by low glucose conditions (Fig. 4E). Thus, these two receptors may have interactive functionality.

Recent studies have begun to implicate Lrp5 as a metabolic regulator, both systemically and locally. However, many of these studies have focused on Wnt ligand-regulated changes in metabolism, and canonical Wnt signaling outputs to explain their phenotypes. For example, in humans, rare mutations in LRP5 control bone and cardio-metabolic disorders, such that gain of function mutations lead to high bone mass and enhanced lower-body fat accumulation, whereas loss of function mutations give low bone mineral density and increased abdominal adiposity [48, 49]. Other investigators have shown that Lrp5 knockout mice show normal glucose levels, but impaired glucose tolerance, thus showing less insulin secretion in response to glucose administration [14]. Dissection of the molecular basis for Lrp5 activity in osteoblasts has shown that Lrp5 controls glucose uptake for the bone marrow stromal cell line ST2 during Wnt-induced osteoblastic differentiation [18]. This study showed that loss of Lrp5 function decreased Wnt-induced differentiation for these cells, but did not inhibit growth. In contrast, our study showed that the growth rate of mammary epithelial cells strictly depends upon Lrp5; indeed, cell viability is severely reduced when knockdown is more complete (J. Martin, C.M. Alexander, unpublished). For mammary epithelial cells, Lrp5 is present in great excess compared to Lrp6 (3-fold), and there is no simultaneous, Wnt-induced differentiation process; thus, it can be unambiguously demonstrated that Lrp5 plays a role in glucose uptake. Indeed, we showed that Lrp5-dependent regulation of glucose uptake in mammary epithelial cells occurs regardless of the presence of Wnt ligands.

Although Lrp5-deficient mammary epithelial cells show some decrease in Wnt transactivational responses (measured using the TOP FLASH reporter), the loss of glucose uptake was not related to canonical βcatenin/TCF signaling. This conclusion is supported by these results: 1) Gain of function for βcatenin/TCF signaling did not induce an increase of glucose uptake, 2) Loss of function for βcatenin/TCF signaling (Lrp6KD or LGK974 treatment) did not decrease glucose uptake. Esen and colleagues also concluded that Wnt-mediated enhancement of glucose uptake was independent of canonical βcatenin/TCF signaling (using a GSK inhibitor, shRNA for βcatenin and the tankyrase inhibitor, XAV939) [18]. They confirmed that βcatenin/TCF signaling induced transcription of IRS1, known to be important to insulin-induced glycogen synthesis in muscle cells [31], but showed that this was not important to glucose uptake in osteoblasts. It is increasingly clear that glucose uptake is a highly regulated process that can determine growth and differentiation. Thus, glucose uptake increases in response to intracellular signals and extracellular cues, and higher glucose supply feeds forward to determine signaling activation and establish homeostasis. Recently, a study of a panel of 46 breast cancer cell lines revealed their remarkable range of glucose uptake rates and glucose dependence [34]. Glucose uptake has been shown to regulate growth of human breast cancer lines, via GLUT1 [33], and malignancy of mouse breast cancer cell lines (via GLUT3 amplification) [50].

One of the intracellular pathways that controls glucose uptake is the mTOR pathway; thus, inhibition of mTORC1 with the specific inhibitor, rapamycin, inhibits glucose uptake in most cell types. We found that rapamycin-treated cells shared symptoms of mitochondrial stress with Lrp5-deficient cells, including higher ROS levels

and p38α activation. Lrp5-deficient cells show decreased activation of mTOR signaling, assayed by phosphorylation of the ribosomal associated proteins, S6 and S6 kinase. However, we could detect no differences in protein amount per cell (measured as protein per cell counted), typically used as an index of relative translation rates, nor did we observe a change in cell size (measured by flow cytometry), typically used as a measure of mTOR activation [51] (data not shown). Interestingly Lrp5-deficient cells show a profound deficiency of S6 protein in lysates analyzed by Western blotting, despite normal levels of S6 mRNA (Fig. 8C). This is an unusual, and possibly unique phenotype, not shared by rapamycin-treated or RICTOR knockdown (mTORC2 loss of function) cells. The function of the S6 protein still remains obscure, though it is poised at the interface of the 40S and 60S subunits of the mature ribosome, suggesting that it could modify translation depending upon signaling inputs [44, 52]. Mice with a non-activatable version of S6 ($rpS6^{P-/-}$) were reported to be viable and grossly normal, though they show subtle alterations in glucose homeostasis, including reduced pancreatic islet function but enhanced insulin sensitivity in peripheral tissues [53].

Glucose uptake is controlled by a series of GLUT transporter proteins, which facilitate glucose transport at the plasma membrane [54, 55]. These channel proteins show different mRNA expression patterns, and highly regulated cell surface presentation. Several studies have shown that the rate of GLUT-dependent glucose uptake can determine mammary epithelial cell growth and the invasive behavior of breast tumor cell lines [33, 50, 56]. Specifically, GLUT1 is the most abundant glucose transporter species in mammary epithelial cells, and knockdown of GLUT1 in mouse mammary tumor cell lines reduces glucose uptake, with a proportional loss of lactate secretion and a

corresponding decrease in growth rates, both in tissue culture and *in vivo* [33]. Our study shows that both glucose-limited and Lrp5 knockdown mammary epithelial cells show proportionally lower glucose consumption, lactate secretion, and oxygen consumption. All three glucose-inhibited conditions (rapamycin-treated, Lrp5 KD and low glucose media) show significantly decreased GLUT1 mRNA expression (approximately 25%), which we assume reflects a compensatory switch to alternate calorie acquisition strategies. Since loss of function for Lrp5 and GLUT1 generate broadly similar phenotypes, we suggest that these two proteins are likely to be functionally interactive.

We conclude that Lrp5 is required for glucose uptake, whether by mouse mammary epithelial cells or human breast cancer cells, and that in this role, it serves to limit and determine cellular growth rate in a Wnt-independent manner. We propose that since the amount of Lrp5 determines metabolism, this in turn determine how cells respond to growth factors. We suggest that since glucose uptake is typically important to breast tumor cells [33, 50], Lrp5-associated glucose processing may become highly significant during breast epithelial cell transformation.

MATERIALS AND METHODS

Flow cytometric purification of EP substrains from the HC11 parental strain, and assay of their tumorigenicity.

Trypsinized HC11 cells were stained according to Kim et al [6]; briefly, cells were incubated with FITC-conjugated CD49f (Cat.# 555735; clone number GoH3; 30 µl/ml) from BD Biosciences, and PE-conjugated EpCAM (Cat.# 118206; clone number G8.8; 0.5 µg/ml), and sorted using a FACS Vantage cell sorter equipped with DiVa software (Becton Dickson, Franklin Lakes, NJ).

To assess their relative tumorigenicity, 4 x 10^5 EPCAM-positive (EP) and EPCAM-negative (EN) cells were suspended in 2 µL media containing Matrigel (2-5 µg/ µL), and transferred to cleared mammary fat pads, as described previously [7, 57, 58]. Mice were assayed by palpation, and 16 weeks after transplantation, fat pads were dissected, processed, and stained with Carmine Red.

Cells purified by flow cytometry (cytosplats) were stained according to Badders et al 2009 [7] and Kim et al [6]; briefly, single cell suspensions were dried briefly onto microscope slides and fixed in ice-cold methanol and acetone for 4 and 2 minutes, respectively. Cell preparations were blocked in 10% non-immune goat serum, and stained using antibodies to K5 and K8 (rabbit and rat primary antibodies respectively) overnight, followed by a rinse and incubation in fluorescent –conjugated secondary antibodies (Alexa546 anti-rat and Alexa488 anti-rabbit antibodies). DAPI was used for nuclear DNA counterstaining and immunofluorescent stains were visualized on a confocal microscope (BioRad MRC1024).

Cell strains, plasmid constructs, transfection and transduction.

Mouse mammary epithelial EP cells, derived as above, and described further in the Results section, were maintained as for parental HC11 cells [26]. Thus, RPMI1640 culture media was supplemented with 10% FBS (Atlanta Biologicals), 5 μg/ml insulin (Sigma-Aldrich), and 10 ng/ml recombinant human EGF (R&D Systems). Expression plasmids are as follows: constitutively active human β-catenin (N-terminal truncation of 47 amino acids; CA-β-cat) was purchased from Addgene (cat# 19287); human Lrp5 was kindly gifted by Brian MacDonald (MacDonald et al., 2011); mouse Wnt3a was kindly gifted by Bart Williams (Van Andel Research Institute, Grand Rapids, MI); Wnt1 described by our previous studies [6, 26]. Cells were transfected with plasmids, or transduced with lentiviral particles expressing shRNAs for Lrp5 or Lrp6 as described by et al [26]. The control plko vector encoding a scrambled shRNA was purchased from Addgene (cat# 1864). The Rictor shRNA constructs were provided by the Broad Institute (kind gift of Dudley Lamming, Department of Medicine) and include the following shRNA sequences (also used by [18]: [CGGTTCATACAAGAGTTATTT] and [CGAGACTTTGTCTGTCTAATT]. Transduced cells were selected for and maintained by addition of 6 μg/ml puromycin to culture media. We designed additional shRNA sequences targeting Lrp5 mRNA for confirmation of our results; Lrp5 shRNA #2 shRNA sequences are [TCAGATACCAGGATCTTTCGG], shRNA#2; [TCATTGATCTCAGTGTTCACA], shRNA#3.

MDA-MB-468 (basal type), MDA-MB231 and Hs578t (both claudin-low), SKBr3 and MCF7 (both luminal) human breast cancer cell strains [34], and mouse breast tumor cell line 4T1 (highly malignant) were obtained from ATCC, and were maintained as per ATCC instructions. 4T07 cells were a kind gift of Brett Morris/Patti Keely (University of

Wisconsin) and were maintained according to Aslakson and Miller (1992)[59]. Lrp5 was knocked down in MDA-MB-231 cells maintained in DMEM supplemented with 5% FBS; briefly, cells were transduced with lentivirus containing pGipz shRNA for LRP5 (Clone ID V3LHS_347020) or pGipz non-silencing control (Clone ID RHS4346), purchased from Open Biosystems. as described by Esen et al [18]. Transduced cells were selected for and maintained in media containing 1.6 ug/mL puromycin.

Quantitative Real Time PCR analysis

RNA isolation, cDNA generation, and amplification by real time PCR was performed as described previously [7, 26].

Gene Name	Forward Primer 5'->3'	Reverse Primer 5'->3'
GLUT1 (slc2a1)	ggcatgtgcttccagtatgt	ccttggtctcagggactttgaag
GLUT2 (slc2a2)	actgggtctgcaattttgtca	gaatgtaaacagggtgaagaccag
GLUT4 (slc2a4)	ggtttccagtatgttgcggat	cctctggtttcaggcacttttag
GLUT6 (slc2a6)	ggctcctatctgtgctgattgc	ccttggcacaaactggacgta
GLUT8 (slc2a8)	ccttcgtgactggctttgctgt	tgggtaggcgatttccgagat
GLUT9 (slc2a9)	gccatcattgcctcgttctgca	tacggcgaagtttgagagccag
RICTOR	cagtgtgaggtcctttccatcc	gccatagatgcttgcgactgtg
HK1	gcctagaccacctgaatgtaac	ggaaggacacggtacactttg
HK2	cctcaagacaaggggaatcttc	cttcacattgatgctgtcgtca
IRS1	atgccaaacctcctgttgag	cttctgggccatagtagcattc
IRS2	ctgccagcacctatgcaa	ttttcaacatggcggcgat
IRS4	aatggactttgccagacgag	gcagatctggagtagacaaagatg
LDHA	tcgatcccatttccaccatg	tcttcctcaggagtcagtgtc

LDHB	ccgtgtctaccatggtgaa	tcatcgtccttcagcttctga
PDK1	ttacggattgcccatatcacg	gattctgtcgacagagccttaatg
PDK2	tcatctatctgaaggccctgt	cgatacgtcgatgtgttcttgg
PDK3	agtgaaccaagggatgcatc	gctctctggttgacttgcag
PKM1	gcagcagcttggatagttctca	gaagatgccacggtacagatg
PKM2	attatcgtgctcaccaagtctg	gaagatgccacggtacagatg

Western blotting analysis of cell lysates

Primary mammary epithelial cells were isolated from chopped mammary glands as previously described, and directly lysed for protein analysis (Badders et al., 2009). For analysis of cultured cells, cells were either solubilized in standard lysis buffer (25 mM HEPES, pH 7.4, 300 mM NaCl, 1.5 mM MgCl2, 1 mM EGTA, 50 mM glycerophosphate, 0.5% Triton X-100) or in RIPA lysis buffer (20 mM Tris-HCl (pH 7.5), 150 mM NaCl, 1 mM Na2EDTA, 1 mM EGTA, 1% NP-40, 1% sodium deoxycholate, 2.5 mM sodium pyrophosphate, 1 mM glycerophosphate) with freshly added protease and phosphatase inhibitors (ThermoFisher Scientific). Western blotting of SDS-PAGE gels was performed as described previously, using the following primary antibodies from Cell Signaling Technology: anti-Lrp5 (cat# 5731), anti-Lrp6 (cat# 3395), anti-GAPDH (cat# 2118), anti-p-Lrp6 (cat# 2568), anti-p-AKT (T308) (cat# 2965), anti-p-AKT(S473) (cat# 4058), anti-AKT (cat# 4685), anti-p-p70 S6 kinase (T389) (cat# 9205), anti-p70 S6 kinase (cat# 2708), anti-p-4EBP1 (T37/46) (cat# 2855), anti-4EBP1 (cat#9452), anti-p-S6 Ribosomal Protein (S235/236) (cat# 2211), anti-S6 Ribosomal Protein (cat# 2217), anti-p-SAPK/JNK (T183/Y185) (cat# 4668), anti-SAPK/JNK (cat# 9252), anti-p-p38 (T180/Y182) (cat#

9215), anti-p38 (cat# 9212), anti-p-ERK1/2 (T202/Y204) (cat# 4377), anti-ERK1/2 (cat# 4695), anti-p-LKB1 (S428) (cat# 3482), anti-LKB1 (3047), anti-p-AMPKα (T172)(cat# 2535), and anti-AMPKα (cat# 2603). Anti-β-actin antibody was purchased from Sigma (cat# A5441) and anti-Vinculin antibody was purchased from Millipore (cat# 95-386).

Small molecule inhibitors and growth factors

EP cells were treated for 48 h with the following small molecule inhibitors at the indicated doses: 500 μM phenformin (Sigma, cat# P7045), 10 nM rotenone (Sigma, cat#R8875), 10 μM UO126 (Promega, cat# V1121), 10 nM LGK974 (Xcessbio, cat#M60106), rapamycin (concentrations as indicated; Calbiochem, cat# 553211), 2-Deoxy-D-Glucose (2-DG) (Sigma, cat# D8375). The following growth factors were used at the concentrations indicated for proliferation and glucose uptake assays: 50 ng/ml recombinant mouse Wnt3a (R&D systems, cat# 1324-WN-010-CF), 2 μg/ml insulin (Sigma, cat# I1882), 50 ng/ml recombinant EGF (R&D systems, cat# 236-EG-200), and 50 ng/ml recombinant FGF (R&D systems, cat# 233-FB-01M). Growth factors or inhibitors were added to a basal media comprising 2% FBS, PenStrep antibiotic and 6 μg/ml puromycin diluted in RPMI 1640 media.

Assay of cell number

For assessment of relative cell number, cells were plated at a density of 7 x 10^4 cells/ml in 24-well plates. The next day, cells were changed to test condition media, and 48 hours later, cells were rinsed with PBS, fixed with ice-cold methanol for 20 min, and stained with 1% crystal violet solution (Sigma, cat# CO775) for 30 min. Plates were washed 3x with deionized water and dried overnight before assay at OD595 (calculated using ImageJ software). This assay was compared with direct assay of cell number done

by trypsinization and counting (data not shown), to confirm that it could be applied as a surrogate for cell number. Relative differences in cell growth were quantified as percent differences in cell number, OD595 [test - control/control]; the control condition for each assay is indicated. For proliferation assays in response to glucose deprivation, cell strains were pre-incubated for 48 hours in culture media made with RPMI lacking glucose. The fetal bovine serum batch used for these experiments (Atlanta Biologicals) contained 110 mg/dL glucose, therefore the “low glucose” condition contained 22 mgs glucose per liter of media.

Dual luciferase assay

Canonical Wnt signaling activity was measured using the TOPFLASH reporter assay as described by Goel et al [26], with the following modification: 5 x 10^4 EP cells in a well of a 24 well plate were transduced with Super TOPFLASH reporter plasmid (0.25 µg), together with renilla luciferase (0.01 µg).

Glucose uptake and lactate efflux assays

Cells were seeded in 24-well plates at a density of 7.5 x 10^4 cells/ml in complete culture media. The next day, media was replaced with phenol-red free RPMI supplemented with 2% FBS and antibiotics. Next day, media containing test compounds was added, and cells were incubated for an additional 24 h. Media was harvested from cells, and cells were washed, fixed, and stained with crystal violet; glucose and lactate concentrations were determined using colorimetric kits from Eton Biosciences (cat#120003100A and cat# 1200011002, respectively) according to manufacturer’s instructions. Percent difference in glucose or lactate uptake/efflux for Lrp5 KD or Lrp6 KD cells was calculated relative to control (plko) cells, and all values were normalized to the

crystal violet (CV/OD595) staining intensity. Briefly, media samples were removed before and after incubation with a known number of cells (measured by CV/OD595), glucose concentrations were assayed, and the glucose consumed/cell was calculated (Δglucose/CV).

ATP assay

Cells were plated in 6 cm^2 dishes at 7.5 x 10^4 cells/ml in triplicate and incubated in RPMI medium. Cells were trypsinized, counted, and 1 x 10^6 cells per replicate were assayed for ATP/cell, according to manufacturer's instructions (BioVision; cat# K354-100).

Analysis of oxygen consumption rate (OCR) and extracellular acidification rate (ECAR)

Cells were seeded at a density of 10,000 cells/well in RPMI media in a 96-well plate. A total of five replicate wells per cell strain were plated. Next day, cells were washed 3 times with test media consisting of un-buffered, phenol-red free RPMI (Sigma, cat# R1383), 2% FBS, 1 mM glutamine, and antibiotics. OCR and ECAR were measured using the Seahorse XFe96 Extracellular Flux Analyzer.

To normalize OCR and ECAR to cell number, a standard curve of cells (0-20,000) of each strain were plated into parallel tissue culture plates, and stained with crystal violet. OCR and ECAR values were calculated using Seahorse Wave Software.

Analysis of intracellular ROS levels

Cells were plated at 7.5 x 10^4 cells/ml in 10 cm dishes and incubated in RPMI media as described previously for glucose and lactate assays. Cells were trypsinized, resuspended in PBS and stained for 30 min with H2DCFDA in a tissue culture incubator (37^{o}C, 5% CO2) (Life Technologies cat# D-399). Cells were washed once with PBS and

resuspended in PBS + 2% FBS containing 50 nM TOPRO3 (Life Technologies, cat# T3605). For a positive control, cells were treated with hydrogen peroxide (200 μM) for 10 min prior to analysis by flow cytometry. Data was collected from 20,000 live cells (per replicate) using a BD Sciences LSR II flow cytometer, and median staining intensity was calculated using FlowJo software.

Statistical Analysis

All experiments were performed with at least three replicates, repeated three times. Statistical significance was determined by performing a two-tailed student's T-test and significance is reported as $p<0.05$.

Acknowledgements. Thanks to Dudley Lamming (Department of Medicine) for his kind gift of RICTOR shRNA expression vectors, and to Brett Morris and Patti Keely (Department of Cell and Regenerative Biology) for consultation on analysis of mouse breast tumor cell lines. Many thanks to those who provided critical review and interpretation for this manuscript, including Avtar Roopra, Dudley Lamming and Bart Williams. We are grateful also to our funding sources, T32 CA009135 (ENC and JAM); Era of Hope Scholar Award W81XWH 06-1-0491 (CMA and SYK); P30 CA014520 Cancer Center Core Support for University of Wisconsin (CMA).

Financial Support: T32 CA009135 (ENC); Era of Hope Scholar Award W81XWH-06-1-0491 (CMA); P30 CA014520 Cancer Center Support Grant for University of Wisconsin (CMA)

REFERENCES

1. Schuijers, J. and H. Clevers, *Adult mammalian stem cells: the role of Wnt, Lgr5 and R-spondins.* The EMBO journal, 2012. **31**(12): p. 2685-96.

2. Clevers, H. and R. Nusse, *Wnt/beta-catenin signaling and disease.* Cell, 2012. **149**(6): p. 1192-205.

3. Brennan, K., et al., *Truncated mutants of the putative Wnt receptor LRP6/Arrow can stabilize beta-catenin independently of Frizzled proteins.* Oncogene, 2004. **23**(28): p. 4873-84.

4. Mastroianni, M., et al., *Wnt signaling can substitute for estrogen to induce division of ERalpha-positive cells in a mouse mammary tumor model.* Cancer Lett, 2010. **289**(1): p. 23-31.

5. Alexander, C.M., et al., *Wnt Signaling in Mammary Glands: Plastic Cell Fates and Combinatorial Signaling.* Cold Spring Harbor perspectives in biology, 2012.

6. Kim, S., S. Goel, and C.M. Alexander, *Differentiation Generates Paracrine Cell Pairs that Maintain Basaloid Mouse Mammary Tumors: Proof of Concept.* PLoS One, 2011. **6**(4).

7. Badders, N.M., et al., *The Wnt receptor, Lrp5, is expressed by mouse mammary stem cells and is required to maintain the basal lineage.* PLoS One, 2009. **4**(8): p. e6594.

8. Lindvall, C., et al., *The Wnt signaling receptor Lrp5 is required for mammary ductal stem cell activity and Wnt1-induced tumorigenesis.* J Biol Chem, 2006. **281**(46): p. 35081-7.

9. MacDonald, B.T., et al., *Dissecting molecular differences between Wnt coreceptors LRP5 and LRP6.* PLoS One, 2011. **6**(8): p. e23537.

10. MacDonald, B.T., K. Tamai, and X. He, *Wnt/beta-catenin signaling: components, mechanisms, and diseases.* Dev Cell, 2009. **17**(1): p. 9-26.

11. He, X., et al., *LDL receptor-related proteins 5 and 6 in Wnt/beta-catenin signaling: arrows point the way.* Development, 2004. **131**(8): p. 1663-77.

12. Hey, P.J., et al., *Cloning of a novel member of the low-density lipoprotein receptor family.* Gene, 1998. **216**(1): p. 103-11.

13. Frey, J.L., et al., *Wnt-Lrp5 signaling regulates fatty acid metabolism in the osteoblast.* Molecular and cellular biology, 2015. **35**(11): p. 1979-91.

14. Fujino, T., et al., *Low-density lipoprotein receptor-related protein 5 (LRP5) is essential for normal cholesterol metabolism and glucose-induced insulin secretion.*

Proceedings of the National Academy of Sciences of the United States of America, 2003. **100**(1): p. 229-34.

15. Magoori, K., et al., *Severe hypercholesterolemia, impaired fat tolerance, and advanced atherosclerosis in mice lacking both low density lipoprotein receptor-related protein 5 and apolipoprotein E.* The Journal of biological chemistry, 2003. **278**(13): p. 11331-6.

16. Monroe, D.G., et al., *Update on Wnt signaling in bone cell biology and bone disease.* Gene, 2012. **492**(1): p. 1-18.

17. Cui, Y., et al., *Lrp5 functions in bone to regulate bone mass.* Nature medicine, 2011. **17**(6): p. 684-91.

18. Esen, E., et al., *WNT-LRP5 signaling induces Warburg effect through mTORC2 activation during osteoblast differentiation.* Cell metabolism, 2013. **17**(5): p. 745-55.

19. Danielson, K.G., et al., *Epithelial mouse mammary cell line exhibiting normal morphogenesis in vivo and functional differentiation in vitro.* Proceedings of the National Academy of Sciences of the United States of America, 1984. **81**(12): p. 3756-60.

20. Ball, R.K., et al., *Prolactin regulation of beta-casein gene expression and of a cytosolic 120-kd protein in a cloned mouse mammary epithelial cell line.* The EMBO journal, 1988. **7**(7): p. 2089-95.

21. Campbell, S.M., et al., *A clonal derivative of mammary epithelial cell line COMMA-D retains stem cell characteristics of unique morphological and functional heterogeneity.* Experimental cell research, 1988. **177**(1): p. 109-21.

22. Merlo, G.R., et al., *Growth suppression of normal mammary epithelial cells by wild-type p53.* Oncogene, 1994. **9**(2): p. 443-53.

23. Cong, F., L. Schweizer, and H. Varmus, *Wnt signals across the plasma membrane to activate the beta-catenin pathway by forming oligomers containing its receptors, Frizzled and LRP.* Development, 2004. **131**(20): p. 5103-15.

24. Bilic, J., et al., *Wnt induces LRP6 signalosomes and promotes dishevelled-dependent LRP6 phosphorylation.* Science, 2007. **316**(5831): p. 1619-22.

25. Matsuda, Y., et al., *WNT signaling enhances breast cancer cell motility and blockade of the WNT pathway by sFRP1 suppresses MDA-MB-231 xenograft growth.* Breast cancer research : BCR, 2009. **11**(3): p. R32.

26. Goel, S., et al., *Both LRP5 and LRP6 receptors are required to respond to physiological Wnt ligands in mammary epithelial cells and fibroblasts.* The Journal of biological chemistry, 2012. **287**(20): p. 16454-66.

27. Lum, L. and H. Clevers, *Cell biology. The unusual case of Porcupine.* Science, 2012. **337**(6097): p. 922-3.

28. Liu, J., et al., *Targeting Wnt-driven cancer through the inhibition of Porcupine by LGK974.* Proceedings of the National Academy of Sciences of the United States of America, 2013. **110**(50): p. 20224-9.

29. Proffitt, K.D., et al., *Pharmacological inhibition of the Wnt acyltransferase PORCN prevents growth of WNT-driven mammary cancer.* Cancer research, 2013. **73**(2): p. 502-7.

30. Wang, X., et al., *The development of highly potent inhibitors for porcupine.* Journal of medicinal chemistry, 2013. **56**(6): p. 2700-4.

31. Yoon, J.C., et al., *Wnt signaling regulates mitochondrial physiology and insulin sensitivity.* Genes Dev, 2010. **24**(14): p. 1507-18.

32. Bogan, J.S., *Regulation of glucose transporter translocation in health and diabetes.* Annual review of biochemistry, 2012. **81**: p. 507-32.

33. Young, C.D., et al., *Modulation of glucose transporter 1 (GLUT1) expression levels alters mouse mammary tumor cell growth in vitro and in vivo.* PLoS One, 2011. **6**(8): p. e23205.

34. Timmerman, L.A., et al., *Glutamine sensitivity analysis identifies the xCT antiporter as a common triple-negative breast tumor therapeutic target.* Cancer Cell, 2013. **24**(4): p. 450-65.

35. Liu, Y., et al., *A small-molecule inhibitor of glucose transporter 1 downregulates glycolysis, induces cell-cycle arrest, and inhibits cancer cell growth in vitro and in vivo.* Molecular cancer therapeutics, 2012. **11**(8): p. 1672-82.

36. Bjorklund, P., et al., *The internally truncated LRP5 receptor presents a therapeutic target in breast cancer.* PLoS One, 2009. **4**(1): p. e4243.

37. Hardie, D.G., *Molecular Pathways: Is AMPK a Friend or a Foe in Cancer?* Clinical cancer research : an official journal of the American Association for Cancer Research, 2015.

38. Wagner, E.F. and A.R. Nebreda, *Signal integration by JNK and p38 MAPK pathways in cancer development.* Nature reviews. Cancer, 2009. **9**(8): p. 537-49.

39. Wallace, D.C., *Mitochondria and cancer.* Nature reviews. Cancer, 2012. **12**(10): p. 685-98.

40. Yecies, J.L. and B.D. Manning, *mTOR links oncogenic signaling to tumor cell metabolism.* Journal of molecular medicine, 2011. **89**(3): p. 221-8.

41. Madiraju, A.K., et al., *Metformin suppresses gluconeogenesis by inhibiting mitochondrial glycerophosphate dehydrogenase.* Nature, 2014. **510**(7506): p. 542-6.

42. Zoncu, R., A. Efeyan, and D.M. Sabatini, *mTOR: from growth signal integration to cancer, diabetes and ageing.* Nature reviews. Molecular cell biology, 2011. **12**(1): p. 21-35.

43. Oh, W.J. and E. Jacinto, *mTOR complex 2 signaling and functions.* Cell Cycle, 2011. **10**(14): p. 2305-16.

44. Ruvinsky, I. and O. Meyuhas, *Ribosomal protein S6 phosphorylation: from protein synthesis to cell size.* Trends in biochemical sciences, 2006. **31**(6): p. 342-8.

45. Gong, Y., et al., *Wnt isoform-specific interactions with coreceptor specify inhibition or potentiation of signaling by LRP6 antibodies.* PLoS One, 2010. **5**(9): p. e12682.

46. Ettenberg, S.A., et al., *Inhibition of tumorigenesis driven by different Wnt proteins requires blockade of distinct ligand-binding regions by LRP6 antibodies.* Proc Natl Acad Sci U S A, 2010. **107**(35): p. 15473-8.

47. Inoki, K., et al., *TSC2 integrates Wnt and energy signals via a coordinated phosphorylation by AMPK and GSK3 to regulate cell growth.* Cell, 2006. **126**(5): p. 955-68.

48. Loh, N.Y., et al., *LRP5 Regulates Human Body Fat Distribution by Modulating Adipose Progenitor Biology in a Dose- and Depot-Specific Fashion.* Cell metabolism, 2015. **21**(2): p. 262-72.

49. Krishnan, V., H.U. Bryant, and O.A. Macdougald, *Regulation of bone mass by Wnt signaling.* J Clin Invest, 2006. **116**(5): p. 1202-9.

50. Onodera, Y., J.M. Nam, and M.J. Bissell, *Increased sugar uptake promotes oncogenesis via EPAC/RAP1 and O-GlcNAc pathways.* The Journal of clinical investigation, 2014. **124**(1): p. 367-84.

51. Wu, L. and R. Derynck, *Essential role of TGF-beta signaling in glucose-induced cell hypertrophy.* Developmental cell, 2009. **17**(1): p. 35-48.

52. Magnuson, B., B. Ekim, and D.C. Fingar, *Regulation and function of ribosomal protein S6 kinase (S6K) within mTOR signalling networks.* The Biochemical journal, 2012. **441**(1): p. 1-21.

53. Ruvinsky, I., et al., *Ribosomal protein S6 phosphorylation is a determinant of cell size and glucose homeostasis.* Genes & development, 2005. **19**(18): p. 2199-211.

54. Zhao, F.Q., *Biology of glucose transport in the mammary gland.* Journal of mammary gland biology and neoplasia, 2014. **19**(1): p. 3-17.

55. Mueckler, M. and B. Thorens, *The SLC2 (GLUT) family of membrane transporters.* Molecular aspects of medicine, 2013. **34**(2-3): p. 121-38.

56. Wahdan-Alaswad, R., et al., *Glucose promotes breast cancer aggression and reduces metformin efficacy.* Cell Cycle, 2013. **12**(24): p. 3759-69.

57. Liu, B.Y., et al., *The transforming activity of Wnt effectors correlates with their ability to induce the accumulation of mammary progenitor cells.* Proc Natl Acad Sci U S A, 2004. **101**(12): p. 4158-63.

58. Kim, S., A. Roopra, and C.M. Alexander, *A phenotypic mouse model of basaloid breast tumors.* PLoS One, 2012. **7**(2): p. e30979.

59. Aslakson, C.J. and F.R. Miller, *Selective events in the metastatic process defined by analysis of the sequential dissemination of subpopulations of a mouse mammary tumor.* Cancer research, 1992. **52**(6): p. 1399-405.

Figure 1

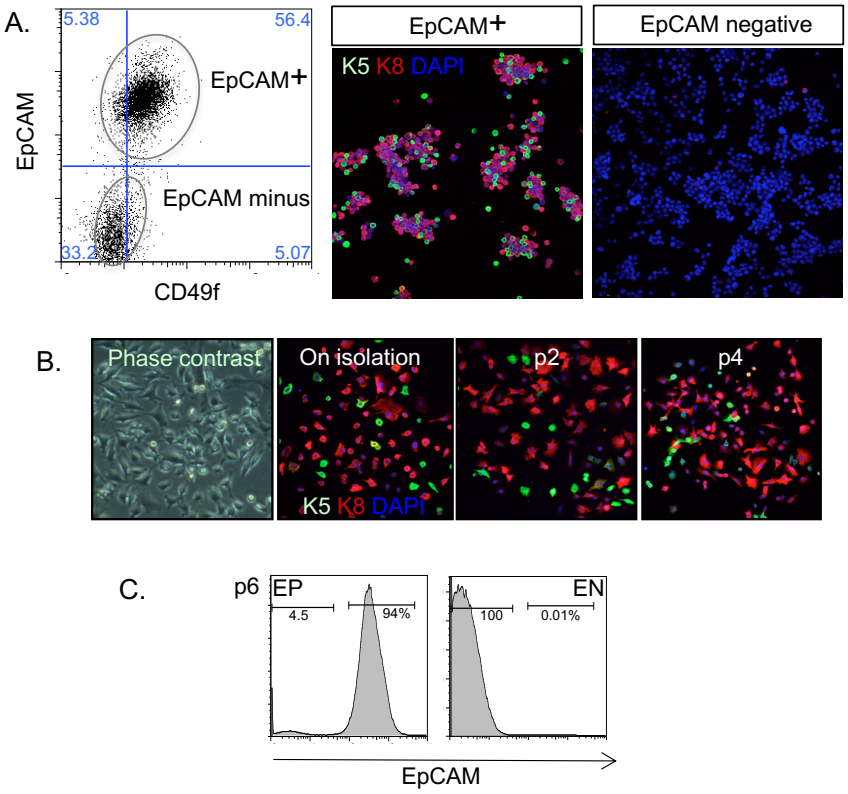

D.

Cell type	No. of cells	Tumors
EpCAM+	400,000 cells	0/6
EpCAM-	400,000 cells	6/6

Figure. 1. Re-derivation of EP mammary epithelial cells. A. HC11 cells were stained with antibodies to EpCAM and CD49f, and flow sorted into EpCAM-positive (**EP**) and EpCAM-negative (**EN**) fractions. Post sorting, cell aliquots were fixed and stained with epithelial markers, anti-keratin5 (K5) and keratin-8 (K8) antibodies (nuclei were counterstained with DAPI, blue). Lineage specification is indicated as either basal /myoepithelial (K5-positive, green) or luminal (K8-positive, red). Note EN cells are entirely negative for keratin expression. B. To test the stability of EP cell phenotype, cells were passaged, and samples at each passage were analyzed for their keratin expression (as for A). C. After 6 passages, cells were re-analyzed by flow cytometry, to show that EP cells maintained EpCAM expression, and EN cells were consistently EPCAM-negative. D. EP or EN cells (4×10^5) were inoculated into mammary fat pads and tumor formation was measured 12 weeks later.

Figure 2

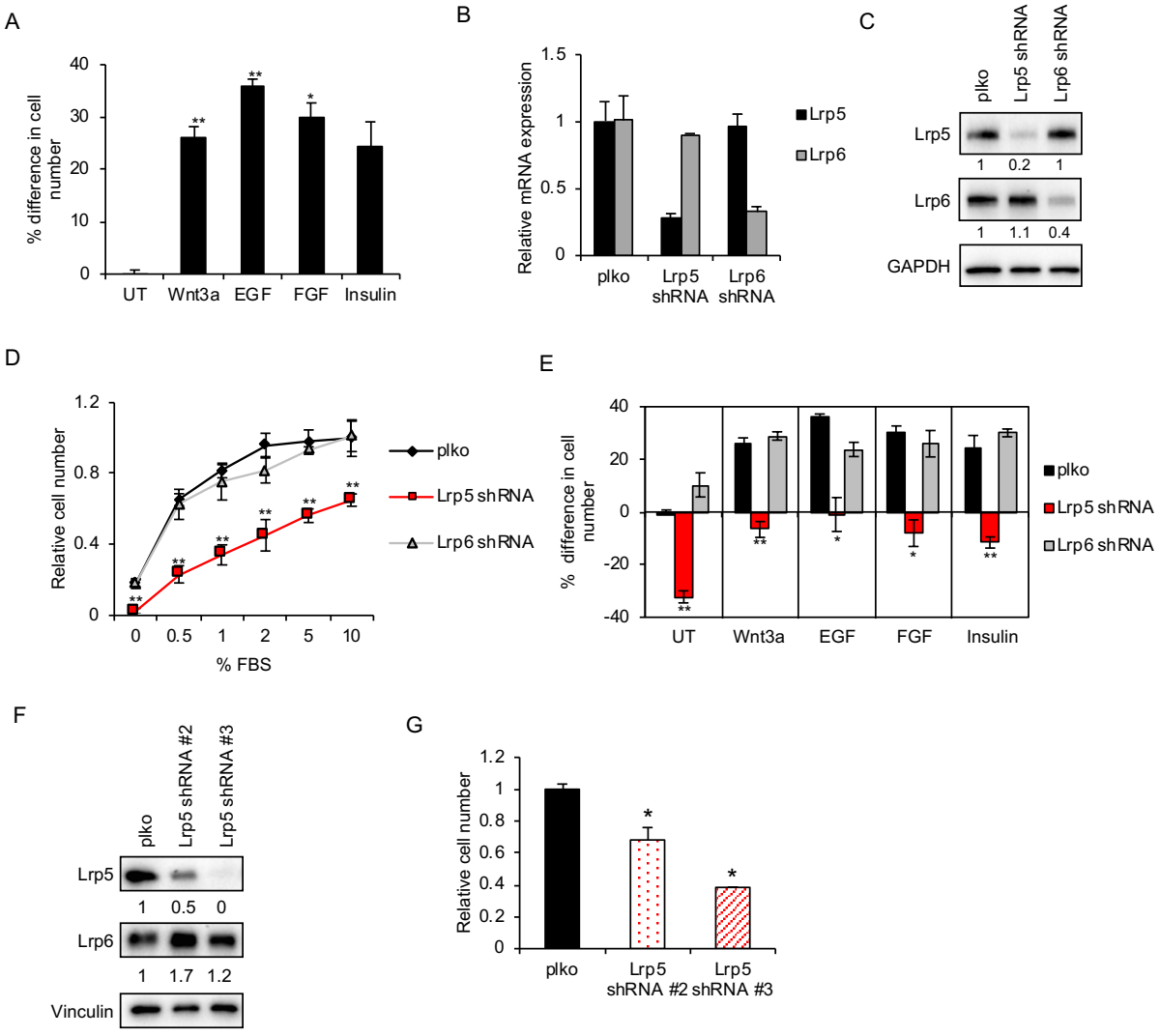
A
% difference in cell number
UT
Wnt3a
EGF
FGF
Insulin
B
Relative mRNA expression
Lrp5
Lrp6
plko
Lrp5 shRNA
Lrp6 shRNA
C
plko
Lrp5 shRNA
Lrp6 shRNA
Lrp5
Lrp6
GAPDH
D
Relative cell number
% FBS
plko
Lrp5 shRNA
Lrp6 shRNA
E
% difference in cell number
UT
Wnt3a
EGF
FGF
Insulin
plko
Lrp5 shRNA
Lrp6 shRNA
F
plko
Lrp5 shRNA #2
Lrp5 shRNA #3
Lrp5
Lrp6
Vinculin
G
Relative cell number
plko
Lrp5 shRNA #2
Lrp5 shRNA #3

Figure 2. Lrp5 regulates mammary epithelial cell growth. A. EP mammary epithelial cells were treated with Wnt3a, Egf, Fgf, insulin or no additions (basal media (UT) contains 2% fetal bovine serum) for 48 hours, and cell number was assayed using crystal violet staining (CV/OD595nm). (Results are reported as % difference in cell number relative to control, plko-transduced cells in basal media. B. EP mammary epithelial cells were stably transduced with lentiviruses encoding a scrambled shRNA (plko), Lrp5 shRNA, or Lrp6 shRNA, and puromycin-selected. Knockdown efficiency was assessed by RT-qPCR of Lrp5 and Lrp6 mRNAs (relative expression of each was normalized to expression in plko control line). C. EP cell strains were analyzed by Western blotting for Lrp5 and Lrp6 (loading control is GAPDH). D. Growth curves for EP cell strains in response to increasing serum concentration (0-10% FBS) were assayed 48 hours after plating (CV/OD595nm). Results are displayed as cell numbers relative to control (plko cells in 10% FBS). E. The growth of EP cell strains was determined after 48 h treatment with specific ligands: Wnt3a [50 ng/ml], Insulin [2 μg/ml], EGF [50 ng/ml], or FGF [50 ng/ml], and expressed with respect to plko cells in basal media (2% serum; untreated, UT). Percent difference in cell number was normalized to control (plko) cells cultured in basal media. F. Two more shRNA constructs (shRNA#2 and #3) for Lrp5 were tested for % knockdown, by Western blotting analysis. G. These Lrp5 KD cell strains were assayed for cell number relative to control (plko) cells, 48 hours after plating. Statistical significance is shown for Lrp5 KD versus control plko cells **$p<0.005$ *$p<0.05$.

Figure 3

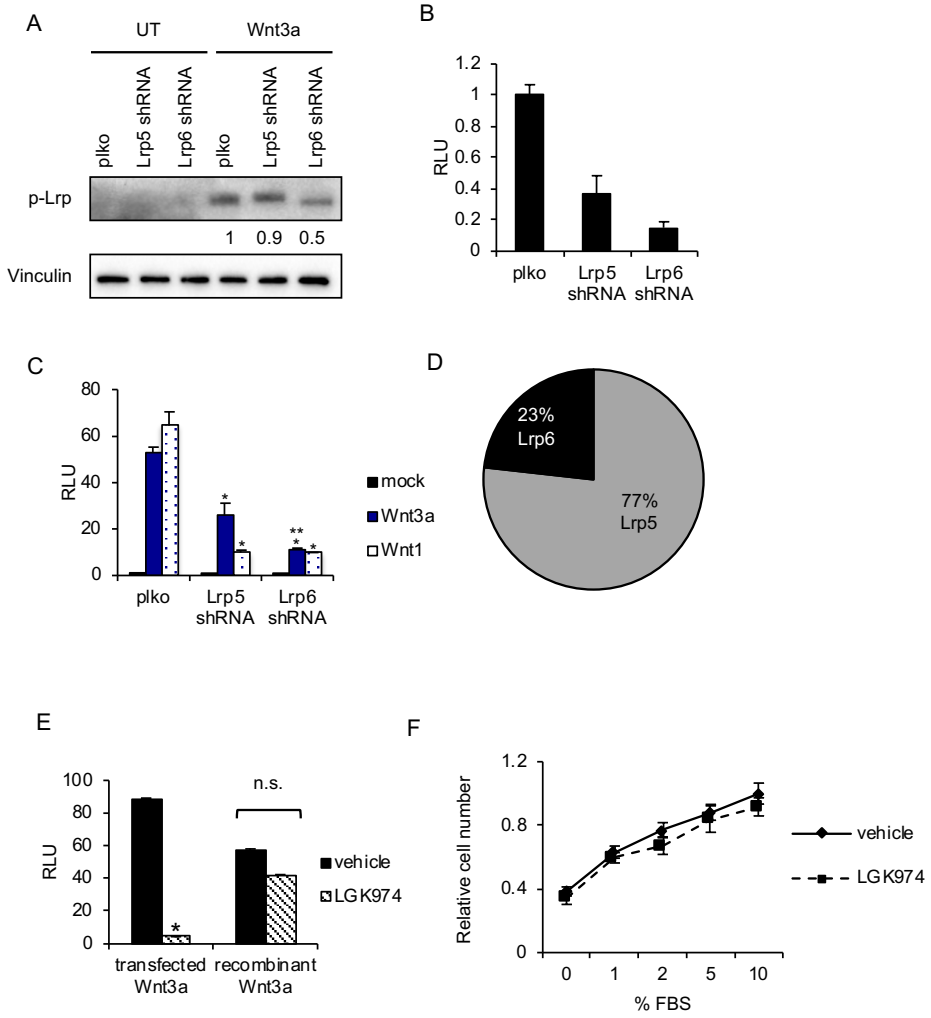
A
UT
Wnt3a
plko
Lrp5 shRNA
Lrp6 shRNA
plko
Lrp5 shRNA
Lrp6 shRNA
p-Lrp
1 0.9 0.5
Vinculin
B
RLU
1.2
1
0.8
0.6
0.4
0.2
0
plko
Lrp5 shRNA
Lrp6 shRNA
C
RLU
80
60
40
20
0
plko
Lrp5 shRNA
Lrp6 shRNA
mock
Wnt3a
Wnt1
D
23% Lrp6
77% Lrp5
E
RLU
100
80
60
40
20
0
n.s.
transfected Wnt3a
recombinant Wnt3a
vehicle
LGK974
F
Relative cell number
1.2
0.8
0.4
0
0
1
2
5
10
% FBS
vehicle
LGK974

Figure 3. Lrp5 does not signal through the canonical Wnt pathway to regulate cell growth. A. Relative activation of Lrp receptors in LrpKD strains was determined after treatment of cells with Wnt3a [50 ng/ml] for 1 hr, followed by Western blot analysis of phospho-Lrp levels. B. Basal levels of TCF/βcatenin transactivation were measured in un-stimulated EP cell strains by transfection of the Wnt βcatenin/TCF transactivation reporter, super TOPFLASH (and a *Renilla* normalization control), followed by assay of relative light units (RLU) 48 hours later (normalized to control (plko) cells). C. To examine Wnt-induced canonical TCF/βcatenin transactivation, EP cell strains were transfected with plasmids encoding Wnt3a, Wnt1, or GFP (mock), together with super TOPFLASH/renilla, and RLU were assayed 48 hours later (normalized to mock transfected control (plko) cells). Statistically significant differences between RLU assays of plko compared to Lrp5 or Lrp6KD cells are shown (*) and between Lrp5 and Lrp6KD cells (**), $p<0.05$. D. The relative amounts of Lrp5 and Lrp6 for EP cells was deduced by comparison of myc-tagged Lrp constructs [26]. E. To evaluate whether autocrine Wnt ligands are produced by EP cells, cells were transfected with superTOPFLASH/renilla, and either dual-transfected with a Wnt3a expression plasmid, or treated with recombinant Wnt3a [50 ng/ml], in the presence or absence of the PORCN inhibitor LGK974 [10 nM], followed by assay of RLU. n.s., not significant. F. EP cells were treated with LGK974 in the presence of various serum concentrations, and cell number assayed 48 hours later (CV/OD595). Control cells (plko cells in 10% serum) were set to 1.

Figure 4

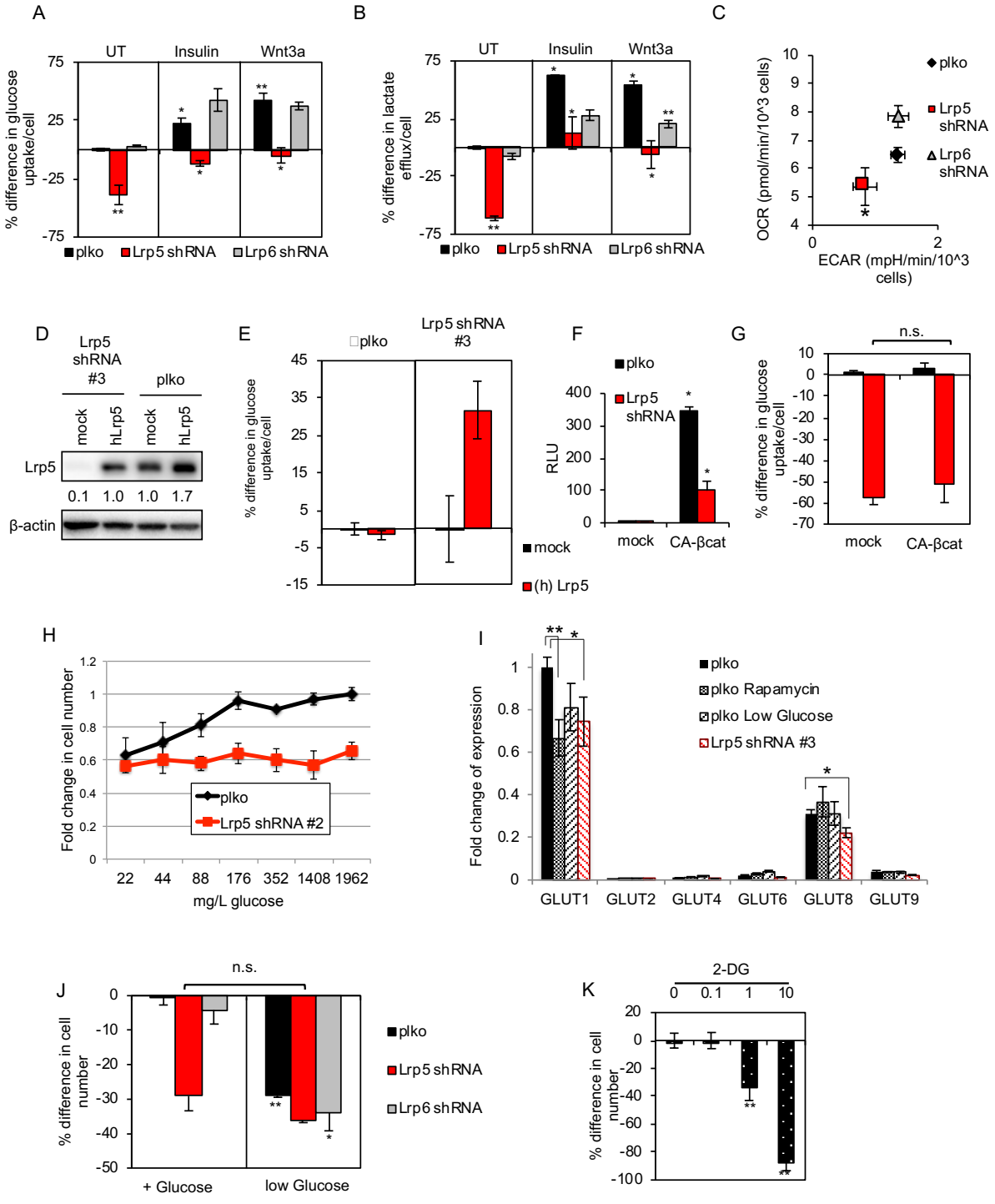
A
UT
Insulin
Wnt3a
% difference in glucose uptake/cell
plko
Lrp5 shRNA
Lrp6 shRNA
B
% difference in lactate efflux/cell
C
OCR (pmol/min/10^3 cells)
ECAR (mpH/min/10^3 cells)
plko
Lrp5 shRNA
Lrp6 shRNA
D
Lrp5 shRNA #3
plko
mock
hLrp5
Lrp5
β-actin
0.1 1.0 1.0 1.7
E
plko
Lrp5 shRNA #3
% difference in glucose uptake/cell
mock
(h) Lrp5
F
plko
Lrp5 shRNA
RLU
mock
CA-βcat
G
n.s.
% difference in glucose uptake/cell
mock
CA-βcat
H
Fold change in cell number
plko
Lrp5 shRNA #2
22 44 88 176 352 1408 1962
mg/L glucose
I
Fold change of expression
plko
plko Rapamycin
plko Low Glucose
Lrp5 shRNA #3
GLUT1 GLUT2 GLUT4 GLUT6 GLUT8 GLUT9
J
n.s.
% difference in cell number
plko
Lrp5 shRNA
Lrp6 shRNA
+ Glucose
low Glucose
K
2-DG
0 0.1 1 10
% difference in cell number

Figure 4. Lrp5 regulates glucose uptake in mammary epithelial cells. A. Glucose uptake was measured for EP cell strains over a 48 hour period. Results are expressed relative to control cells (plko) in basal conditions (UT). B. Lactate accumulation was measured for media collected in parallel. C. The oxygen consumption rate (OCR) and extracellular acidification rate (ECAR) for each EP cell strain was analyzed using the Seahorse Biosciences Flux Analyzer (normalized per cell). D. Human Lrp5 (hLRP5) was over-expressed in Lrp5KD cells (Lrp5 shRNA#3 knockdown) and control (plko) cells, and the amounts of Lrp5 analyzed by Western blotting. E. The effect of over-expressed hLrp5 on glucose uptake was assayed (24 hour period) for plko cells (left hand side) and as a rescue of Lrp expression in Lrp5 KD cells (shRNA#3; right hand side). F. To test the effect of gain of function of canonical TCF/βcatenin transactivation on glucose uptake, EP cells were transfected with a plasmid encoding constitutively active βcatenin (CA-βcat), together with super TOP-FLASH/*Renilla*. Cell lysates were analyzed 24 hours later and RLU was calculated relative to control (plko) cells transfected with a mock plasmid. G. These cells were analyzed for their glucose consumption (24 hour consumption). n.s., not significant. H. Glucose dose response curve for EP cells and EP/Lrp5 KD (shRNA#2) cells, grown for 72 hours in RPMI/2% FBS with the glucose concentrations indicated; cell numbers assayed by CV stains. I. Expression of mRNAs for various GLUT species (GLUT1, 2, 4, 6, 8, 9; GLUT3 not detected) were assayed by qPCR in EP cells transduced with Lrp5 shRNA (#2) or control lentiviral vector (plko), in either control conditions, or growing in low glucose (0.12 mM or 22 mg/L) or 10 nM rapamycin for 24 hours. All mRNA amounts are expressed with respect to GLUT1 expression by control EP cells. J. EP cell strains were grown in media with glucose (11.1 mM or 2 g/L), or in low glucose (glucose

concentration in 2% FBS, for this serum batch, 0.12 mM or 22 mg/L), and cell number was assayed 48 hours later (CV/OD595). Percent difference in cell number was calculated relative to control (plko) cells cultured in the presence of glucose. K. EP cells were grown in various concentrations of 2-deoxyglucose, an inhibitor of glucose uptake, and cell number was assayed and reported relative to cells treated with vehicle. Statistical significance is reported as follows, $^{**}p<0.005$ $^{*}p<0.05$.

Figure 5

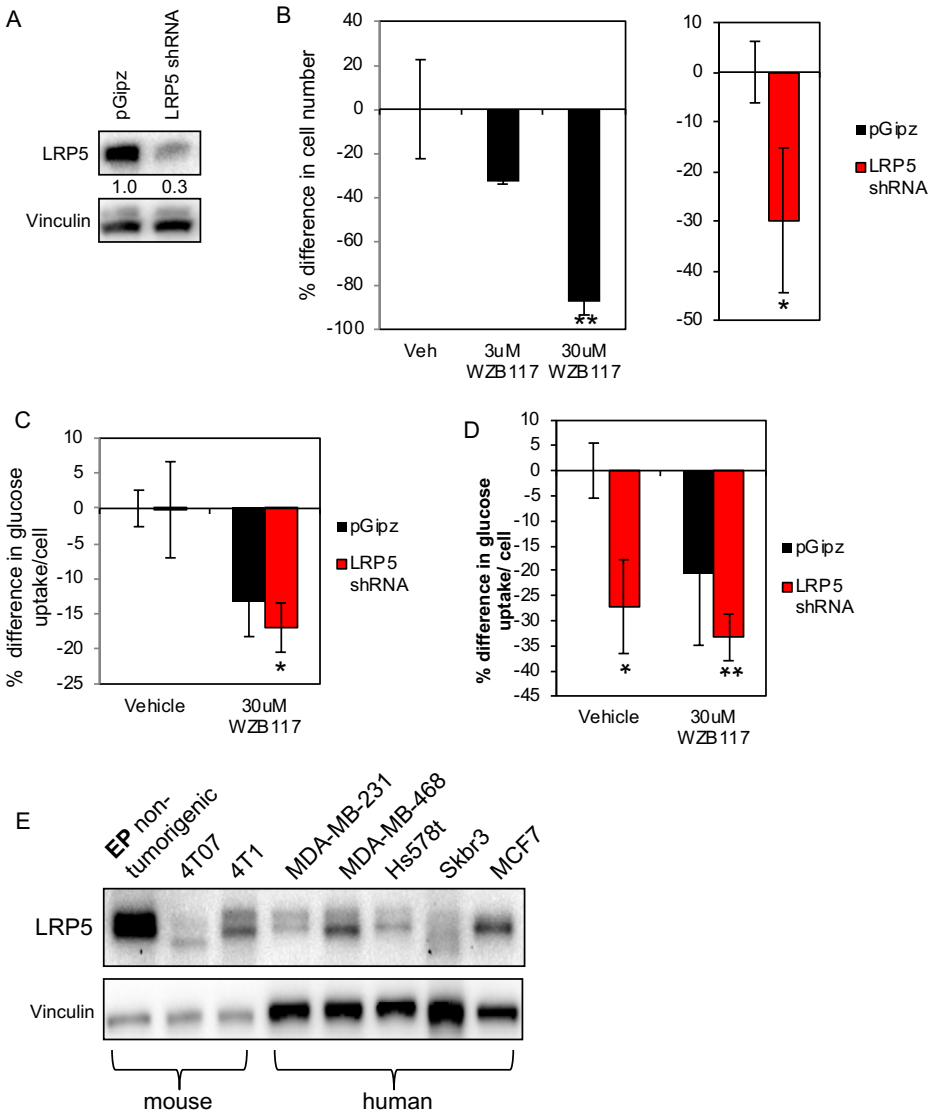
A
pGipz
LRP5 shRNA
LRP5
1.0
0.3
Vinculin
B
% difference in cell number
Veh
3uM WZB117
30uM WZB117
pGipz
LRP5 shRNA
C
% difference in glucose uptake/cell
Vehicle
30uM WZB117
D
% difference in glucose uptake/ cell
E
EP non-tumorigenic
4T07
4T1
MDA-MB-231
MDA-MB-468
Hs578t
Skbr3
MCF7
LRP5
Vinculin
mouse
human

Figure 5. Lrp5 controls glucose uptake and growth of MDA-MB-231 human breast cancer cells. A. MDA-MB-231 cells transduced with lentiviruses containing either pGipz non-silencing control or LRP5 shRNA were analyzed by Western blotting to assess efficiency of knockdown. B. MDA-MB-231 cells were plated at 3.0 x 10^4 cells/mL in 24-well plates and treated with the GLUT1 inhibitor WZB117; change in cell number was assessed 48hrs after administering the inhibitor. Growth of LRP5 knockdown and pGipZ control cells was likewise assessed after 48 hrs (in low glucose media/22 mg/L. C. Glucose uptake was assessed in vehicle (pGipZ-transduced) and Lrp5 knockdown MDA-MB-231 cells in full media (with 2 g/L glucose) plated 6.0 x 10^4 cells/mL. As a control, cells were treated with WZB117 for 24 hrs. D. In parallel, glucose uptake was assessed for MDA-MD-231 cells cultured in RPMI without glutamine for 24 hrs. E. LRP5 expression was analyzed in a panel of normal and breast cancer cell lines from mouse and human sources, by Western blot. **$p<0.005$ *$p<0.05$.

Figure 6

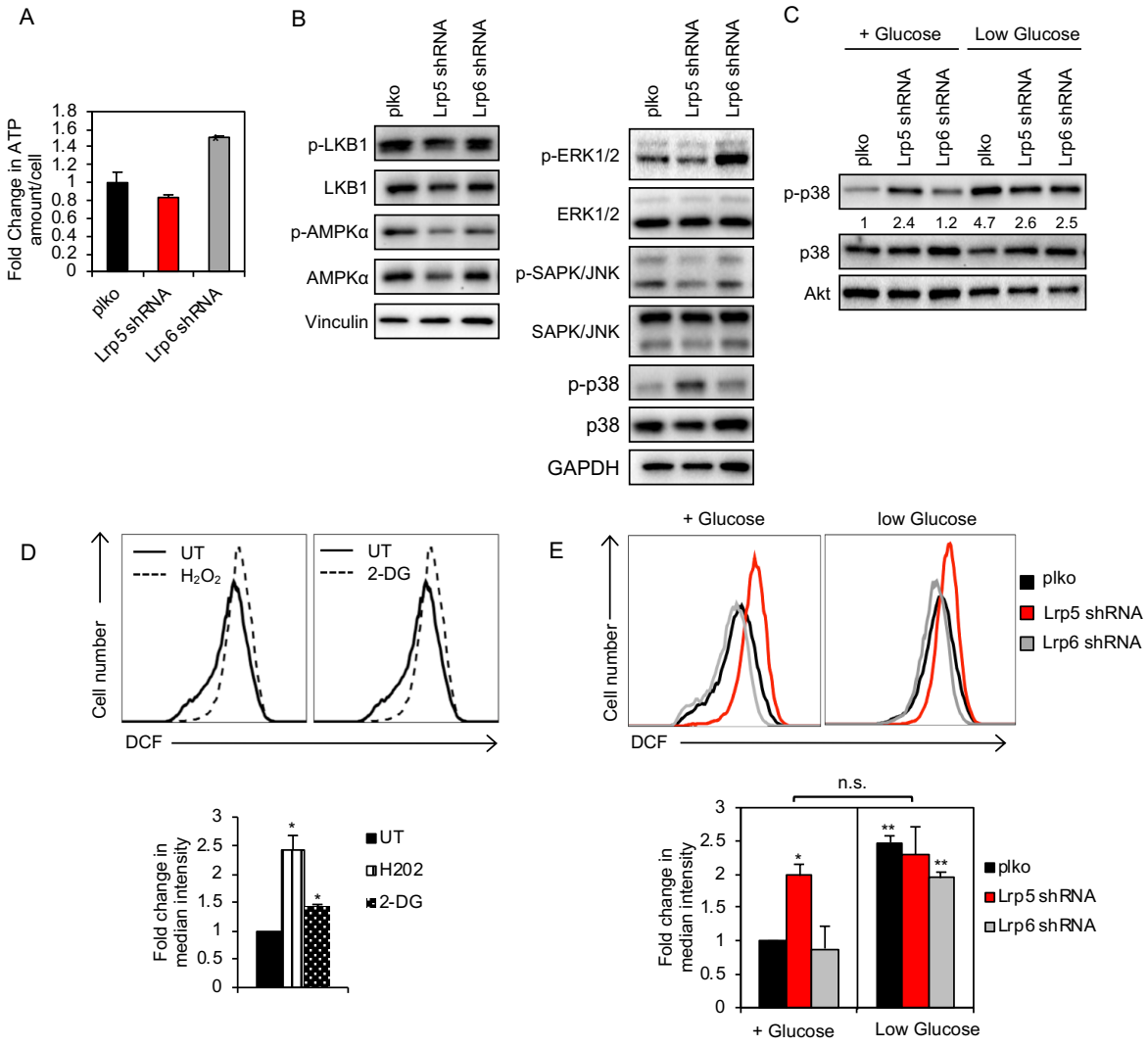
A
Fold Change in ATP amount/cell
1.8
1.6
1.4
1.2
1
0.8
0.6
0.4
0.2
0
plko
Lrp5 shRNA
Lrp6 shRNA
B
plko
Lrp5 shRNA
Lrp6 shRNA
p-LKB1
LKB1
p-AMPKα
AMPKα
Vinculin
p-ERK1/2
ERK1/2
p-SAPK/JNK
SAPK/JNK
p-p38
p38
GAPDH
C
+ Glucose
Low Glucose
plko
Lrp5 shRNA
Lrp6 shRNA
p-p38
1
2.4
1.2
4.7
2.6
2.5
p38
Akt
D
UT
H2O2
2-DG
Cell number
DCF
Fold change in median intensity
UT
H202
2-DG
E
+ Glucose
low Glucose
plko
Lrp5 shRNA
Lrp6 shRNA
Cell number
DCF
n.s.
Fold change in median intensity
+ Glucose
Low Glucose
plko
Lrp5 shRNA
Lrp6 shRNA

Figure 6. Lower glucose uptake by EP cells increases ROS levels and p38α activation. A. ATP levels were measured for EP cell strains and normalized to cell number. Fold change in ATP amount/cell was normalized to control (plko) cells cultured in basal media. B. Lysates of EP cell strains were analyzed by Western blotting for activation of several metabolic sensors and regulators, together with controls (vinculin and GAPDH). C. EP cell strains were incubated with or without glucose (48 h), and cell lysates were analyzed by Western blotting for relative activation of p38α. D. EP cells were treated with 2-DG [1 mM] (right panel), or with H_2O_2 [0.2 mM] as a positive control (left panel), and ROS levels were measured by staining cells with intracellular DCF dye followed by flow cytometry (quantified in panel below). Fold change in median intensity of DCF staining was normalized to control cells cultured in basal media. E. ROS levels for the EP cell strains were determined after 48 hours of culture in the presence or absence of glucose. Statistical comparisons are shown with respect to control, plko cells in glucose-containing media, **$p<0.005$ *$p<0.05$. n.s., not significant.

Figure 7

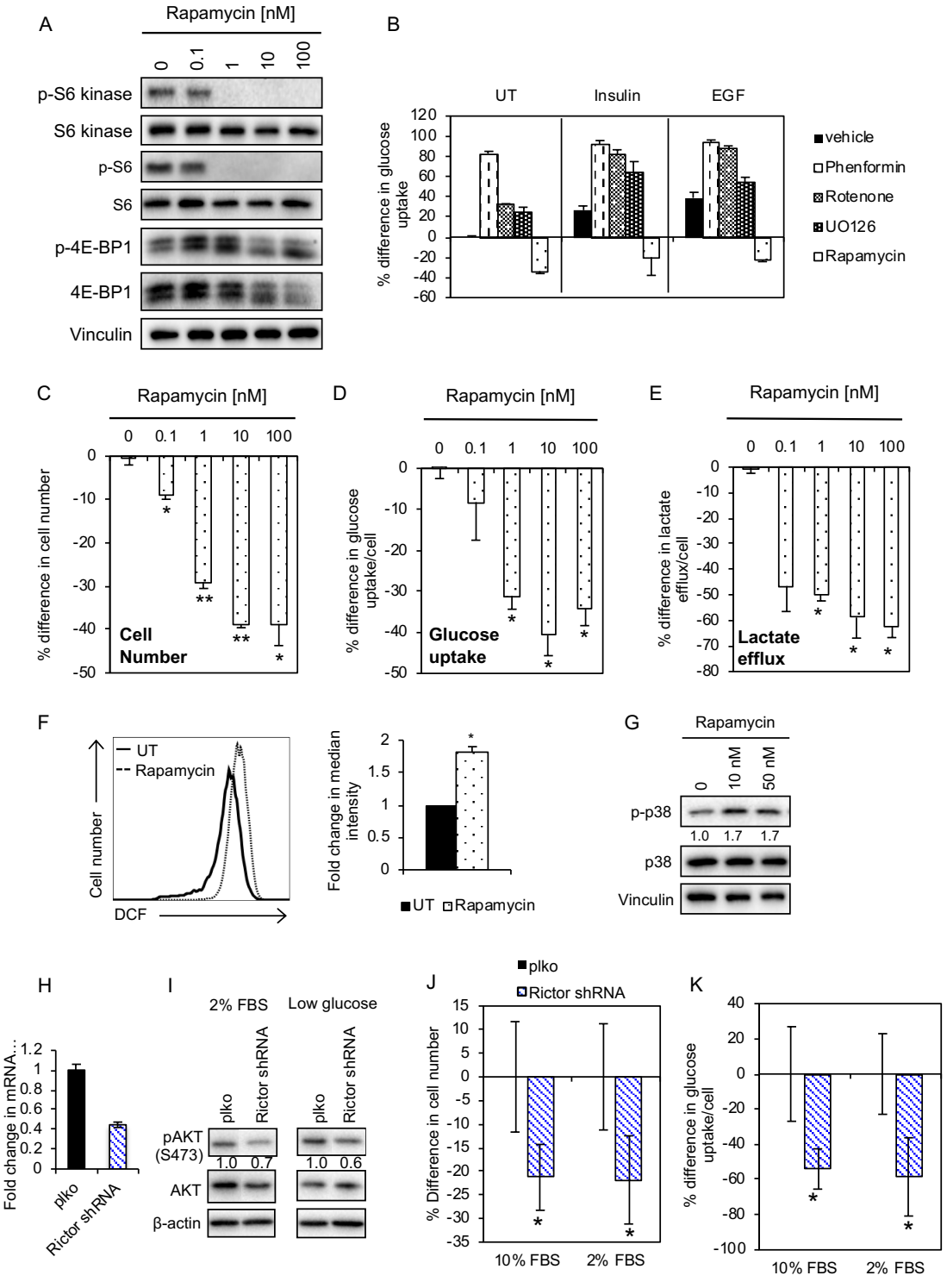
A
Rapamycin [nM]
0
0.1
1
10
100
p-S6 kinase
S6 kinase
p-S6
S6
p-4E-BP1
4E-BP1
Vinculin
B
UT
Insulin
EGF
% difference in glucose uptake
vehicle
Phenformin
Rotenone
UO126
Rapamycin
C
Rapamycin [nM]
% difference in cell number
Cell Number
D
Rapamycin [nM]
% difference in glucose uptake/cell
Glucose uptake
E
Rapamycin [nM]
% difference in lactate efflux/cell
Lactate efflux
F
UT
Rapamycin
Cell number
DCF
Fold change in median intensity
UT
Rapamycin
G
Rapamycin
0
10 nM
50 nM
p-p38
1.0 1.7 1.7
p38
Vinculin
H
Fold change in mRNA...
plko
Rictor shRNA
I
2% FBS
Low glucose
plko
Rictor shRNA
pAKT (S473)
1.0 0.7
1.0 0.6
AKT
β-actin
J
plko
Rictor shRNA
% Difference in cell number
10% FBS
2% FBS
K
% difference in glucose uptake/cell
10% FBS
2% FBS

Figure 7. Both rapamycin and RICTOR/mTORC2 knockdown phenocopy Lrp5 knockdown. A. EP cells were treated for 48 hours with rapamycin at the doses indicated, and lysates were analyzed by Western blotting for mTORC1 target proteins, S6, S6 kinase and 4E-BP1 (vinculin is a loading control). B. EP cells were treated with the metabolic inhibitors indicated, and glucose uptake was assayed after 48 hours. C-E. The effect of 48 hours of rapamycin treatment on cell number, glucose uptake and lactate efflux were assayed (as described for Fig. 4). F. ROS levels were assayed by DCF staining and flow cytometric analysis. All results were normalized to EP cells treated with vehicle. G. Relative activation of p38α was measured by Western blotting. H. EP cells were transduced with shRNA species for RICTOR, a component of the mTORC2 complex. I. Lysates of EP cells (control and shRNA RICTOR), cultured in 2% serum or low glucose (22 mg/L) for 24 hrs, were analyzed by Western blotting for their relative pAkt activation (S473; together with total Akt and a βactin loading control). J. RICTOR KD cells strains were growth in 2 or 10% serum (as indicated) for 48 hours, and cell number assayed. K. Glucose uptake was assessed for these cells, over 24 hrs in EP cells. **$p<0.005$ *$p<0.05$.

Figure 8

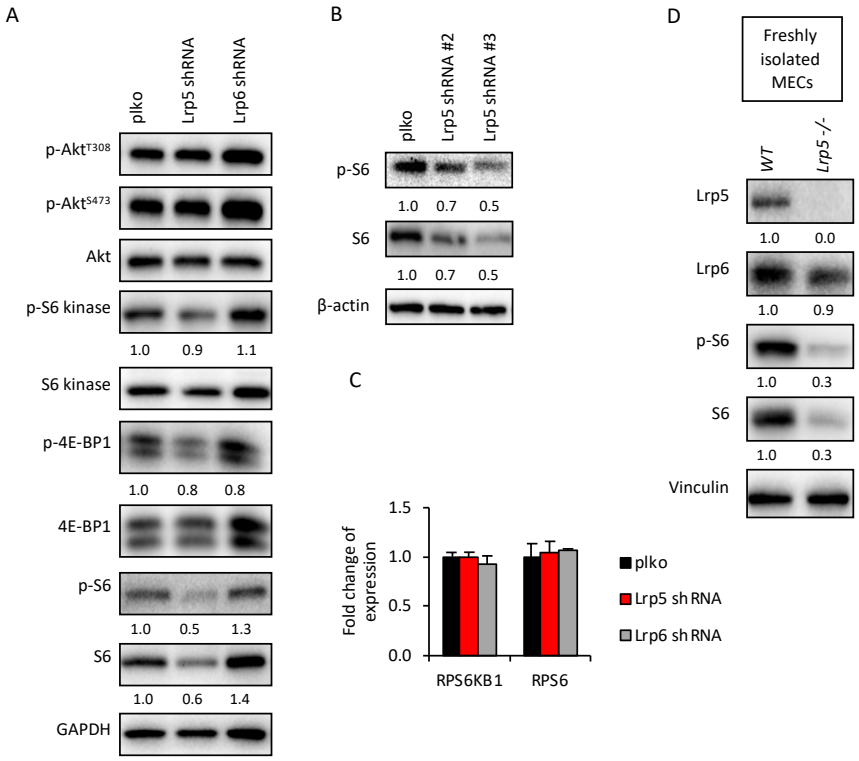

Figure 8. Lrp5 knockdown cells show a specific S6 signature. A. The relative activation of Akt, S6, S6 kinase and 4E-BP1 was analyzed by Western blotting of lysates of EP cell strains. B. Similar analysis of EP cell strains knocked down using shRNA#2 and #3. C. Assay of expression of S6 and S6 kinase mRNAs in Lrp5 KD EP cells, by qPCR. D. Assay of lysates of primary mammary epithelial cells isolated from *lrp5-/-* or control (C57Bl6) mammary glands, by Western blotting.

Chapter III

Alternative splicing and cleavage of GLUT8

This Chapter has been submitted for publication:

Joshua A. Martin, Katherine A. Senn, Ildiko Kasza, Heidi Dvinge

and Caroline M. Alexander

Contributions: Figures 1C , 2A, 4D, 4E, 4F, S1, S3, were performed by K. S. & H. D. Figures 7, 8, S4, S6, S7, S8 were performed by I. K. All remaining experiments were performed by J. M.

ABSTRACT

The GLUT (*SLC2*) family of membrane-associated transporters are described as glucose transporters. However, this family is divided into three classes, and although the regulated activity of Class I transporters is becoming better understood, Class III protein functions continue to be obscure. Genomic analysis of data from breast tumors and normal tissues shows that GLUT8 is one of only two Class III *SLC2* family members consistently expressed in breast epithelial cells, and that GLUT8, like several other *SLC2* loci, is produced as a set of alternatively spliced isomers that vary at the crucial regulatory N- and C-termini. A variant GLUT8 mRNA isomer predominates in tumor cells but does not encode a stable protein. As expected, loss of GLUT8 does not affect glucose uptake, and indeed the mRNA expression level of GLUT8 is 5-fold lower than the predominant glucose transporter at the cell surface, GLUT1. However, we show that the GLUT8 protein is cleaved at the carboxy-terminus to generate a membrane-associated peptide that becomes separated from the rest of the GLUT8 protein, enriched in a distinct vesicular population. Given its localization at a major metabolic hub (the late endosomal/lysosomal interface), and its regulated cleavage reaction, we speculate that GLUT8 may serve as a metabolic sensor.

INTRODUCTION

Transport of hexose sugars is performed by at least two families of integral membrane channels, where the GLUT (*SLC2*) family of transporters mediates bidirectional and energy-independent glucose transport. By sequence comparison, this family comprises 14 members, divided into 3 classes [1-3], with specific expression patterns and affinities for hexose sugars. Loss of function of the Class I GLUT proteins in mice and humans tends to have profound phenotypes [1]. Defying predictions, the GLUT4 knockout mouse was found to have remarkably normal glucose levels, turning attention of investigators to other *SLC2* family members with potentially overlapping or redundant functions [4].

Thus, structural homology comparisons have placed 5 proteins in Class III of the *SLC*2 proteins (GLUT-6, -8, -10, -12 and HMIT), and functional evaluation has shown that these proteins can indeed transport hexoses across a gradient [1, 5]. GLUT8 is the best-studied Class III member; indeed three independent groups cloned and characterized GLUT8, and showed that it was not essential for glucose uptake in cells or mice [6-8]. The phenotypes of GLUT8 knockout mice are subtle, including hypoactive sperm, hyperproliferation of hippocampal cells and resistance to hepatosteatosis in mice fed high fructose [9-13]. Subtle phenotypes are also typical *in vitro*; for example, unlike GLUT1, high throughput short term CRISPR screening modalities of cultured cancer cell lines do not identify GLUT8 as an essential gene [14, 15].

Furthermore, although full-length GLUT8 cDNA is stable upon ectopic expression in cells, neither the exogenous nor endogenous proteins are conclusively present on the cell surface [5]. Indeed, this protein has the classic di-leucine intracellular motif (in the N-

terminal cytoplasmic domain) that targets integral membrane proteins to the late endosomal/lysosomal vesicular compartment. Several groups have therefore speculated that GLUT8 might mediate transport of hexoses, or other metabolites, from compartment to cytosol [16-19].

In this manuscript, we show that there are issues that have confounded the investigation of GLUT8. For example, a number of alternatively spliced mRNA variants are made from the gene locus (as documented by the genome database and confirmed by our analysis). The most common in cultured cells (variant 3, v3) does not encode a viable protein. Several *SLC2* mRNAs show alternative splice forms that specifically affect the crucial regulatory N- and C-terminal cytoplasmic domains. We also show that the GLUT8 protein is cleaved, releasing a 10 kDa membrane-associated carboxy-terminal domain, which becomes enriched in a distinct and separate vesicular population, and speculate that this may provide a clue to GLUT8 function.

RESULTS

Patterns of expression for each GLUT species are revealed from *in silico* Northern data derived from the Genotype-Tissue Expression (GTEx) project (Fig. 1A): GLUT species are clustered according to their degree of shared expression. This analysis confirms and expands Northern blot data from tissue mRNA analysis published in other studies [1, 20]. GLUT1 and GLUT3 show high and widespread expression, lower in tissues that specialize in systemic glucose regulation, such as liver, muscle and pancreas, where other GLUT mRNA species predominate. GLUT2, -7 and -14 show the most restricted expression pattern; GLUT2 is expressed only in liver and small intestine. The rest are divided into two clusters, one comprising GLUT4, -10, -8 and -11 (expressed widely and at relatively high levels) and the other comprising GLUT5, -12, -6, -13 and -9 (showing lower and more specific expression patterns). In particular, GLUT5 is most abundant in testis and small intestine; GLUT12 in stomach, prostate and esophagus; GLUT6 in blood (and spleen); GLUT13 in cervix; GLUT9 in kidney and bladder, where it has been shown to be a high capacity urate transporter [21].

Assuming that multiple GLUT species could be involved in maintaining glucose uptake into cancer cells, we compared the relative expression of all 14 *SLC2* genes from three distinct classes (Fig. 1B) in breast tumors *in vivo* and breast cancer cell lines *in vitro*, using publicly available RNA Seq data [22, 23] (Fig. 1C). This shows that, of the class I transporters, GLUT1 mRNA is most abundantly expressed in both tumors and cell lines. In tumors, mean expression is 75±80 TPM, nearly 3-fold higher than normal near-adjacent tissue (26.2 ± 12.6 TPM); in cell lines in culture, average expression is even higher (127 ± 102 TPM). Indeed, the variability of GLUT1 expression is so high that the

cell lines in the top decile show 15-fold more expression than those in the lowest decile (379 versus 25 TPM).

Of the other class 1 transporters, GLUT3 mRNA is next most abundant (14.2 ± 13.2 TPM), showing less expression in tumor tissue than normal tissue (26.0 ± 23.7 TPM). Expression is however highly variable in cell lines (lowest and highest deciles are 0.05 to 181 TPM). Indeed, breast cancer cells massively over-expressing GLUT3 have been shown to depend upon this transporter for their metastatic behavior [24]. Of the class II GLUT transporters, only GLUT11 is significantly expressed in tumors (7.9 ± 4.6 TPM) and tumor cell lines (15.3 ± 8.9 TPM). Tumor expression reflects that of normal breast tissue (7.2 ± 1.7 TPM).

Of the class III GLUT transporters, GLUT8 and GLUT10 are expressed *in vivo* in breast tumors (16.2 ± 9.7 and 15.1 ± 23.1 TPM respectively), in normal tissues (12.2 ± 4.2 and 10.9 ± 4.2 TPM) and *in vitro* in breast tumor cell lines (9.3 ± 6.3 and 26.9 ± 37.4 TPM). GLUT10 shows the most highly variable expression in breast tumors and cell lines (0.3 to 113 TPM highest and lowest decile for the group of 79 cell lines). Although consistently over-expressed in tumors, none of the GLUT loci are located in the commonly amplified chromosomal domains of breast tumors (chromosomal locations are indicated in Table 1).

Breast tumors are grouped into sub-types according to their tumor driver and genetic profile. To delve deeper into potential correlations of GLUT isotype expression and breast tumor subtype, we evaluated GLUT mRNA expression for each of 5 tumor sub-types (basal, HER2, Luminal-A, Luminal-B, Normal-like), using normal adjacent tissue as a comparison (Fig. 2A). GLUT1 was always the most abundant mRNA species.

Of the remaining GLUT species, only GLUT10 and GLUT6 were consistently upregulated: >4-fold in basal tumors and significantly increased in HER2 over-expressing tumors (Fig. S1). GLUT4 is under-expressed in tumors compared to the near adjacent “normal” samples; these normal samples are enriched in GLUT4-expressing fatty tissue, highlighting the caution required to interpret these comparative data. We tested the relative expression of GLUT species by RT-qPCR assay of breast epithelial cells in culture (Fig. 2B) and found that the ratios of GLUT mRNAs were preserved from tumors *in vivo* to cell lines *in vitro* and from mouse to human.

GLUT1 is described as responsible for “basal” glucose uptake, though its activity is now known to be highly regulated, either by growth factor stimulation, or by starvation [25-27] Indeed, GLUT1 has been shown to be key to both the growth of mouse breast tumor cells and to HER2-induced mouse breast cancer initiation [28, 29], and GLUT1 deficiency syndromes produce predictable phenotypes [30]. Low expression of Class III GLUT mRNAs could imply that GLUT8 and -10 are insignificant contributors to glucose transport, however, examination of gene and protein sequences for GLUT8 and -10 suggest that there is considerable evolutionary pressure to maintain these species. Thus, the GLUT8 gene is arranged into 10 exons (Table 1, Fig. 3A), encoding 12 transmembrane domains, where the boundaries of each exon are embedded within sequences that encode the 20 amino acid, highly conserved trans-membrane domains (TM; Fig. 3B, C). For this purpose, the human GLUT8 sequence is compared with 3 other species, mouse, rat and cow. The GLUT8 protein is known to be glycosylated, as predicted from the sequence, and also contains several conserved residues, including a canonical di-leucine motif in the N-terminal domain that directs the trafficking of this

protein to late endosomes/lysosomes (Fig. 3B) [16, 20]. The hinge region between TM6 and TM7, the N-terminal cytoplasmic domain, and the extracellular loop (TM9-TM10) show relatively lower conservation, typical also of GLUT1 [31].

By interrogation of the UCSC and NCBI databases, we noticed that several GLUT loci exist as alternatively spliced isomers (Table 1). GLUT1, GLUT3, GLUT10 and GLUT12 species have only one full-length isomer in human and mouse, but in contrast, GLUT2, GLUT4, GLUT6 and GLUT8 exist as several alternatively spliced mRNA variants. Notably, splice variants are predicted to produce alterations in the N- and C-termini of the proteins, where these domains are known to be key regulatory and signaling domains for characterized species.

Using GLUT8 as an example of this phenomenon, we investigated the expression of the principal mRNA isomers of GLUT8, together with their translation in human tissues and tumors. Three species of mRNA are transcribed from the GLUT8 locus, v1 (full-length), v2, missing exon 9 and a section of the C-terminus, and v3, missing exons 2 and 3 (Fig. 4A). We determined that the v2 variant showed little or no expression in breast tumors or cell lines, and focused instead on v1 and v3 as the primary products of the *SLC2A8* locus. The relative amount of v1 and v3 mRNAs was determined by RT-PCR, firstly for MB231 breast cancer cells, using primers that cross exons 1-4 (Fig. 4B), and secondly using variant-specific primers for a panel of cell lines and normal human tissues (Fig. 4C). This latter assay is calibrated to report copy number of GLUT8 variants per ng RNA. Enriched sources of GLUT8 mRNA include testes and liver [8], confirmed here. For normal tissues, the v3 isomer comprises approximately 5-10% of total GLUT8 mRNA; this is also true for the untransformed breast epithelial cell line (MCF10A). For cancer

cell lines, this exon2-3 deleted v3 isomer is abundant, and can be predominant. Several studies have described a single, 2.1 kB GLUT8 mRNA on Northern blots of normal tissues [6-8, 32]; this matches our findings for normal tissues, where we find the full-length (v1) variant predominates.

To ask whether this truncated form is present also *in vivo* in breast tumors, we assayed junction-specific RNA-Seq products, and measured their relative frequency (Fig. 4D). Splice junctions that characterize v2 and v3 are shown in red. First, we noticed that the GLUT8 locus shows depleted read-through of exons2 and 3; compare the relative frequency pattern for GLUT8 exons with the more typical pattern shown by GLUT1 (Fig. 4E). *In vitro* assay of breast cancer cells using PCR-based DNA polymerases showed that this block could be relieved by solutions designed to read through high % GC content, and indeed, exons2 and 3 of GLUT8 show >80% GC content (Fig. S2), for both mouse and human sequences. Regardless of the depletion of sequences representing exons 1-4, assay of v3 shows that this isomer exists at a significant frequency in breast tumors *in vivo*.

To test whether this expression pattern was specific to breast tumors, we expanded the assay of GLUT8 exon expression to a panel of 33 tumor types (Fig. 4F). We conclude that amongst all tumor types, breast tumors show average expression of GLUT8, and depletion of 5' exons of mRNAs from *SLC2A8* in the RNA Seq libraries is typical. The pattern of exon representation in any given tumor was remarkably similar (Fig. S3). Interestingly however, one tumor type in particular, chromophobe renal cell carcinoma (KICH) shows much higher expression of GLUT8 than usual (4-fold); whereas

acute myelogenous leukemia (LAML) shows little/no expression. Chromophobe kidney tumors show unusual metabolic adaptations [33, 34].

To test whether alternatively spliced GLUT8 isomers could be functional, we subcloned cDNAs for each of v1, v2 and v3 into expression vectors. We also compared the expression pattern of two FLAG-tagged variants of v1 (one with the FLAG tag at the C-terminus and the other at the N-terminus). The putative trans-membrane proteins encoded are illustrated in Fig. 5A. To accurately describe the proteins made (and endogenously expressed proteins), we made a new polyclonal antibody to the TM6-7 cytoplasmic loop (called BBA1). We made this antibody because none of the commercial antisera we evaluated showed increased signal with ectopic expression, or reduced signal with knockdown (Table S1). More detailed evaluation of the specificity of BBA1 is provided as Fig. S4 (assay of immunofluorescent stains of cells with a knockdown of GLUT8 and cells with expression constructs), and in Western blotting data shown in Figs. 5 and 6.

We tested the three alternatively spliced mRNAs for their expression in HEK293T and MB231 cells; we found that v1 and v2 proteins are stably expressed, but v3 is not (Fig. 5B, S5). Adding a FLAG tag to either the C- or N-terminus had no effect on total GLUT8 production (Fig. 5C). We evaluated whether the proteins being expressed showed the activities expected. Cells over-expressing GLUT1 showed a large increase in glucose uptake activity; cells expressing GLUT8 did not (Fig. 5D), confirming prior studies. Vice versa, cells with a knockdown of GLUT1 showed reduced glucose uptake whereas GLUT8 knockdown cells showed no effect (Fig. 5E). Note that the proteins described here were expressed from retroviral expression vectors; surprisingly, they did

not show the same properties when synthesized from lentiviral expression vectors (data not shown).

When we evaluated the glycosylation pattern of GLUT8 proteins, we were surprised to find that PNGase treatment reduced the diffuse bands (from 45-60 kDa) to two bands, instead of the expected single band (Fig. 6A). This was not true for GLUT1 from these same lysates (data not shown). Using the termini-specific FLAG tagged constructs, we showed that a FLAG-tagged peptide was derived from the C-terminal domain, with approximate molecular weight of 10kDa (shown on the scheme drawn as Fig. 6B). We predict that this peptide would stay membrane-bound, since it contains at least two trans-membrane domains. Interestingly, the putative cleavage site is situated in transmembrane domain 10 (TM10) which is 100% conserved (Fig. 3C). We tested whether the C-terminal FLAG-tagged v3 construct was capable of producing a carboxy-terminal peptide and found no evidence of FLAG containing peptides either by immunofluorescence or Western blotting (Fig. S5 and data not shown). The exact insertion points of the FLAG tags are detailed in Fig. 6C.

Cleavage by regulated contact with membrane domain-specific proteases can be an important regulatory reaction, notably for metabolic sensors. Thus, for sensors such as SREBP (a sterol sensor), release from one organelle to another allows cleavage by two processive proteases, turning a membrane-bound protein into a transcriptional co-activator. Therefore, we evaluated the subcellular localization of GLUT8 in more detail, testing for a shift in the subcellular localization of the cleaved carboxy-domain. Previous studies of GLUT8 have shown that this protein accumulates in the late endosome/lysosome compartment, after cycling to the plasma membrane followed by

internalization and retention on the limiting membrane of the lysosome, via the di-leucine N-terminal signal. This was true both for the endogenous and for the exogenously expressed proteins [16, 18]. We evaluated the subcellular localization of the GLUT8 full-length v1 protein in MB231 cells and confirmed that both C-terminal tagged, and untagged proteins co-located with a late endosome/lysosome compartment (Fig. 7A, B). For comparison, cells over-expressing GLUT1 showed a classic plasma membrane-associated pattern, with no significant co-localization to lysosomes (Fig. 7C). Other co-localization assays excluded early endosomes, endoplasmic reticulum and peroxisomes as sites of significant accumulation (Fig. S6).

To test whether the cleaved peptide was located in the same place as the cleaved N-terminal domain, we compared the staining pattern of anti-GLUT8 (BBA1) with the staining pattern of anti-FLAG (Fig. 8). As a test of the optical integrity of the images, we stained the FLAG epitope with a mixture of red- and green-conjugated secondary antibody and showed there was no significant chromatic aberration at the magnifications presented (Fig. S7). Co-stain of the FLAG epitope together with the central loop epitope (BBA1) showed combinations of color signals, orange where both epitopes are together in the full-length GLUT8 protein, or separated into red (majority N-terminal GLUT8 protein, after cleavage of carboxyterminal peptide) or green (C-terminal peptide) (Fig. 8). Note that the total immunofluorescent signal is lower for the C-terminal FLAG tagged protein than the corresponding N-terminal tagged version, despite similar amounts assayed by Western blotting (Fig. S8); this suggests that the FLAG-tagged C-terminus may be complexed, and therefore masked for immunofluorescent assay. Thus, the GLUT8-derived C-terminal peptide, absent the N-terminal di-leucine retention motif, becomes

enriched in a separate vesicular population than both the cleaved N-terminus and the full-length GLUT8 proteins.

DISCUSSION

We have shown that the GLUT8 transmembrane protein is cleaved from the rest of the protein, to generate a carboxy-terminal membrane-associated peptide, that translocates to a different vesicular population. In this study, approximately 50% of GLUT8 protein is present in the cleaved form. This cleavage occurs whether the protein is FLAG-tagged or not, thus the tagging process itself does not disturb the natural processing reaction. It is likely that some of the C-terminal FLAG-tagged protein is present in a larger complex, since some signal is masked to immunohistochemical detection. Although GLUT8 proteins have been expressed in various cell types before [6, 9, 16, 18, 19], our study applied a unique combination of reagents to make this discovery. Thus, instead of the more typical N-terminal tagging, we built a GLUT8 species with a C-terminal tag and used a novel, and demonstrably specific, antibody to the central cytoplasmic loop, which became separated from the carboxy-terminal epitope during processing.

Given that GLUT8 is actively retained at the endosomal-lysosomal boundary by the N-terminal di-leucine motif, it is not surprising that the carboxy-domain accumulates in a different vesicular population [16]. The full-length and N-terminal cleaved protein may retain a hexose-binding activity, but cleaved protein is unlikely to show transporter activity (which depends upon 12 trans-membrane domains). Interestingly, out of all the trans-membrane domains, the only domain 100% conserved across species is trans-membrane domain 10, that we predict be the site of carboxy-terminal cleavage for GLUT8.

Given this processing pattern of GLUT8 protein, perhaps it is useful to consider other examples of membrane-tethered signaling molecules that are activated by

cleavage. Thus the sterol sensor SREBP is a membrane-located protein, sequestered in the ER, and released to the Golgi when local cholesterol concentration is low [35, 36]. In the Golgi, it comes into contact with two proteases, the first one (SIP) cleaves SREBP between two trans-membrane domains, inside the Golgi lumen; this becomes a substrate for the intramembrane protease, S2P, which clips off a soluble short carboxy-terminal peptide which, together with a series of co-activators, create nuclear transcription complexes that induce expression of enzymes in the cholesterol biosynthetic cascade. The effect of loss of function of this sensor only becomes apparent upon cholesterol deprivation.

Furthermore, whether endogenously or exogenously expressed [16, 18], GLUT8 is at a cellular hub of metabolic decision-making, the late-endosomal/lysosomal limiting membrane. For example, this lipid membrane senses amino acids that activate the Ragulator complex, recruiting the mTORC1 complex to the lysosomal membrane [37-40]. There are trafficking proteins such as the GTPase Rab7 the direct traffic within the endo-lysosomal system, to mediate endocytic sorting, lysosomal biogenesis and phagocytosis [41]. This hub location also modulates mitochondrial homeostasis [42, 43] and regulates the protein and lipid content of the plasma membrane and other vesicular populations [41, 44]. Perhaps related to this suggestion, DeBosch and colleagues showed that livers of male GLUT8 knockout mice directed aberrant PPARα-regulated fasting responses [45]. In summary, GLUT8 is present at a signaling hub, and is cleaved in a manner that evokes a metabolic sensor.

It is also useful to consider the fact that several molecules that share a sequence template with transporters have been adapted to become sensors instead, for example

there are channel proteins of yeast that bind to glucose but do not facilitate transport [46, 47]. Instead, glucose binding activates complex formation with signaling kinases to initiate glucose-dependent metabolic and behavior adaptations [48]. Another example is the mammalian sodium glucose co-transporter, SGLT3, which is present at the plasma membrane and binds glucose but does not transport it; this molecule initiates membrane de-polarization of neuronal cells in response to glucose [49]. There is precedent for adaptations of transporters to become proteins that use metabolites as signals.

Our investigation suggests that GLUT8 mRNA expression assays do not accurately reflect its presence at the protein level. Although GLUT8 shows low/mid-level co-expression across a broad range of tissues, including the breast tumors examined in this study, the GLUT8 locus, like 50% of the other *SLC2* loci, is expressed as several alternatively spliced isomers. In particular, tumor cells show a high frequency of expression of the v3 GLUT8 variant, which has two 5' exons missing, displacing the putative protein synthesis start site downstream to exon 6. As predicted from the translation motifs in the mRNA, and the unusual topography of the projected protein, this v3 protein is not synthesized. Therefore, despite expression of GLUT8 mRNA, we predict that most tumors will show low/absent function of this locus.

The chromophobe kidney tumor (KICH or ChRCC) shows notably higher expression of GLUT8 v1 than any other type. This tumor is characterized by the accumulation of defective mitochondria, induced expression of mitochondrial enzymes, disrupted autophagy/lysosomal trafficking, and systemically activated adenosine monophosphate-activated protein kinase (AMPK), a marker of metabolic stress [33, 34].

High GC content (potentially also associated with a secondary structure or knot) of exons 2 and 3 in GLUT8, together with the relatively low expression levels, make it difficult to quantify the relative expression of v1 and v3, and may confound other mRNA assays. The other variant described in the databases, v2, encodes a viable protein (albeit with the C-terminal facing outward), but v2 was not significantly expressed in breast tumors *in vivo* or breast cancer cell lines *in vitro*. Unlike v3, this variant is relatively simple to assay (using a signature exon 9 deletion) and should be considered for specific assay in other cell types. Another report of GLUT8 mRNA isomers described minor (<1% total) variants of GLUT8 mRNA, none the same as the variants described here and in the databases [50]; their significance *in vivo* is perhaps uncertain.

Only the two major Class I glucose transporters at the cell surface, GLUT1 and GLUT3, occur as just one isomer in both mouse and man. Likewise, of the Class III transporters, only GLUT10 and GLUT12 occur as one full-length isomer. GLUT2, -4 and -8 show several isomers that affect the N- and C-termini of their putative protein products. These termini face the cytoplasm and promote accurate trafficking and responsivity to regulators like growth factors [26, 51-53]. Precedent for significant functional differences for GLUT variants comes from the study of GLUT9, which is directed to the basolateral or apical surface of kidney epithelial cells by alternative splicing of N-termini [54, 55], and GLUT4 in adipocytes [56].

In summary, we have tested the properties of several alternatively spliced GLUT8 mRNA isomers described in tissues and tumors *in vivo* and have shown that at least two of these are translated into stable proteins. One isomer (v3) is common in tumors and is not translated. We have revealed that full-length GLUT8 shows a regulated cleavage

reaction, and that the C-terminal peptide becomes enriched in a separate vesicular population. We propose that this observation points to a potential function for this enigmatic protein channel as a metabolite sensor.

MATERIALS AND METHODS

Gene expression and splicing analysis

RNA-seq data from The Cancer Genome Atlas [22] was analyzed as previously described [57]. Briefly, unprocessed RNA-seq reads were mapped to the UCSC hg19 human genome assembly using Bowtie [58] and RSEM [59], with a maximum of two mismatches per read and ignoring reads mapping to 100 or more positions within the genome. Alignments with mapq scores of 0, or with a splice junction overhang of less than 6bp were removed. The resulting unaligned reads were mapped to a splice junction annotation derived from MISO v2.0 [60] and gene isoforms in the UCSC KnownGene track [61] and Ensembl database [62] using TopHat2 [PMID: 23618408]. The resulting RNA-seq read alignments were combined into a single BAM file per sample. Gene expression levels were quantified with RSEM as transcripts per million (TPM), and normalized using a trimmed mean of M values (TMM) scaling factor [63] derived from all protein-coding genes. The intrinsic breast cancer subtypes were derived from the PAM50 classifier [64] in the genefu R package, using the TMM-normalized expression of all fifty genes and the scaled centroids from pam50.robust. All samples with a subtype probability above 0.5 were included into the analysis. All exon-covering and junction-spanning reads within GLUT8 were extracted directly from the BAM files based on genomic coordinates of GLUT8 exons. Average exon coverage per nucleotide was calculated by adjusting for exon length. All BAM data extraction and manipulation was done using the GenomicRanges suite of tools in R [PMID: 23950696]. Differential gene expression between breast cancer subtypes and samples from the adjacent normal tissue (N=111) was calculated by edgeR [PMID: 19910308], after removing all genes with less than 20

reads in half or more of the normal samples. *P*-values were adjusted for multiple testing using the Benjamini-Hochberg approach.

Quantitative Real-Time PCR

Total RNA from human tissues were purchased from Takara Bio USA. RNA was isolated from tissue culture cells using the RNeasy mini kit according to instructions (Qiagen, Catalog #74104). cDNA was prepared using QuantiTect Reverse Transcription Kit (Qiagen, Catalog #205311) and RT-qPCR was performed as previously described [65] using Sybr Select Master Mix (Applied Biosystem, Catalog #4472918). Relative gene expression was determined using the comparative $\Delta\Delta$Ct method. To quantify the number of copies of GLUT8 transcript variants, we generated a standard curve using dilutions of linearized GLUT8 v1 or v3 plasmid. Primer sequences are provided in Supplemental Table 1.

Cell Culture and growth assay

All human cell lines were from ATCC (HEK293T/17, MDA-MB-231, MCF7, MCF10A, HepG2). HepG2 stocks were maintained according to ATCC recommendations; MDA-MB-231 (**MB231**) and MCF7 stocks were maintained in DMEM with 4.5g/L glucose (Gibco cat#11965), 5% fetal bovine serum (FBS; VWR cat#89510-194) and 1% penicillin/streptomycin (Gibco, cat#15140122). MCF-10A cells were maintained in DMEM/F12 (Gibco cat#10565042), 5% Horse serum, EGF 20 ng/mL (R&D system cat# 236-EG), Hydrocortisone 0.5 mg/ml (Sigma Aldrich cat# H0888), Cholera Toxin 100ng/mL (Sigma Aldrich cat# C8052), Insulin 10 μg/mL (Sigma Aldrich cat# I1882) and 1% penicillin/streptomycin (Gibco, cat#15140122). HEK293T/17 (**293T**) were maintained in DMEM with 1.0g/L glucose, sodium pyruvate and HEPES (Gibco

cat#12320032), 5% FBS and 1% PenStrep. The isolation of mouse mammary epithelial untransformed cells (MMEC) was described by Chin et al; untransformed cells were cloned from cell populations flow sorted as EpCAM-positive HC11 cells (EP cells)[65].

Cell number was assayed using FluoReporter Blue dsDNA quantitation kit according to instructions with the following modifications (Molecular Probes cat# F2962); plates were washed briefly in PBS and frozen at -80^{o}C. The plates were then thawed and 200 μl of water was added to each well followed by 1-hour incubation at room temperature. Cell lysis was completed by freezing the plates again at -80^{o}C. 100 μl of the cell lysate was transferred to black well 96-well plates, together with 100μl of Hoechst33258 diluted in TNE buffer, and plates assayed on a CLARIOStar fluorescent plate reader.

Knockdown of GLUT8 or GLUT1

Human GLUT8 shRNA clones TRCN0000300122 or TRCN0000300180 and human GLUT1 clones TRCN0000418550 or TRCN0000424768 were purchased from Sigma-Aldrich. A control non-targeting shRNA (*scramble*) was from Addgene (cat# 1864). Lentiviral shRNA constructs were packaged in 293T cells by transfection of psPAX2 (Addgene cat# 12260) and pMD2.G (Addgene cat# 12259) and shRNA plasmid using Lipofectamine LTX (Invitrogen, cat#15338100). Supernatants were harvested and filtered using 0.45 μm sterile filters. Cells were transduced by combining 0.5 mL of viral supernatant with 1.0x10^{5} cells and 10 ug/mL Polybrene (Sigma Aldrich cat #107689). The viral titer for scramble control construct was greater than the specific GLUT8 knockdown construct. After 48 hrs, infected cells were selected with 1.6 μg/mL puromycin (Sigma-Aldrich cat#P9620).

Assembly and transduction of GLUT8 expression vectors. 1. Generation of GLUT8 variant 1 expression construct. GLUT8 expression constructs were generated from GLUT8 clone 4641145 (Genbank#BC019043; Dharmacon, cat#MHS6278-202832055). The retroviral GLUT8 variant 1 expression construct (pQCXIP puromycin^R backbone) containing portions of the 5' and 3'UTRs was generated by PCR amplification (Forward Primer 5'- CTGCTGGGATCCGGCGGTTCAGGCG-3' and Reverse Primer 5'-CTGCTGGAATTCGGTTTGTTTTTTTTTGCTGTTTATT), then digested and subcloned between BamHI and EcoRI sites of pQCXIP. For this study, a GLUT8 v1 version that was non-degradable by GLUT8 sh180 was generated with synonymous mutations introduced into 3 sites by performing mutagenesis using the primer 5'-CTCCCTCATGCTGCTTCTGATGTGTTTTATGCCCGAGACCCC-3'. Mutagenesis PCR reaction products were treated with DpnI and then transformed in Stbl3 *E.coli*, followed by sequencing to confirm accuracy. All cloning was performed using Q5 polymerase (NEB, cat#M0491). All the GLUT8 constructs used in this study were generated from the initial non-degradable GLUT8.

Generation of GLUT8 variants 2 and 3 constructs

GLUT8 variant 2 and GLUT8 variant 3 were derived from the variant 1 construct by deletion mutagenesis: For variant 2, the deletion of exon 9 was generated using the variant 2 primer 5'-ATGTGCCTCTTCATCGCCGGAGGTCCTCAGGCC-3'. For variant 3 the deletion of exons 2 and 3 was generated using the variant 3 primer 5'CCTCCTGGCGGCAGGTCTACATCTCCGAAATCGCC-3'.

Generation of GLUT8 variant 1 and 3 FLAG tag constructs

To insert a FLAG tag into the N-terminus of GLUT8 variant 1, the plasmid was amplified using the primer 5'- GGCCGCCGACATGGATTATAAAGATGATGATGATAAA ACGCCCGAGGACC-3'. To insert a FLAG tag into the C-terminus of GLUT8 (variant 1 and 3) the respective plasmids were amplified using the primer 5'- CCCATTTTGAGGGGCGAGATTATAAAGATGATGATGATAAATGACAGCCACTCACT AGGG-3'.

Generation of GLUT1 expression construct

GLUT1 expression constructs were generated from GLUT1 clone#40085220 (Genbank#BC121804; Dharmacon, cat #MHS6278-211690539). The retroviral GLUT1 expression construct (pQCXIP puromycin^R backbone) was generated by amplifying the GLUT1 ORF using the Forward Primer 5'- CTGCTGGCGGCCGCATGGAGCCCAGCA-3' and Reverse Primer 5'-CTGCTGGGATCCTCACACTTGGGAATCAG-3'. The PCR product was then digested and subcloned between the NotI and BamHI sites of pQCXIP. All constructs were sequenced to confirm accuracy.

Retroviral constructs were packaged in 293T cells by transfecting pQCXIP (Clontech) with pMD.Gag-Pol [66] and pVSVG [67] packaging plasmids using Lipofectamine LTX (Invitrogen, cat#15338100). Supernatants were harvested and filtered using 0.45 μm sterile filters. Transduction by retrovirus was performed by spinoculation; briefly, 1 mL of viral supernatant was combined with $2.0x10^5$ cells followed by a 2-hour centrifugation at 1200g at room temperature. The cells were then resuspended in media and plated. After 48 hours, infected cells were selected using 1.6 μg/mL puromycin (Sigma-Aldrich cat#P9620).

Western blotting, Antibody probes and PNGase treatment

Proteins were analyzed by SDS-PAGE with Western blotting as follows. Cells were lysed in RIPA lysis buffer (25 mM Tris-Cl pH7.4, 150 mM NaCl, 1% Triton X-100, 1% Sodium Deoxycholate, 0.1% Sodium Dodecyl Sulfate) with the addition of Halt Protease Inhibitor (Pierce, Catalog #78430) and Halt Phosphatase Inhibitor (Pierce, Catalog #78428), for 10 minutes at 4^{o}C on a rocker. Lysates were cleared, protein concentration assayed and 10-20 μg of protein lysate separated by SDS-PAGE and transferred to PVDF membranes, blocked in 5% dry milk in TBS with 0.1% Tween-20.
A novel antibody to GLUT8 (named **BBA1**) was raised in rabbits using a 15 amino acid peptide (^{227}GSEQGWEDPPIGAEQ^{241}) from the long cytoplasmic loop between transmembrane domains 6 and 7 of GLUT8. This peptide shows zero homology with other GLUT species, and is included in both GLUT8 variants, v1 and v3. Other antibodies used in this study are tabulated below, including the rabbit anti-GLUT1, a generous gift of Dr. Steven M. Anderson, University of Colorado-Denver.

To study the non-glycosylated GLUT proteins, cell lysates were de-glycosylated using PNGase F (R&D systems, cat#9109-GH) according to the manufacturer's instructions.

Glucose Uptake assay

Glucose uptake was assayed using 1.0 mCi/mL 2-[1,2-^{3}H (N)]-deoxy-D-Glucose (**^{3}H-2DG**; Perkin Elmer, cat#NET549A). Cells were plated at 2.5x10^{4} cells/well in 24-well plates in complete growth media and incubated in 37^{o}C incubator overnight. The following day the cells were rinsed in PBS, then 0.5 ml warm media without glucose (Gibco, cat#11966 with 5% FBS) was added for 10 mins at 37^{o}C. 2μCi ^{3}H-2DG was added to each well and incubated for 10 mins. Uptake was halted by washing the cells in ice-cold

PBS three times, then cells were lysed in 400 μL of 10 mM Tris Cl (pH8.0) with 0.1% SDS, and samples counted by liquid scintillation. Glucose uptake was normalized to cell number by analyzing a parallel 24-well plate using FluoReporter Blue, as described above.

Immunofluorescence staining

Cells were seeded onto chamber slides, incubated at 37°C for 48hrs, and fixed in 4% paraformaldehyde (PFA) for 15 mins at room temperature. The PFA was removed, slides washed 3 times in PBS, followed by permeabilization in 0.01% Saponin in PBS for 5 mins at room temperature. Samples were blocked using 5% goat serum and 0.01% Saponin in PBS for 1 hour at room temperature, then incubated with primary antibodies, diluted in PBS containing 5% goat serum and 0.01% saponin, overnight in humidified chambers at 4°C. Slides were washed in TBS-Tween (0.1%), 3 times for 5 minutes each, and incubated with secondary antibodies (tabulated below) for 1hr at room temperature in diluent, followed by washing (as above) and visualization.

Target	**Source**	**Working dilution** (IHC)
ß-ACTIN	Mouse; Sigma #A5441	--
EEA1	Rabbit; ThermoFisher MA5-147494	1: 1000
FLAG	Rabbit; Cell Signaling #CS14793	1: 800
FLAG	Mouse; Sigma #F3165	0.5 μg/ml
GLUT8	Rabbit; Biobasic Inc; BBA1	1:100
GLUT1	Rabbit; S. Anderson (UC Denver)	0.2 ng/ml

LAMP1	Mouse; DHSB #H4A3	1: 100
PDI	Rabbit; Cell Signaling #CD3501	1: 1000
PMP70	Rabbit; Invitrogen #PA1-650	5 μg/ml
Vinculin	Mouse; Millipore #05-386	---
Mouse	Goat; Alexa546; ThermoFisher #A11030	1: 500
Rabbit	Goat; Alexa488; ThermoFisher #A11034	1: 500
Mouse	Goat; Alexa488; ThermoFisher #A11029	1: 500
Rabbit	Goat; HRP; Invitrogen, cat#G-21234	---
Mouse	Donkey; HRP; Jackson, cat#715-035-151	---

Acknowledgements. This manuscript is dedicated to our brilliant and gentle co-author, Dr. Heidi Dvinge, who passed away suddenly and tragically on September 30th, 2019. Thanks for generous advice from Dr. Aussie Suzuki and Nate Sherer (McArdle Laboratory) on the calibration of confocal microscopic images and the utilization of retroviral expression vectors. The results published here are, in part, based upon data generated by the TCGA Research Network: http://cancergenome.nih.gov. The Genotype-Tissue Expression (GTEx) Project was supported by the Common Fund of the Office of the Director of the National Institutes of Health, and by NCI, NHGRI, NHLBI, NIDA, NIMH, and NINDS. The data used for the analyses described in this manuscript were obtained from the GTEx Portal on 09/03/2019. We appreciate the expert assistance of the Small Molecule Screening Facility (University of Wisconsin Carbone Cancer Center Support Grant; P30 CA014520). JM, IK and CMA were supported by RO1 GM113142,

and a Cancer Biology training award to JM (T32 CA009135). Antibody production was assisted by support from the UW SDRC grant P30 AR066524, funded by the National Institute of Arthritis and Musculoskeletal and Skin Diseases (NIAMS).

REFERENCES

1. Mueckler, M. and B. Thorens, *The SLC2 (GLUT) family of membrane transporters.* Mol Aspects Med, 2013. **34**(2-3): p. 121-38.

2. Joost, H.G., et al., *Nomenclature of the GLUT/SLC2A family of sugar/polyol transport facilitators.* Am J Physiol Endocrinol Metab, 2002. **282**(4): p. E974-6.

3. Zhao, F.Q. and A.F. Keating, *Functional properties and genomics of glucose transporters.* Current genomics, 2007. **8**(2): p. 113-28.

4. Mueckler, M. and G. Holman, *Homeostasis without a GLUT.* Nature, 1995. **377**(6545): p. 100-1.

5. Schmidt, S., H.G. Joost, and A. Schurmann, *GLUT8, the enigmatic intracellular hexose transporter.* Am J Physiol Endocrinol Metab, 2009. **296**(4): p. E614-8.

6. Ibberson, M., M. Uldry, and B. Thorens, *GLUTX1, a novel mammalian glucose transporter expressed in the central nervous system and insulin-sensitive tissues.* J Biol Chem, 2000. **275**(7): p. 4607-12.

7. Carayannopoulos, M.O., et al., *GLUT8 is a glucose transporter responsible for insulin-stimulated glucose uptake in the blastocyst.* Proc Natl Acad Sci U S A, 2000. **97**(13): p. 7313-8.

8. Doege, H., et al., *GLUT8, a novel member of the sugar transport facilitator family with glucose transport activity.* J Biol Chem, 2000. **275**(21): p. 16275-80.

9. Adastra, K.L., et al., *Slc2a8 deficiency in mice results in reproductive and growth impairments.* Biol Reprod, 2012. **87**(2): p. 49.

10. Schmidt, S., et al., *Deletion of glucose transporter GLUT8 in mice increases locomotor activity.* Behav Genet, 2008. **38**(4): p. 396-406.

11. Gawlik, V., et al., *Targeted disruption of Slc2a8 (GLUT8) reduces motility and mitochondrial potential of spermatozoa.* Mol Membr Biol, 2008. **25**(3): p. 224-35.

12. Membrez, M., et al., *GLUT8 is dispensable for embryonic development but influences hippocampal neurogenesis and heart function.* Mol Cell Biol, 2006. **26**(11): p. 4268-76.

13. Debosch, B.J., et al., *Glucose transporter 8 (GLUT8) mediates fructose-induced de novo lipogenesis and macrosteatosis.* J Biol Chem, 2014. **289**(16): p. 10989-98.

14. Meyers, R.M., et al., *Computational correction of copy number effect improves specificity of CRISPR-Cas9 essentiality screens in cancer cells.* Nat Genet, 2017. **49**(12): p. 1779-1784.

15. Tsherniak, A., et al., *Defining a Cancer Dependency Map.* Cell, 2017. **170**(3): p. 564-576 e16.

16. Diril, M.K., et al., *Lysosomal localization of GLUT8 in the testis--the EXXXLL motif of GLUT8 is sufficient for its intracellular sorting via AP1- and AP2-mediated interaction.* FEBS J, 2009. **276**(14): p. 3729-43.

17. Piroli, G.G., et al., *Peripheral glucose administration stimulates the translocation of GLUT8 glucose transporter to the endoplasmic reticulum in the rat hippocampus.* J Comp Neurol, 2002. **452**(2): p. 103-14.

18. Augustin, R., J. Riley, and K.H. Moley, *GLUT8 contains a [DE]XXXL[LI] sorting motif and localizes to a late endosomal/lysosomal compartment.* Traffic, 2005. **6**(12): p. 1196-212.

19. Gomez, O., et al., *Differential expression of glucose transporter GLUT8 during mouse spermatogenesis.* Reproduction, 2006. **131**(1): p. 63-70.

20. Joost, H.G. and B. Thorens, *The extended GLUT-family of sugar/polyol transport facilitators: nomenclature, sequence characteristics, and potential function of its novel members (review).* Mol Membr Biol, 2001. **18**(4): p. 247-56.

21. Caulfield, M.J., et al., *SLC2A9 is a high-capacity urate transporter in humans.* PLoS Med, 2008. **5**(10): p. e197.

22. Cancer Genome Atlas, N., *Comprehensive molecular portraits of human breast tumours.* Nature, 2012. **490**(7418): p. 61-70.

23. Marcotte, R., et al., *Functional Genomic Landscape of Human Breast Cancer Drivers, Vulnerabilities, and Resistance.* Cell, 2016. **164**(1-2): p. 293-309.

24. Onodera, Y., J.M. Nam, and M.J. Bissell, *Increased sugar uptake promotes oncogenesis via EPAC/RAP1 and O-GlcNAc pathways.* The Journal of clinical investigation, 2014. **124**(1): p. 367-84.

25. Roy, S., et al., *Autophagy-Dependent Shuttling of TBC1D5 Controls Plasma Membrane Translocation of GLUT1 and Glucose Uptake.* Mol Cell, 2017. **67**(1): p. 84-95 e5.

26. Wu, N., et al., *AMPK-dependent degradation of TXNIP upon energy stress leads to enhanced glucose uptake via GLUT1.* Mol Cell, 2013. **49**(6): p. 1167-75.

27. Olsen, J.M., et al., *Glucose uptake in brown fat cells is dependent on mTOR complex 2-promoted GLUT1 translocation.* The Journal of cell biology, 2014. **207**(3): p. 365-74.

28. Young, C.D., et al., *Modulation of glucose transporter 1 (GLUT1) expression levels alters mouse mammary tumor cell growth in vitro and in vivo.* PLoS One, 2011. **6**(8): p. e23205.

29. Wellberg, E.A., et al., *The glucose transporter GLUT1 is required for ErbB2-induced mammary tumorigenesis.* Breast Cancer Res, 2016. **18**(1): p. 131.

30. Hully, M., et al., *From splitting GLUT1 deficiency syndromes to overlapping phenotypes.* Eur J Med Genet, 2015. **58**(9): p. 443-54.

31. Deng, D., et al., *Crystal structure of the human glucose transporter GLUT1.* Nature, 2014. **510**(7503): p. 121-5.

32. Scheepers, A., et al., *Mouse GLUT8: genomic organization and regulation of expression in 3T3-L1 adipocytes by glucose.* Biochem Biophys Res Commun, 2001. **288**(4): p. 969-74.

33. Rathmell, W.K., J.C. Rathmell, and W.M. Linehan, *Metabolic Pathways in Kidney Cancer: Current Therapies and Future Directions.* J Clin Oncol, 2018: p. JCO2018792309.

34. Joshi, S., et al., *The Genomic Landscape of Renal Oncocytoma Identifies a Metabolic Barrier to Tumorigenesis.* Cell Rep, 2015. **13**(9): p. 1895-908.

35. Shimano, H. and R. Sato, *SREBP-regulated lipid metabolism: convergent physiology - divergent pathophysiology.* Nat Rev Endocrinol, 2017. **13**(12): p. 710-730.

36. DeBose-Boyd, R.A. and J. Ye, *SREBPs in Lipid Metabolism, Insulin Signaling, and Beyond.* Trends Biochem Sci, 2018. **43**(5): p. 358-368.

37. Zoncu, R., et al., *mTORC1 senses lysosomal amino acids through an inside-out mechanism that requires the vacuolar H(+)-ATPase.* Science, 2011. **334**(6056): p. 678-83.

38. Sancak, Y., et al., *Ragulator-Rag complex targets mTORC1 to the lysosomal surface and is necessary for its activation by amino acids.* Cell, 2010. **141**(2): p. 290-303.

39. Colaco, A. and M. Jaattela, *Ragulator-a multifaceted regulator of lysosomal signaling and trafficking.* J Cell Biol, 2017. **216**(12): p. 3895-3898.

40. Kvainickas, A., et al., *Retromer and TBC1D5 maintain late endosomal RAB7 domains to enable amino acid-induced mTORC1 signaling.* J Cell Biol, 2019.

41. Langemeyer, L., F. Frohlich, and C. Ungermann, *Rab GTPase Function in Endosome and Lysosome Biogenesis.* Trends Cell Biol, 2018. **28**(11): p. 957-970.

42. Wong, Y.C., et al., *Regulation and Function of Mitochondria-Lysosome Membrane Contact Sites in Cellular Homeostasis.* Trends Cell Biol, 2019. **29**(6): p. 500-513.

43. Stroupe, C., *This Is the End: Regulation of Rab7 Nucleotide Binding in Endolysosomal Trafficking and Autophagy.* Front Cell Dev Biol, 2018. **6**: p. 129.

44. Thelen, A.M. and R. Zoncu, *Emerging Roles for the Lysosome in Lipid Metabolism.* Trends Cell Biol, 2017. **27**(11): p. 833-850.

45. Mayer, A.L., et al., *Enhanced Hepatic PPARalpha Activity Links GLUT8 Deficiency to Augmented Peripheral Fasting Responses in Male Mice.* Endocrinology, 2018. **159**(5): p. 2110-2126.

46. Johnston, M. and J.H. Kim, *Glucose as a hormone: receptor-mediated glucose sensing in the yeast Saccharomyces cerevisiae.* Biochem Soc Trans, 2005. **33**(Pt 1): p. 247-52.

47. Rolland, F., J. Winderickx, and J.M. Thevelein, *Glucose-sensing mechanisms in eukaryotic cells.* Trends Biochem Sci, 2001. **26**(5): p. 310-7.

48. Snowdon, C. and M. Johnston, *A novel role for yeast casein kinases in glucose sensing and signaling.* Mol Biol Cell, 2016. **27**(21): p. 3369-3375.

49. Diez-Sampedro, A., et al., *A glucose sensor hiding in a family of transporters.* Proc Natl Acad Sci U S A, 2003. **100**(20): p. 11753-8.

50. Romero, A., et al., *Expression of GLUT8 in mouse intestine: identification of alternative spliced variants.* J Cell Biochem, 2009. **106**(6): p. 1068-78.

51. Macintyre, A.N., et al., *The glucose transporter Glut1 is selectively essential for CD4 T cell activation and effector function.* Cell Metab, 2014. **20**(1): p. 61-72.

52. Waldhart, A.N., et al., *Phosphorylation of TXNIP by AKT Mediates Acute Influx of Glucose in Response to Insulin.* Cell Rep, 2017. **19**(10): p. 2005-2013.

53. Dotimas, J.R., et al., *Diabetes regulates fructose absorption through thioredoxin-interacting protein.* Elife, 2016. **5**.

54. Bibee, K.P., et al., *The apical sorting signal for human GLUT9b resides in the N-terminus.* Mol Cell Biochem, 2013. **376**(1-2): p. 163-73.

55. Augustin, R., et al., *Identification and characterization of human glucose transporter-like protein-9 (GLUT9): alternative splicing alters trafficking.* J Biol Chem, 2004. **279**(16): p. 16229-36.

56. Buchner, D.A., et al., *Zinc finger protein 407 (ZFP407) regulates insulin-stimulated glucose uptake and glucose transporter 4 (Glut4) mRNA.* J Biol Chem, 2015. **290**(10): p. 6376-86.

57. Dvinge, H. and R.K. Bradley, *Widespread intron retention diversifies most cancer transcriptomes.* Genome Med, 2015. **7**(1): p. 45.

58. Langmead, B., et al., *Ultrafast and memory-efficient alignment of short DNA sequences to the human genome.* Genome Biol, 2009. **10**(3): p. R25.

59. Li, B. and C.N. Dewey, *RSEM: accurate transcript quantification from RNA-Seq data with or without a reference genome.* BMC Bioinformatics, 2011. **12**: p. 323.

60. Katz, Y., et al., *Analysis and design of RNA sequencing experiments for identifying isoform regulation.* Nat Methods, 2010. **7**(12): p. 1009-15.

61. Meyer, L.R., et al., *The UCSC Genome Browser database: extensions and updates 2013.* Nucleic Acids Res, 2013. **41**(Database issue): p. D64-9.

62. Flicek, P., et al., *Ensembl 2013.* Nucleic Acids Res, 2013. **41**(Database issue): p. D48-55.

63. Robinson, M.D. and A. Oshlack, *A scaling normalization method for differential expression analysis of RNA-seq data.* Genome Biol, 2010. **11**(3): p. R25.

64. Parker, J.S., et al., *Supervised risk predictor of breast cancer based on intrinsic subtypes.* J Clin Oncol, 2009. **27**(8): p. 1160-7.

65. Chin, E.N., et al., *Lrp5 Has a Wnt-Independent Role in Glucose Uptake and Growth for Mammary Epithelial Cells.* Mol Cell Biol, 2015. **36**(6): p. 871-85.

66. Ory, D.S., B.S. Neugeboren, and R.C. Mulligan, *A stable human-derived packaging cell line for production of high titer retrovirus/vesicular stomatitis virus G pseudotypes.* Proc. Natl. Acad. Sci. USA, 1996. **93**: p. 11400-11406.

67. Yee, J.K., et al., *A general method for the generation of high-titer, pantropic retroviral vectors: highly efficient infection of primary hepatocytes.* Proc Natl Acad Sci U S A, 1994. **91**(20): p. 9564-8.

Table 1

	Hum chsme	Hum isoforms	Human exons	Mouse exons
GLUT1 *SLC2A1*	1	1		
GLUT2 *SLC2A2*	3	3	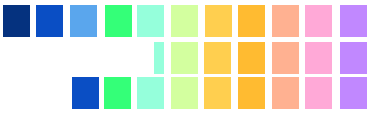	
GLUT3 *SLC2A3*	12	1		
GLUT14 *SLC2A14*	12	4	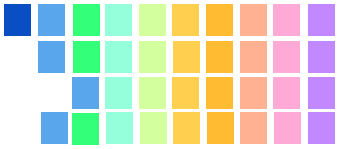	
GLUT4 *SLC2A4*	17	3	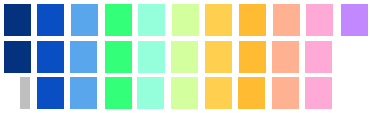	
GLUT6 *SLC2A6*	9	2		
GLUT8 *SLC2A8*	9	3	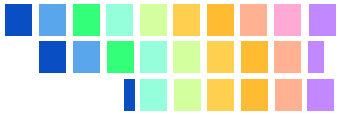	
GLUT10 *SLC2A10*	20	1		
GLUT12 *SLC2A12*	6	1		
HMIT *SLC2A13*	12	2		

Table 1. Alternative splicing of GLUT mRNAs. (Putative) protein-encoding exons for each of 10 GLUT species, 5 Class I GLUTs (GLUT1-4) and 5 Class III GLUTs (GLUT6, 8, 10, 12, 13/HMIT) are compared for human and mouse. The species shown are confirmed alternatively spliced mRNA isomers from the genome database (human:GRCh38/hg38 and mouse: GRCm38/mm10). The color bars are unique to each exon to allow comparison of splicing pattern between GLUT isoforms.

Figure 1

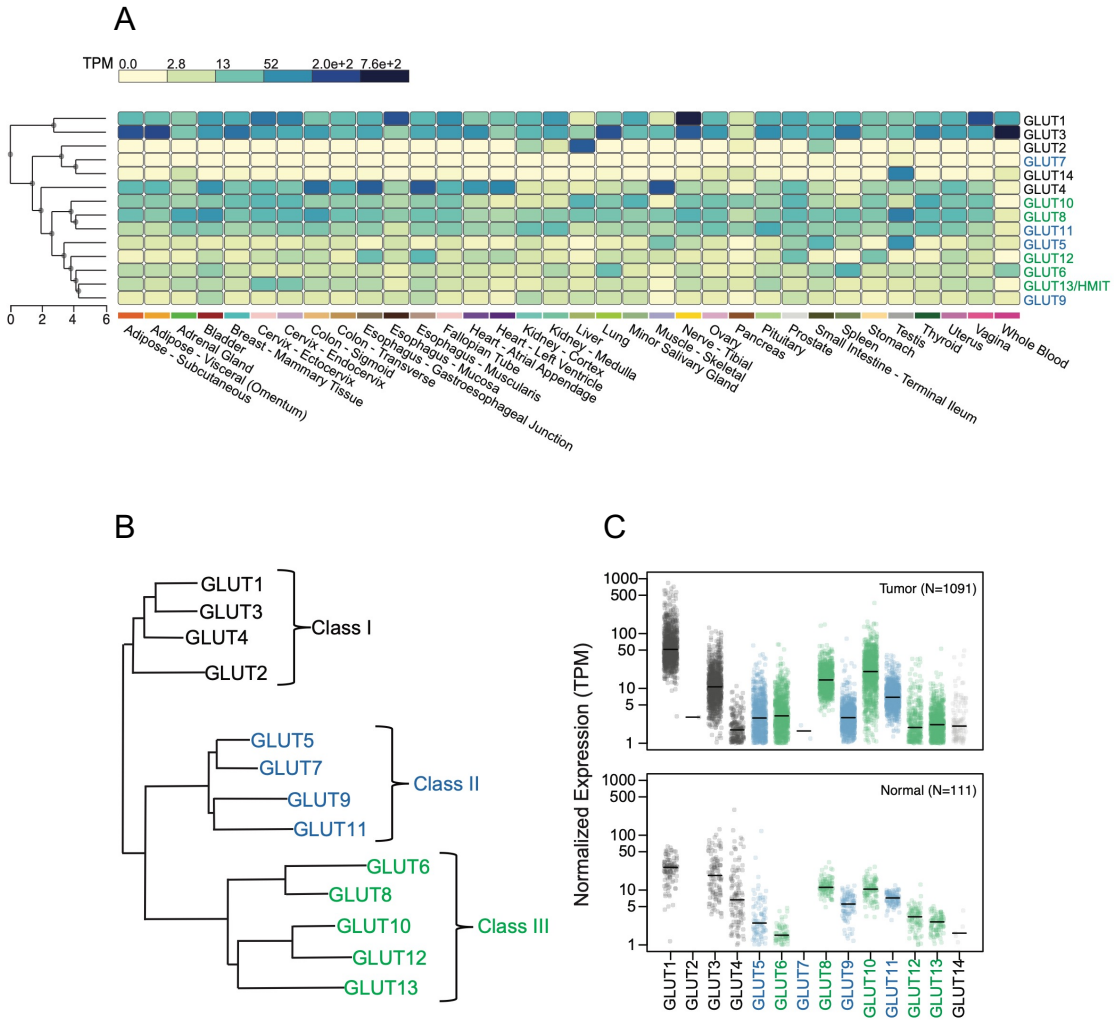

Figure 1. Expression levels of GLUT *SLC2* species in normal tissues and breast tumors. A. Expression levels of each of the 14 Slc2 family members is shown as a heat map of RNA Seq reads (transcripts per kilobase million, TPM) in each of the human tissues indicated (data summarized from GTEx Portal, v8). **B.** The GLUT family dendrogram, redrawn from [2], shows three sub-classes of GLUT proteins (class I, II and III). GLUT14 is not indicated on this scheme; it has now been identified as a paralog of GLUT3, and is therefore grouped with class I *SLC2* species. GLUT13 is more typically called HMIT (H^+-myo-inositol symporter). **C.** Expression of *SLC2* mRNA species is described from the RNASeq database of The Cancer Genome Atlas for breast tumors

(1091 total) [22] and for near-adjacent, non-tumor breast samples (labelled Normal, n=111).

Figure 2

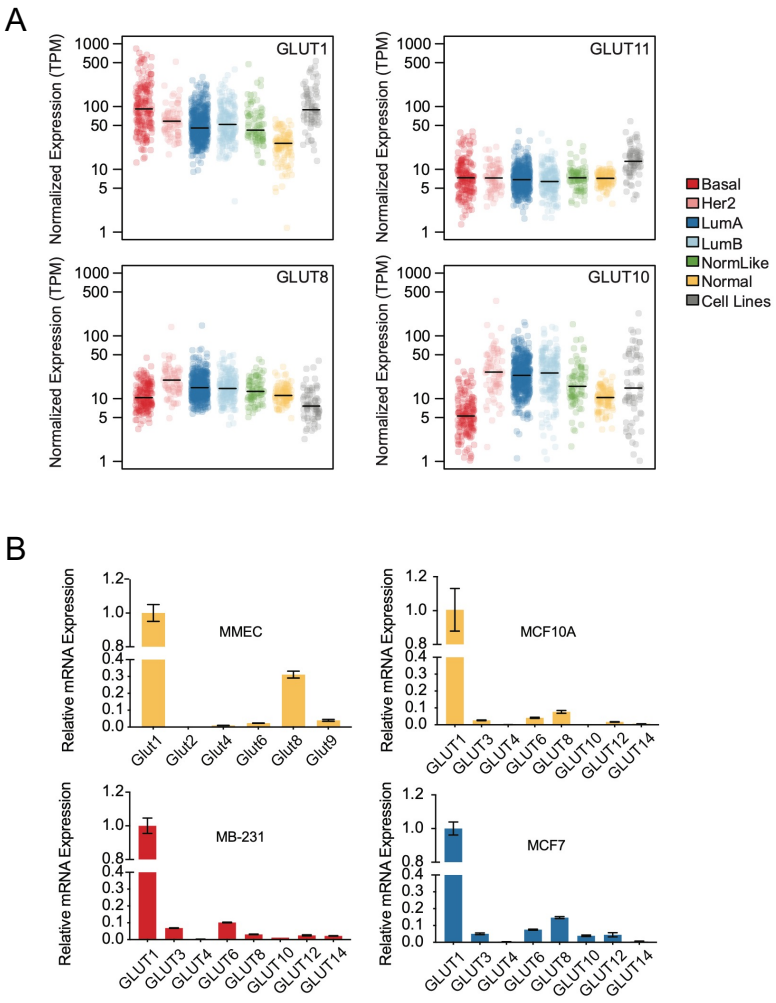

Figure 2. Expression levels of GLUT species in breast tumor subtypes. A. Expression of mRNAs of the most abundant GLUT species from each GLUT class (class I, GLUT1; class II, GLUT11; class III, GLUT8 and 10) is shown for each of the 5 breast tumor sub-types (basal, HER2-positive, luminal A (LumA), luminal B (LumB) and normal-like (NormLike)) and adjacent normal tissues (Normal). Also included is the average expression of 75 cell lines *in vitro* [23]. **B.** Relative mRNA expression level of selected members of the *SLC2* family is shown for a non-transformed **mouse** mammary epithelial cell line (MMEC), non-transformed **human** breast epithelial cells (MCF10A) and two

breast cancer cell lines (MB231 and MCF7 cells), color-coded by their subtype. Expression levels of *SLC* family members is shown with respect to GLUT1 mRNA expression.

Figure 3

A

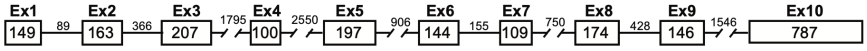

B

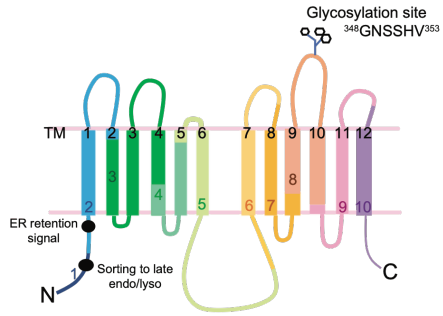

C

Domain	Amino Acids (Q9NY64)	% Identity *Mus musculus*	% Identity *Rattus norvegicus*	% Identity *Bos taurus*
N-term	1:25	72	72	92
TM1	26:46	95.2	95.2	100
TM2	71:91	95	100	95
TM3	97:117	90.5	90.5	85.7
TM4	128:148	100	100	95.2
TM5	157:177	90.5	90.5	95.2
TM6	183:203	90.5	90.5	95.2
Cytoplasmic Loop	204:256	83.3	77.8	70.4
TM7	257:277	85	80	95.2
TM8	293:313	90.5	90.5	95.2
TM9	320:340	81	81	90.5
Extracellular Loop	341:367	60	64	70
TM10	368:388	100	100	100
TM11	405:425	95.2	85.7	90.5
TM12	439:459	77.8	83.3	90.5
C-term	460:477	88.9	94.4	100
Overall Identity	1:477	86.2	85.2	88.9

Figure 3. Mapping of exons to protein structure of GLUT8. **A.** *Schematic diagram showing the GLUT8 locus.* Exon and intron base size (bp) are indicated. **B.** *Schematic of GLUT8 variant 1*, indicating the exon boundaries within the putative protein structure, where each of the trans-membrane (TM) domains is numbered in black, 1-12. Key functional domains are indicated, including the glycosylation site in the ecto-loop between transmembrane domains 9 and 10 and the di-leucine ER-retention and sorting motifs. **C**. *Comparison of GLUT8 protein sequence conservation*, between human GLUT8 (uniprot id. Q9NY64, *Homo sapien*) and three other mammalian species, *Mus musculus (Q9JIF3), Rattus norvegicus (Q9JJZ1), Bos Taurus (P63010).* Trans-membrane domains are 20 amino acids long. Internal cytoplasmic domains include both N- and C-termini and a large loop between transmembrane domains 6 and 7.

Figure 4

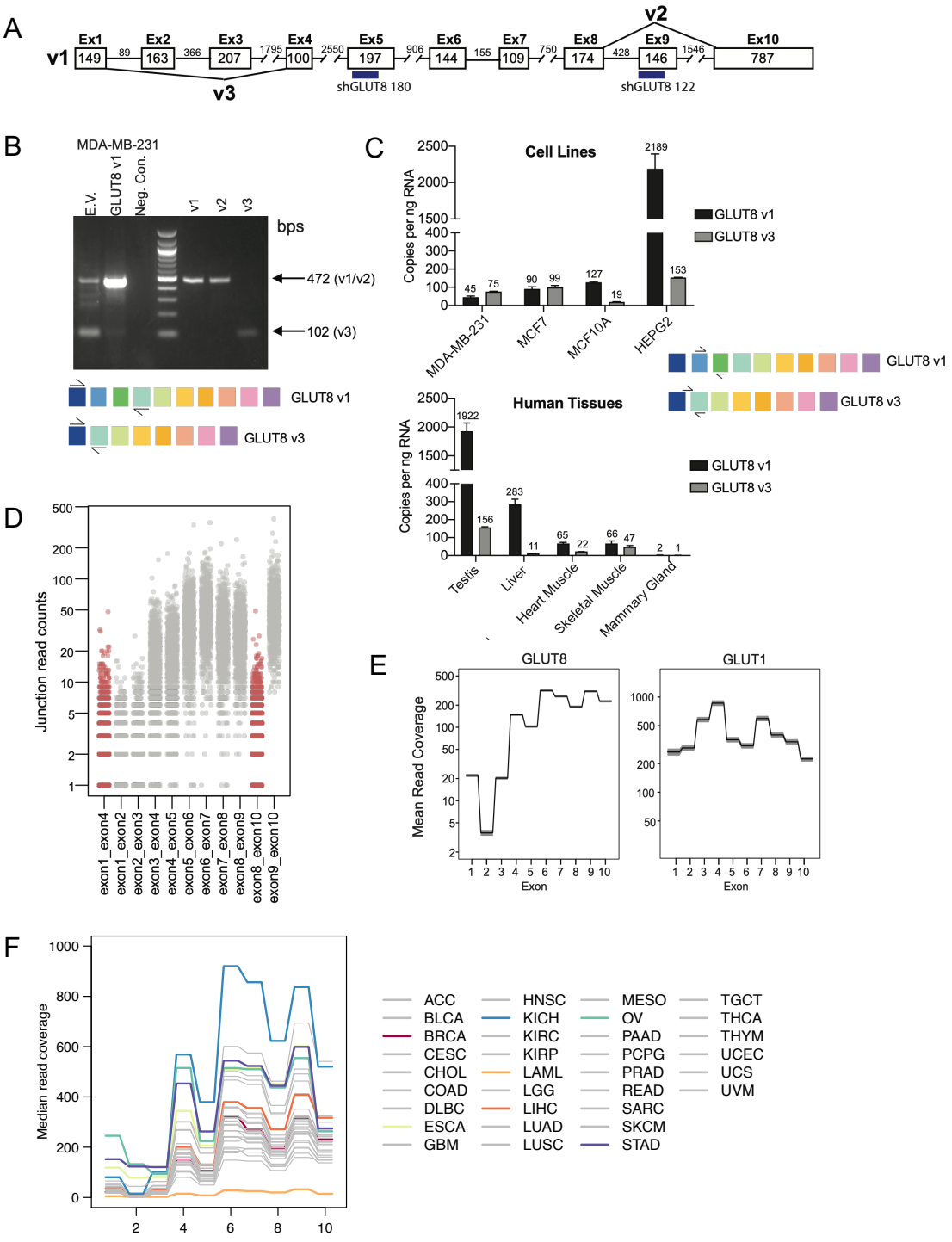

Figure 4. Assay of alternatively spliced isoforms of GLUT8. A. Schematic diagram showing the three alternatively spliced isoforms of GLUT8, v1, v2 and v3. The target

sequences of two of the shRNAs we used (122 and 180) are indicated. **B**. *Assay of endogenous v1 and v3 expression in MB231 cells* (empty vector; EV), and ectopic expression in cells transduced with a vector expressing v1 GLUT8. Primers that cross exons 1 to 4 (as indicated in the schemes below) were used for PCR analysis. Controls (right hand side) show products from v1, v2 and v3 plasmids. **C**. *Frequency of v1- and v3-GLUT8 mRNAs in cells and tissues*. RT-qPCR assay of GLUT8 v1 and v3 expression in human cancer cell lines and normal human tissue, determined using a standard curve of the target amplicon. **D**. *Splicing patterns in vivo*. Exon-Exon junction analysis of GLUT8 mRNAs from TCGA RNA-seq data of breast tumors, showing v2 (ex8-ex10) and v3 (ex1-ex4) in red and canonical exon-exon junctions in grey. **E.** *Assay of relative exon expression*. Analysis of mean read coverage for each exon from breast cancer TCGA RNA-seq data set for GLUT8 and GLUT1. Shaded areas represent the 95% confidence interval (n=1091). F. *Analysis of mean read coverage for a pan-cancer panel.* Labels for each tumor type are excerpted from TCGA. Several tumor types are highlighted for comparison with invasive breast carcinoma (BRCA), and discussed further in results and discussion (ESCA, esophageal carcinoma; KICH, kidney chromophobe; LAML, Acute Myeloid Leukemia; LIHC, Liver hepatocellular carcinoma; OV, Ovarian serous cystadenocarcinoma: STAD, Stomach adenocarcinoma).

Figure 5

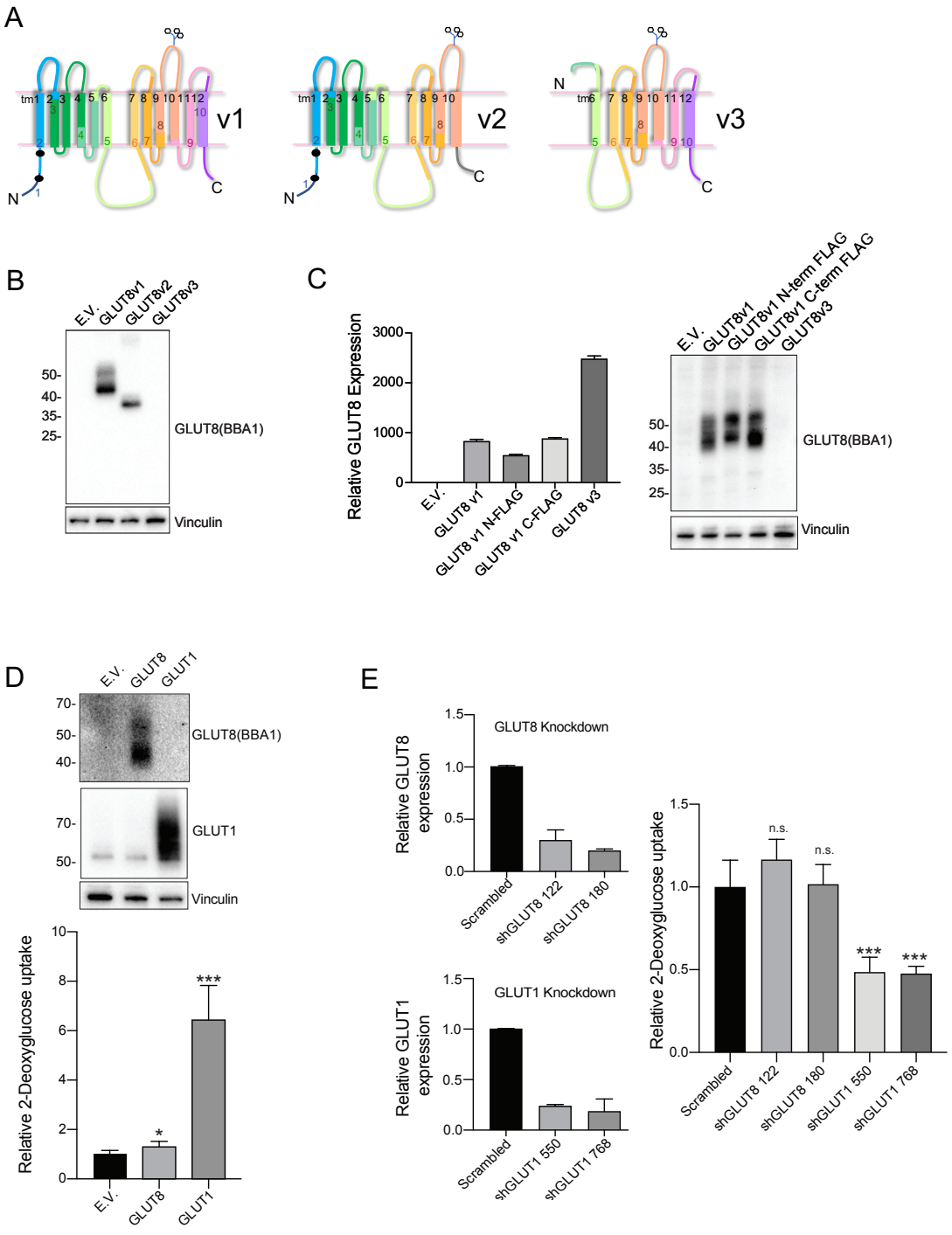
A
v1
v2
v3
N
C
B
E.V.
GLUT8v1
GLUT8v2
GLUT8v3
50-
40-
35-
25-
GLUT8(BBA1)
Vinculin
C
Relative GLUT8 Expression
3000
2000
1000
0
E.V.
GLUT8 v1
GLUT8 v1 N-FLAG
GLUT8 v1 C-FLAG
GLUT8 v3
GLUT8v1 N-term FLAG
GLUT8v1 C-term FLAG
D
E.V.
GLUT8
GLUT1
70-
50-
40-
GLUT8(BBA1)
GLUT1
Vinculin
Relative 2-Deoxyglucose uptake
10
8
6
4
2
0
*
***
E
GLUT8 Knockdown
Relative GLUT8 expression
1.5
1.0
0.5
0.0
Scrambled
shGLUT8 122
shGLUT8 180
GLUT1 Knockdown
Relative GLUT1 expression
shGLUT1 550
shGLUT1 768
n.s.
***

Figure 5. Assay of properties of variant GLUT8 proteins. A. Schematic diagram of GLUT8 v1, v2 and v3 putative protein structures, indicating impact of deletion of exon9 (V2) and exons1-4 (v3). **B**. *Expression of v1, v2 and v3 GLUT8 proteins*. Western blots of lysates from 293T cells transfected with expression constructs. EV, empty vector. **C.** *Expression of v1, FLAG-tagged v1, and v3 expressed in MB231 cells*. RT-qPCR analysis of mRNA from stable GLUT8 over-expressing MB231 cell lines, using a primer set that detects both GLUT8 v1 and v3 isoforms (total GLUT8 assay), and Western blotting of lysates with BBA1, an anti-GLUT8 antibody. Protein loading control is vinculin. **D**. *Assay of glucose transporter activity: gain of function.* (Top) Western blot of protein lysates from MB231 cells transduced with retroviral GLUT8 or GLUT1 constructs, with corresponding assay of relative ^{3}H-2DG uptake. **E.** *Assay of glucose transporter activity: loss of function.* Efficacy of shRNA knockdown of GLUT1 or GLUT8 was assayed (left hand side) and impact of knockdown on ^{3}H-2DG uptake assessed (right hand side). * $p<0.01$; *** $p<0.0001$; n.s, not significant. Results are representative of $n\geq3$ assays.

Figure 6

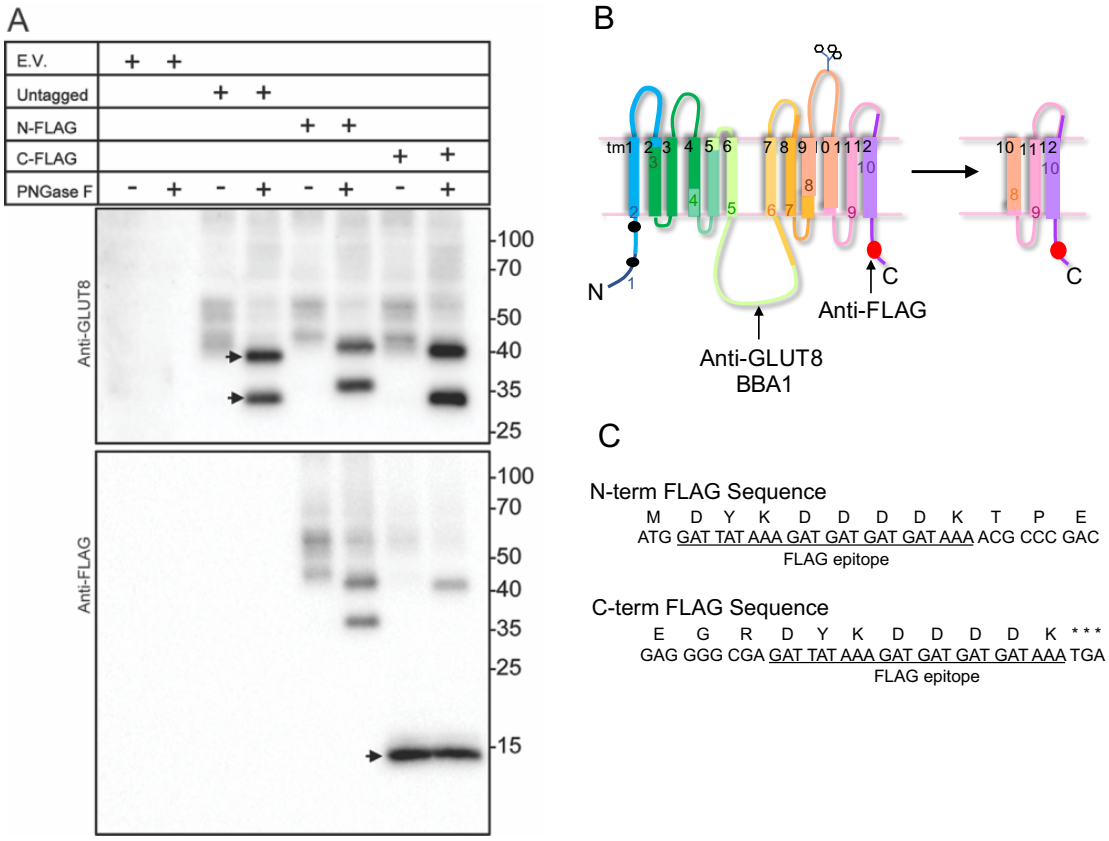

Figure 6. GLUT8 is cleaved at C-terminus to generate a 10kDa peptide. A. Western blot of lysates from MB231 cell lines transduced with retroviral expression constructs indicated. Lysates were treated with PNGase F to remove N-linked glycosylation prior to SDS-PAGE (4-20% gradient gel), and probed with anti-GLUT8 or anti-FLAG antibodies. **B.** Schematic diagram of putative cleavage site within the 10th transmembrane domain of GLUT8, predicted from the sizes of the parent and cleaved de-glycosylated GLUT8 proteins. **C**. The protein and nucleotide sequences of the C-terminal and N-terminal FLAG sites of GLUT8.

Figure 7

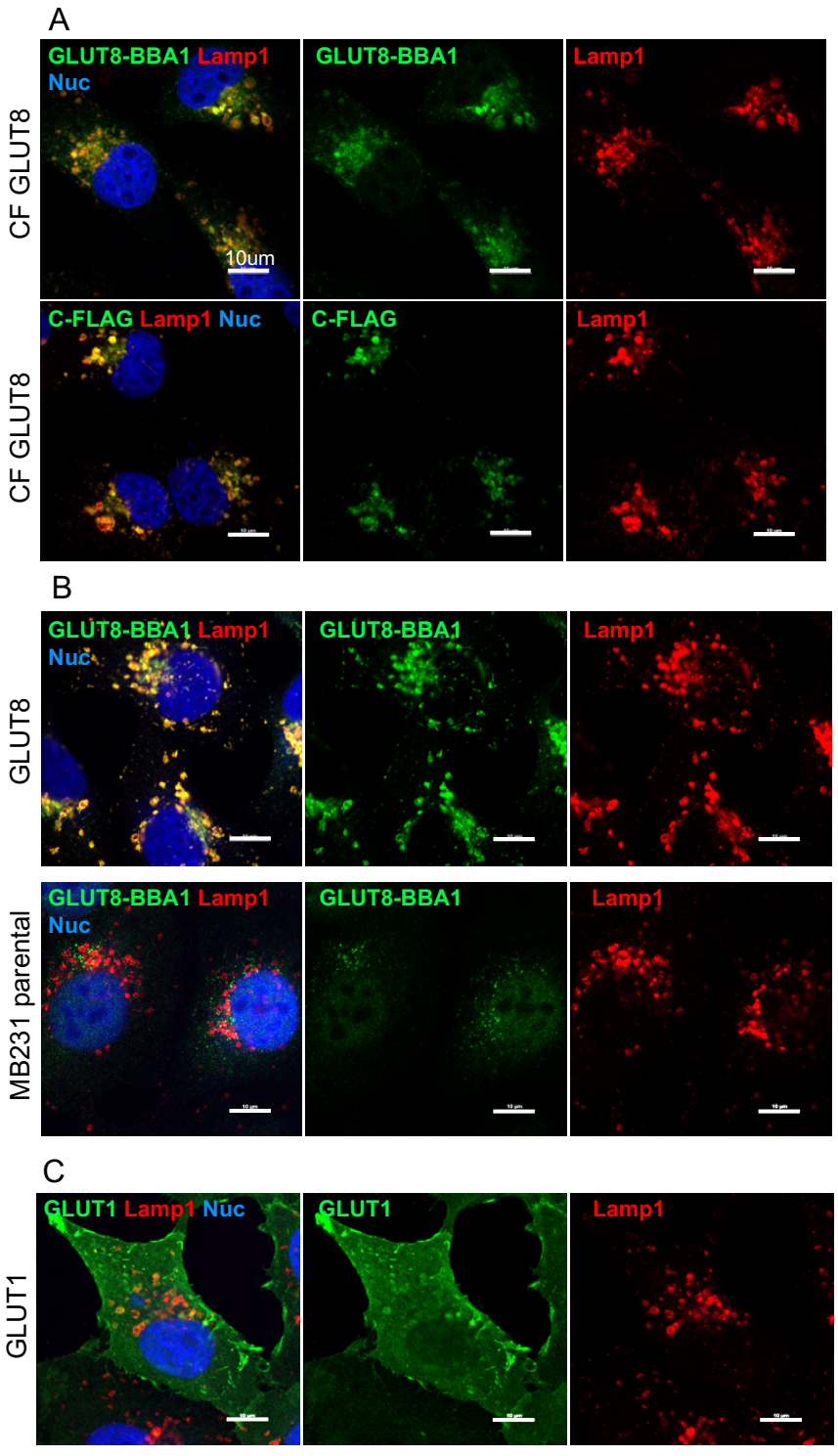
A
CF GLUT8
GLUT8-BBA1 Lamp1 Nuc
10um
GLUT8-BBA1
Lamp1
CF GLUT8
C-FLAG Lamp1 Nuc
C-FLAG
Lamp1
B
GLUT8
GLUT8-BBA1 Lamp1 Nuc
GLUT8-BBA1
Lamp1
MB231 parental
GLUT8-BBA1 Lamp1 Nuc
GLUT8-BBA1
Lamp1
C
GLUT1
GLUT1 Lamp1 Nuc
GLUT1
Lamp1

Figure 7. GLUT8 co-localizes with LAMP1 in the lysosome. **A.** MB231 cells expressing C-terminal-FLAG tagged GLUT8 were stained with anti-GLUT8 and LAMP1; single stains are shown to the right, co-localization to the left; nuclei were stained with DAPI. **B.** MB231 cells expressing untagged GLUT8, and cells without transgenic GLUT8 expression, are compared with the data shown in A, to assess relative distribution of untagged GLUT8 protein, normal lysosome distribution, and endogenous GLUT8 localization. **C.** *GLUT1 distribution.* MB231 cells expressing GLUT1 were stained using the same protocol. Scale bars 10 μM

Figure 8

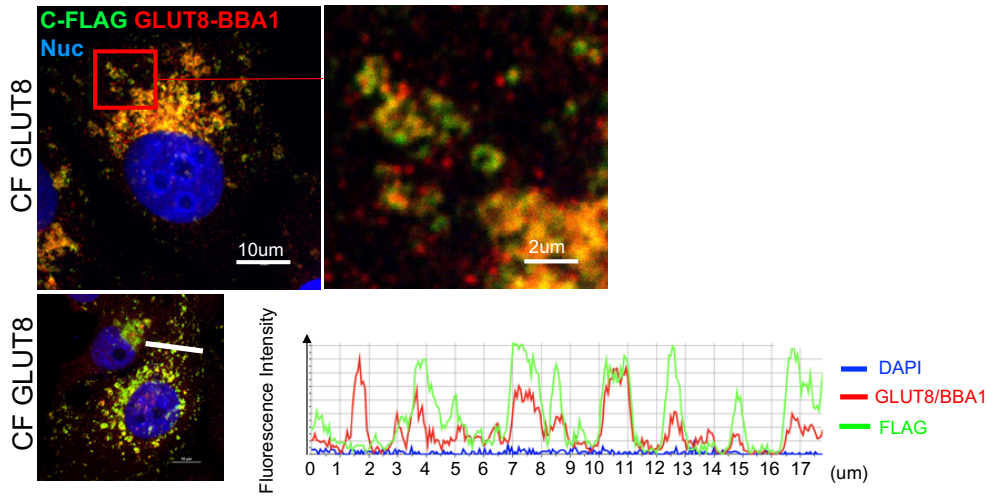

Figure 8. The cleaved C-terminal peptide becomes enriched in a separate vesicular population. Evaluation of co-localization of epitopes from the central loop of GLUT8 (BBA1) and the FLAG-epitope at the C-terminus shows that these epitopes become separated into separate vesicles. An example of images revealing vesicular population with mixed colors is shown (top); quantitative analysis of relative color intensity is shown across a typical section (bottom).

Table S1. Evaluation of specificity of commercial antibodies to GLUT8. BBA1 (in house rabbit polyclonal anti-peptide antibody) passed the quality control assays, defined as loss of signal after knockdown of GLUT8 and gain of signal upon over-expression. The following commercial antibodies were assayed by the same criteria and did not pass:

Antibody **Cat#** **Source**	**Species** **Type**	**Epitope**	**Method tested** **Western blotting (WB)** **Immunofluorescent stain (IF)**
Anti-GLUT8 [EPR9477] #Ab169779 **Abcam**	Rabbit Monoclonal	Not disclosed	WB: 42kDa band is prominent. Failed to show knockdown by shRNA IF: ND
Anti-GLUT8 C-terminus #07-1407 **Millipore**	Rabbit Polyclonal	11 amino acids near the C-terminus	WB: Not compatible IF: Nuclear staining pattern, not decreased by shRNA expression
Anti-GLUT8 #bs-4241R **Bioss**	Rabbit Polyclonal	Immunogen: AAs 278-292	WB: 52, 45, 25kDa bands are prominent. Failed to show knockdown by shRNA. Does not detect overexpression of FLAG tagged GLUT8. IF: Nuclear staining pattern, not sensitive to shRNA expression. No change in signal with overexpression
Anti-GLUT8 #Ab99132 **Abcam**	Rabbi Polyclonal	Peptide derived from range AAs 323-372	WB: 70kDa band is prominent. Not sensitive to KD by shRNA. Does not detect overexpression of FLAG tagged GLUT8 IF: ND
Anti-GLUT8 #Ab191269, **Abcam**	Rabbit Polyclonal	Synthetic peptide: Amino Acids 461-477	WB: Does not detect overexpressed FLAG tagged GLUT8 or endogenous band IF: ND

Primer sequences for qPCR

Gene name	Primer sequence (5'-3') Forward	Reverse	NCBI Ref Seq Id
HPRT	CCTCATGGACTGATTATGGACAG	AATCCAGCAGGTCAGCAAAG	NM_000194
YWHAZ	AAGACAGCACGCTAATAATGC	TTGGAAGGCCGGTTAATTTTC	NM_003406
GLUT1	TTGCAGGCTTCTCCAACTGGAC	ACGAACCAGGAGCACAGTGAAG	NM_006516
GLUT8 all	ACGAACCAGGAGCACAGTGAAG	GATCTCTGACATGAGGAGCCAG	NM_014580, NM_001271712
GLUT8 variant 1	GTTCGGGGCTGTCGTGAC	AGCATCCACACGTCCTGG	NM_014580, NM_001271711
GLUT8 variant 3	TGGCGGCAGGTCTACAT	TGCCGACGACGACCATTA	NM_001271712

Figure S1

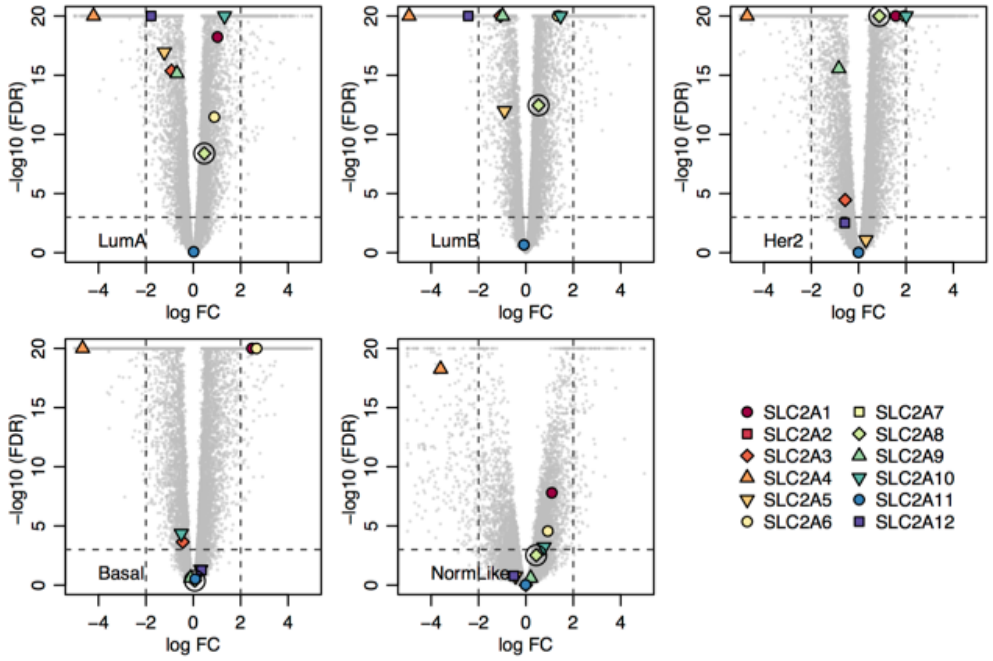

Figure S1. Relative expression of SLC2 family members compared to matched normal breast tissues. Volcano plots show the statistical significance of differences of relative expression of GLUT mRNA family members; GLUT8 mRNA is circled. Dashed lines show commonly used thresholds of statistical significance and fold change.

Figure S2

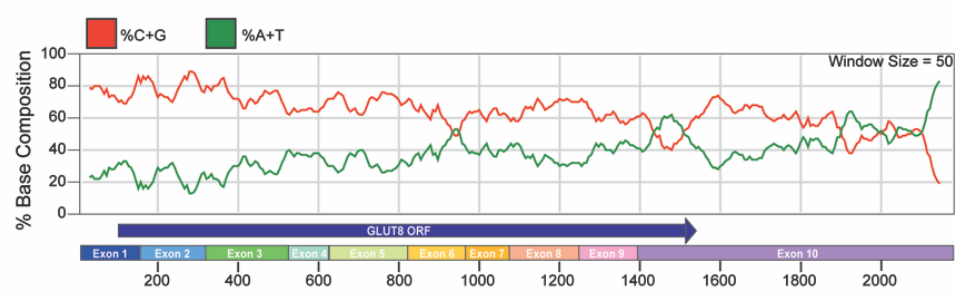

Figure S2. Base composition of GLUT8. Base composition analysis of GLUT8 (NM_014580.4) was performed using MacVector version 17.0.5. Mononucleotide base pairing shown in plot using a base window size of 50.

Figure S3

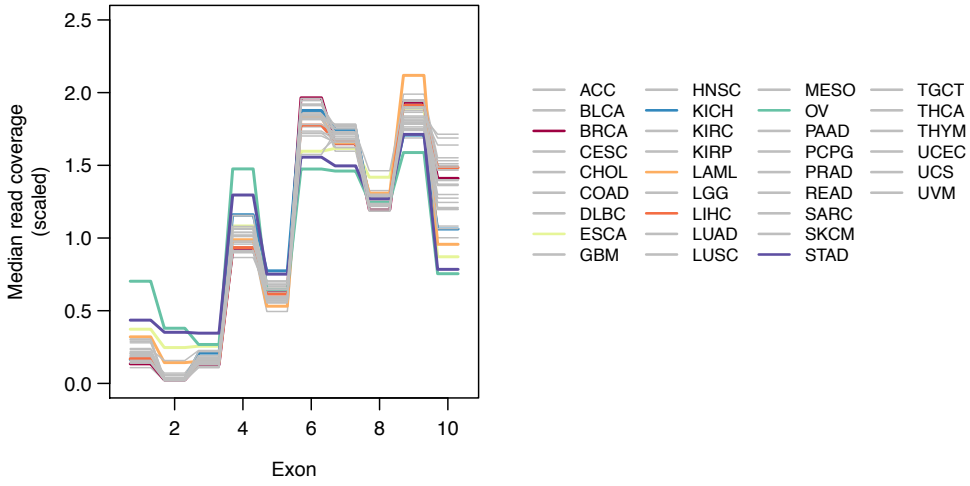

Figure S3. Pan-cancer GLUT8 exon expression. The relative frequency of each exon (1-10) of GLUT8 is shown for 33 different types of tumor, scaled for total frequency of GLUT8 mRNA (partner to Fig. 4F).

Figure S4

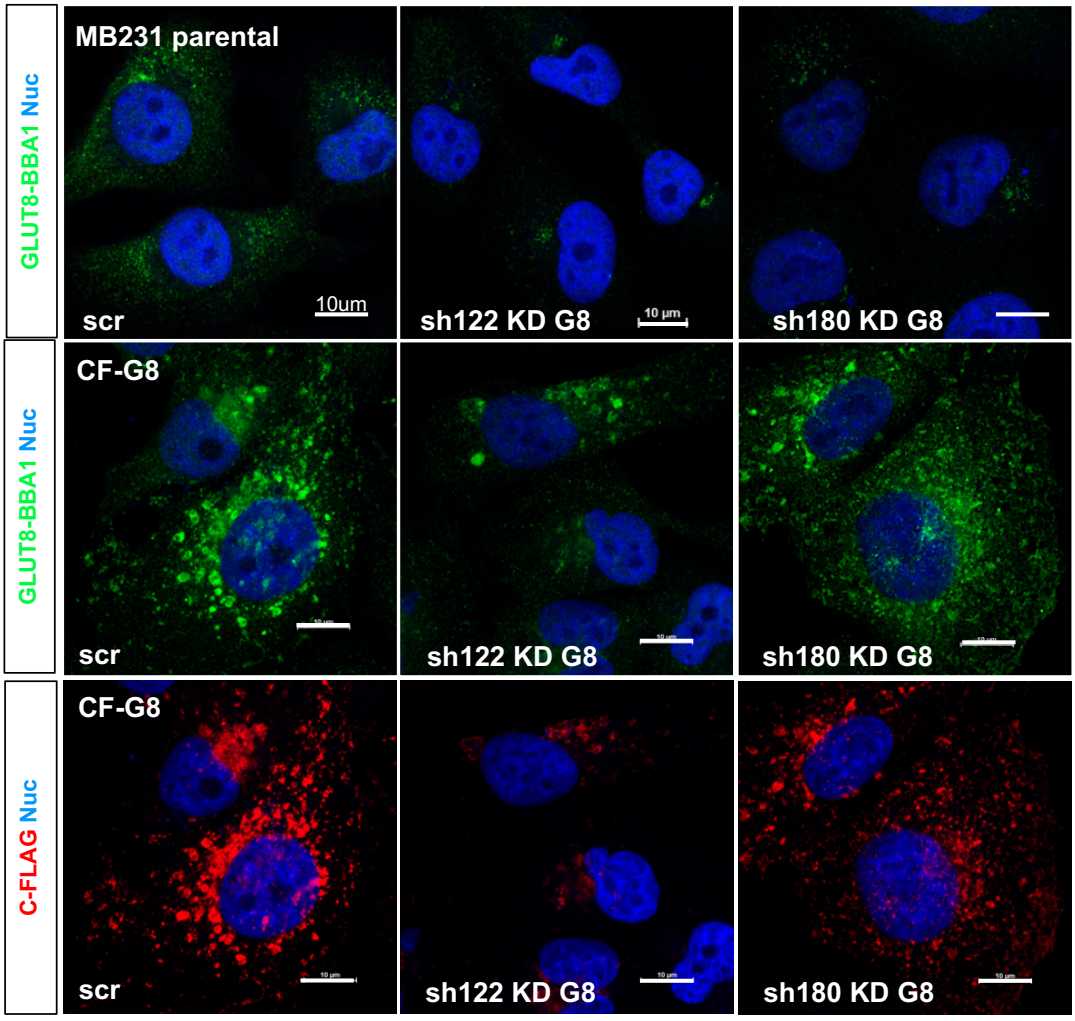

Figure S4. Demonstration of specificity of new rabbit anti-GLUT8 antibody, BBA1. Confocal microscopy of GLUT8 expression in MB231 cells. *Top Row:* parental MB231 cells (low endogenous expression of GLUT8) were transduced lentivirus expressing shRNA-GLUT8 (sh122 or 180; described in Fig. 4A) or scramble (scr) shRNA and stained with BBA1 antibody 48 hours later. *Middle, bottom rows:* MB231 cells stably expressing exogenous C-terminal FLAG GLUT8 were transduced with lentivirus expressing shRNA-

GLUT8 or scramble shRNA and stained with BBA1. The sequence of CF-GLUT8 includes silent mutations that make it non-degradable by sh180. Scale bars show 10μM.

Figure S5

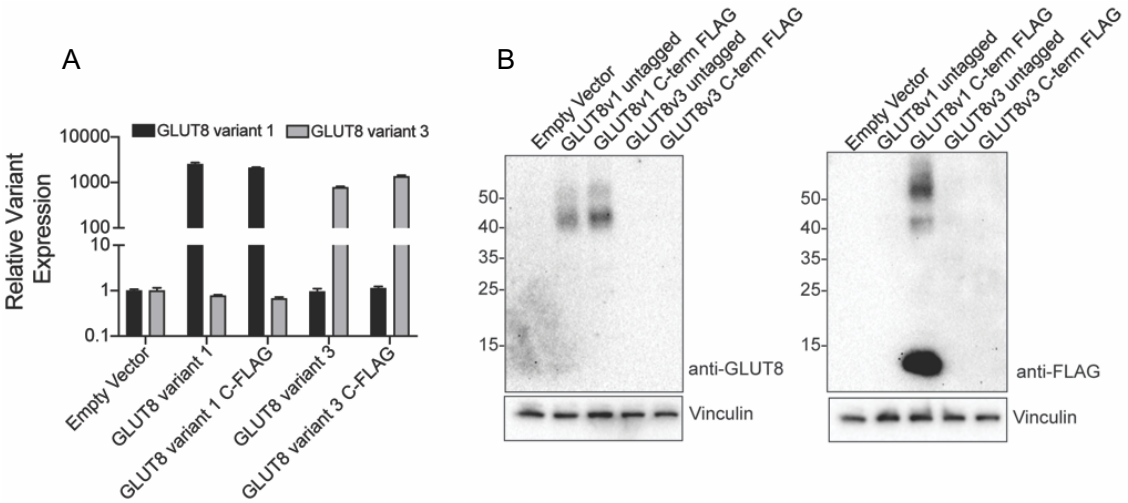

Figure S5. C-terminal FLAG v3 construct does not produce a FLAG tagged C-terminal peptide. A. *Assay of mRNA expression.* qRT-PCR assay of RNA for MB231 cells expressing the constructs indicated. RT-qPCR assay was designed to be selective for v1 and v3 (as described for Fig.4C). **B**. *Assay of protein expression.* Western blot of lysates from the same cells showing that GLUT8-v3 constructs generate neither full-length nor detectable cleaved products.

Figure S6

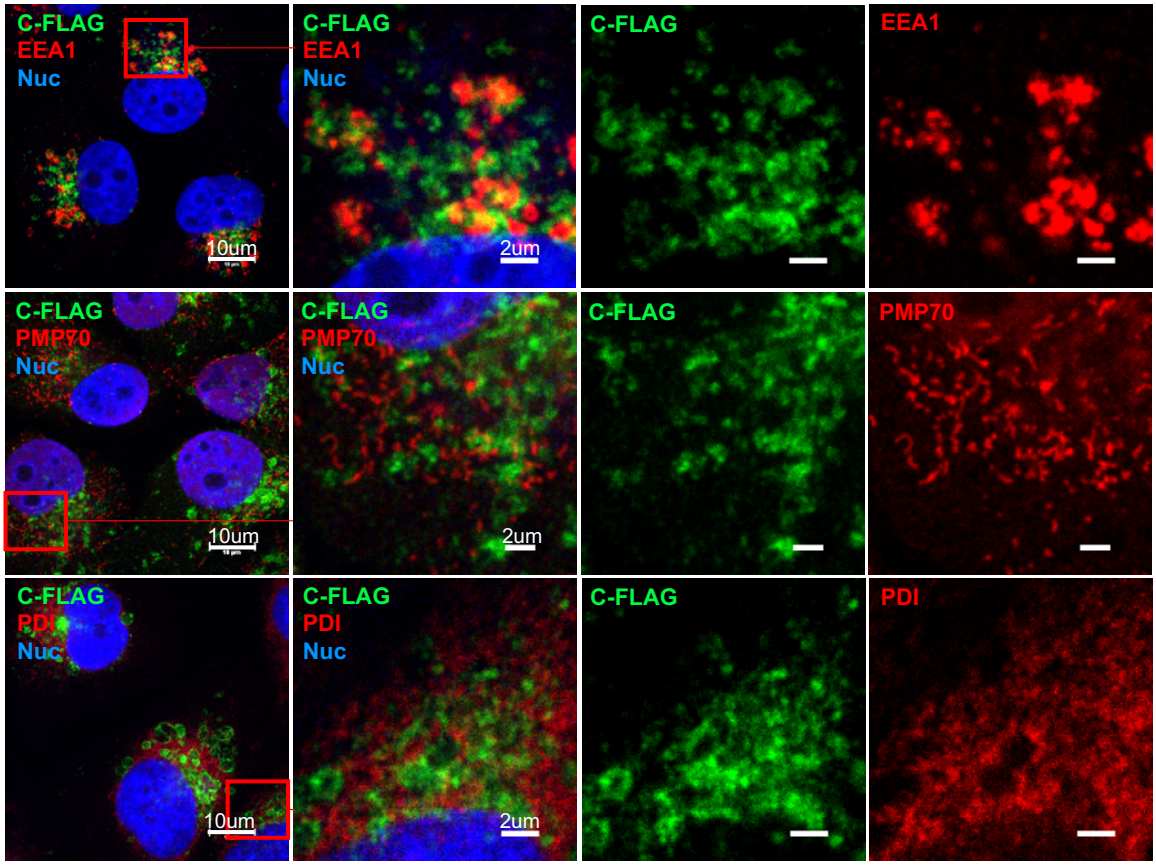

Figure S6. Assay of co-localization of GLUT8 with markers of early endosomes, peroxisomes and endoplasmic reticulum. C-terminal FLAG GLUT8 protein was visualized in MB231 cells (using anti-FLAG), together with the early endosomal marker EEA1, peroxisomal marker PMP70 or endoplasmic reticulum maker PDI.

Figure S7

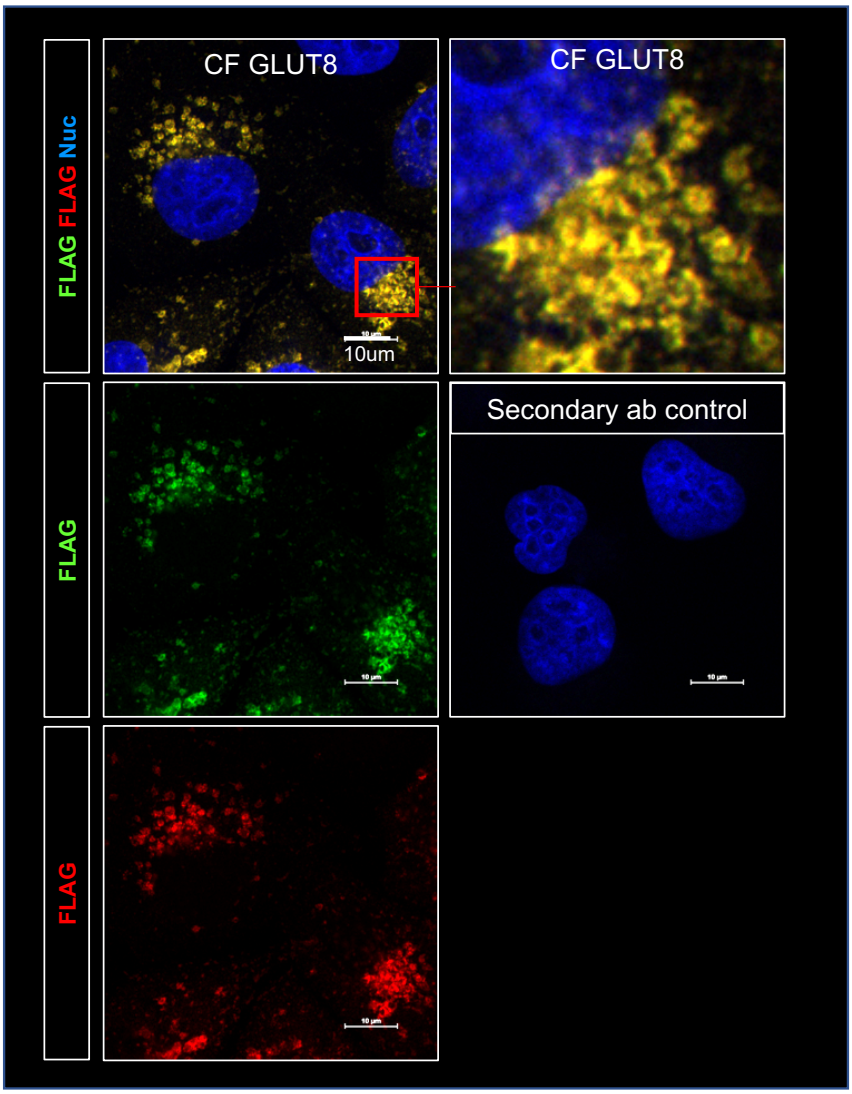

Figure S7. Evaluation of fidelity of diffraction of red and green light (test of chromatic aberration). C-terminal FLAG GLUT8 protein in MB231 cells was visualized after staining with primary anti-FLAG primary antibody and a mixture of anti-mouse secondary antibodies conjugated with Alexa^{488} (green) or Alexa^{546} (red).

Figure S8

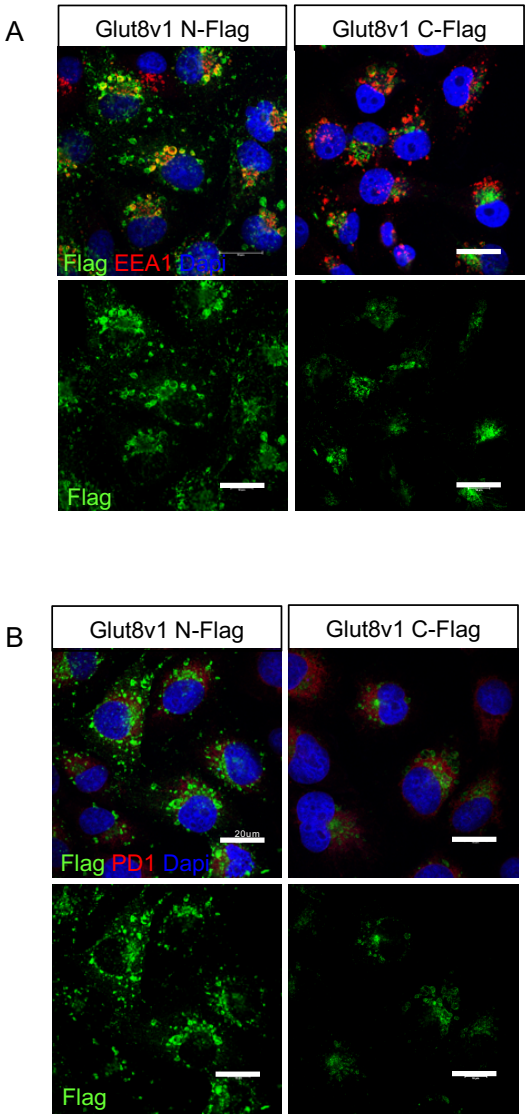

Figure S8. Immunostaining of FLAG suggests masking of C-terminal FLAG epitope. MB231 cells expressing either C-terminal or N-terminal FLAG tagged GLUT8 were stained with anti-FLAG, together with EEA1 (**A**) or PDI (**B**). Compare stain with the Western blotting data of Fig. 6A, which shows that N-FLAG and C-FLAG proteins are present in approximately equal amounts.

Chapter IV

GLUT inhibition and shRNA expression induce senescence in breast cancer cells

Joshua A. Martin, Ildiko Kasza,

and Caroline M. Alexander

Contributions: Figures 1, 2, 3, 4, 5 were performed by J. M. Figures 6, 7 and 8 were performed in collaboration with I. K. and J. M.

ABSTRACT

Actively dividing cells rely on glucose and other nutrients to provide sufficient energy and biosynthetic precursors for rapid cell division. Cellular glucose uptake is mediated by specialized transporters including the GLUT family of glucose transporters. We have previously shown that breast cancer cells express multiple GLUT isoforms, so we explored potential compensatory functions of two of the most prominently expressed isoforms, GLUT1 and GLUT8. To explore GLUT1 and GLUT8 function in breast cancer cells, we used lentiviral-based shRNA-mediated gene silencing and found that, interestingly, shRNA-mediated gene knockdown induced senescence in this cell type. This phenotype resembled the phenotype induced by treatment with the GLUT inhibitor WZB117. However, results from follow-up studies in which we attempted to rescue the observed phenotype by over-expressing the knocked down GLUT isoform, as well as studies involving expression of a control shRNA suggest that the shRNA-induced phenotype is not entirely explained by loss of GLUT expression alone. Thus, additional work is necessary to identify the mechanism underlying the non-specific shRNA-mediated induction of senescence in breast cancer cells.

INTRODUCTION

In cancerous cells, metabolic reprogramming occurs to meet the extensive demand for nutrients needed to support rapid cell division. Glucose, among other fuel sources, is an important component used to meet the demands of proliferating cells. One example of such reprogramming is the utilization of aerobic glycolysis by cancerous cells, a phenomenon otherwise known as the Warburg effect [1]. This process facilitates the conversion of glucose to pyruvate, providing the cell with ample glycolytic intermediates to support macromolecule biosynthesis. Glucose transporters (GLUTs) mediate the first step of this process by mediating ATP-independent transport of glucose across the cell membrane down a concentration gradient [2].

The purpose of this study was to determine if breast cancer cells require the expression of multiple glucose transporters to survive. Our studies focused on GLUT8 and GLUT1 specifically due to their relatively higher mRNA abundance compared to mRNA levels of other SLC2A family members as shown previously (Chapter 3). We found that the cellular response to disruption of glucose metabolism differs from that of inhibition of glucose uptake following exposure to the GLUT inhibitor WZB117. When GLUT8 or GLUT1 expression was knocked down using targeted shRNA constructs, we observed an induction of senescence, which is similar to what we observed following GLUT inhibition by WZB117. However, attempts to rescue the shRNA-induced phenotype suggest that the effect of the shRNAs was not entirely due to loss of GLUT expression alone. Additional experimentation revealed that expression of the non-targeting control TurboGFP shRNA also induced senescence. We propose additional work needs to be done to determine the specificity of shRNA effects in MB-231 cells.

RESULTS

Breast cancer cell lines require glucose for proliferation

To confirm the reliance of breast cancer cell lines on glucose for growth, we first cultured a panel of cell lines in various concentrations of extracellular glucose for a period of 72 hours (Figure 1A). All three cell lines tested demonstrated a definite requirement of extracellular glucose in the culture media for their growth. For the given starting cell density used for MDA-MB-231 (MB-231), MDA-MB-436 (MB-436), and T47D cells, the proliferation rate decreased for cells cultured in ≤10mM glucose compared to cells cultured in 25mM glucose media. Thus, at concentrations at or below 10mM, glucose availability limits growth of breast cancer cells. Differences in growth responses between the various cell lines are likely reflective of the doubling times and rates of glucose consumption of that specific cell line [3].

Given the fructose transport activity of GLUT8, we wanted to test whether fructose could substitute for glucose as the primary hexose source in the culture media [4-6]. To do this, we first dialyzed our fetal bovine serum to remove small molecules (3.5K molecular weight cut-off), including any potential carbon sources. We then added 1mM or 10mM of either glucose or fructose to glucose-free culture media. We cultured MB-231 cells for 72 hours to assess the effects of varying hexose sources on proliferation. Fructose availability alone as an energy source was not sufficient to support proliferation of MB-231 cells. Growth curves for both fructose concentrations (1mM and 10mM) paralleled the lack of proliferation in cells cultured in serum alone without glucose or any other hexose source. Cells cultured in 10mM glucose with either normal serum or dialyzed serum doubled nearly every 24 hours, which demonstrates that serum dialysis does not

strip away any necessary growth-promoting factors, and that the concentration of extracellular glucose alone is the sole determinant of proliferation in our culture system (Figure 1B).

Given the reliance of MB-231 cells on extracellular glucose, we suspected that growth of these cells would also be susceptible to inhibition by glucose transport inhibitors. To test this, we treated MB-231 cells with the GLUT inhibitor WZB117 [7]. Treatment with increasing concentrations of WZB117 demonstrated a dose-dependent effect on cell number after 48 hours, and a 50% reduction in cell number at 30μM (Figure 4.1C). These results correspond to previously reported effects on growth of other cancer cell lines [7]. We confirmed WZB117(30μM) inhibited GLUT transport activity by measuring the uptake of the glucose analog H^3 2-deoxyglucose. 30μM WZB117 decreased glucose uptake by 40% in MB-231 cells (Figure 1C). Next, we explored the effect of the glucose analog and glucose metabolism inhibitor 2-deoxyglucose (2-DG) on growth of MB-231 cells. As expected, proliferation of MB-231 cells was inhibited in the presence of 2-DG in a dose-responsive manner, and a 50% reduction in cell number was observed following exposure to a 5mM dose for 48 hours (Figure 4.1D).

Previously, WZB117 was shown to cause cell cycle arrest and senescence in the A549 lung cancer cell line [7]. When we examined the induction of senescence using the three growth inhibitory conditions, WZB117(30μM), 2-DG(5mM), and low glucose, in MB-231 cells, WZB117 treatment induced senescence with approximately 25% of the cells staining positive for senescence-associated β-galactosidase activity (SA-βgal) (Figure 2A, B). To confirm that the length of exposure to the various growth inhibitory conditions was sufficient to induce senescence, we examined cell treated for 72-96 hours. MB-231

cells cultured in low glucose and 2-DG had near background levels of senescence at the timepoints measured, approximately 5% and 0.5%-1%, respectively.

Expression of GLUT targeting shRNA causes growth arrest

Given our previous results, we concluded that breast cancer cell lines are reliant on extracellular glucose for cell growth, and that inhibition of glucose uptake by WZB117 induces senescence. Previously, we identified the expression of multiple GLUT isoforms in breast cancer cells, therefore we sought to determine which of the expressed GLUTs, if any, are required for growth (Chapter 3). We used lentiviral-based shRNA-mediated knockdown of the two most abundant GLUTs from our cell line panel, GLUT1 and GLUT8 (Table 1), to examine the importance of these isoforms for cell growth. This approach also allowed us to test whether these GLUT isoforms serve any redundant functions in breast cancer cells. Targeting GLUT1 using two shRNAs, shGLUT1 550 and shGLUT1 768, resulted in growth arrest in MB-231 cells (Figure 3A). This result was expected given the previous result with WZB117, a known GLUT1 inhibitor. Interestingly, GLUT8 knockdown by two GLUT8-targeting shRNA, shGLUT8 122 and shGLUT8 180, also caused growth arrest (Figure 3B). This finding suggested the two GLUT species are not functionally redundant and that both are required for proliferation. During our knockdown studies, we noticed a discernable change in cellular morphology with our cultures containing round, larger, and flat cells when expressing GLUT1 or GLUT8 shRNAs. Therefore, we stained for SA-β-gal activity (Figure 3C) and found that within 6 days of transduction with lentiviral constructs expressing the two GLUT1 and two GLUT8 shRNA species, MB-231 cells were more than 50% positive for SA-β-gal. Background SA-β-gal staining determined based on expression of a scrambled shRNA control construct

showed that only 3% of cells exhibited positive staining. This result suggests that growth arrest by GLUT1 and GLUT8 shRNA expression was due to induction of senescence. Although the induction of senescence was more dramatic with GLUT knockdown versus WZB117 treatment, our results confirm that GLUT inhibition by either pharmacologic or genetic means induces senescence. The similarity in phenotypes observed following either knockdown of GLUT1 or GLUT8 suggests the two GLUT proteins do not play a compensatory role and are required for growth independently of each other.

Expression of shRNA-resistant GLUT constructs does not rescue growth arrest

We previously tested multiple commercially available antibodies to verify our GLUT8 targeting shRNAs are disrupting GLUT8 protein expression but found that none of the tested antibodies could detect knockdown or overexpression (or both) of GLUT8 in MB-231 cells (Chapter 3). Thus, in order to support our knockdown studies, we pursued multiple rescue strategies in order to attribute the observed senescence phenotype specifically to loss of GLUT8 expression. The first rescue strategy involved designing a GLUT8 shRNA that targets a region in the 3'UTR of endogenous GLUT8. Expression of this shRNA would not affect expression of exogenous GLUT8, which lacks the 3'UTR (Figure 4A). A stable MB-231 cell line that over-expresses GLUT8 without a 3'UTR was generated. The stable GLUT8 overexpression line was then transduced with the newly generated GLUT8 3'UTR-shRNAs. The GLUT8 overexpression line was then monitored for evidence of rescue of the growth phenotype. Cells over-expressing non-targetable GLUT8 displayed an abnormal cell morphology when transduced with either version of the GLUT8 3'UTR-shRNA. Interestingly, the same changes in cell morphology were also observed in the control cell line (cells stably transduced with an empty vector) (Figure

4B). Neither cell line was affected by transduction with the scrambled shRNA control. Despite expression of GLUT8 mRNA at levels approximately 100-fold higher than control, the expression construct failed to rescue the observed growth phenotype (Figure 4B).

We wondered whether the failure to rescue GLUT8 knockdown was a consequence of unexpected off-target effects from the UTR-targeted shRNAs, or a result of requirement of the 3'UTR for appropriate translation of the GLUT8 transcript, which is similar to what has been shown for the channel protein hERG [8]. To address these possibilities, we designed a GLUT8 mRNA (referred to as GLUT8 DR180) that would be resistant to knockdown by shGLUT8 180 expression. This alternative shRNA construct was generated by introducing 3 synonymous point mutations in the shRNA binding sequence of the mRNA (Figure 4C). This approach allowed us to express a GLUT8 mRNA that contains both the 5' and 3' UTRs to rescue the GLUT8 knockdown phenotype. We generated stable MB-231 cells expressing the GLUT8 DR180 construct. We then transduced these cells with the shGLUT8 180-containing lentivirus using our standard protocol and examined the effect of the shRNA on mRNA expression levels and on overall cell proliferation. The GLUT8 DR180 construct was overexpressed 100-fold compared to the Empty Vector control when infected with the non-targeting Scrambled shRNA control (Figure 4D). While the GLUT8 DR180 line had a reduction in total mRNA when transduced with shGLUT8 180, overall GLUT8 expression remained more than 50-fold higher than the control cell line. Despite the robust residual expression of GLUT8 mRNA in our stable GLUT8 DR180 line, the rescue construct was unable to overcome the effect of the GLUT8 targeting shRNA (Figure 4D). Thus, proliferation was static in the

knockdown cell lines and the GLUT8 DR180 over-expressing cell lines remained susceptible to the effects of shRNA-mediated knockdown.

Given the failure of stable GLUT8 DR180 expression to rescue knockdown, we considered the possibility that the relatively high level of expression of GLUT8 from our overexpression lines was disrupting post-translational modifications and/or localization of GLUT8. To address this possibility, we adapted our GLUT8 DR180 construct to an inducible system to allow controlled, low-level expression. We confirmed inducible mRNA expression from our GLUT8 inducible construct by RT-qPCR (Figure 5C). We determined doxycycline treatment for 24 hours induced expression 2 to 14-fold above endogenous levels depending on doxycycline concentration therefore we used 6.25ng/mL to 25.0ng/mL doxycycline to induce expression during the rescue experiment. The rescue was performed by inducing expression of GLUT8 DR180 with doxycycline for 24 hours. The cells were transduced with GLUT8 shRNA, and then we examined the effect of GLUT8 shRNA on cell growth. To verify that expression of GLUT8 from our GLUT8 DR180 construct was resistant to shGLUT8 180 knockdown, we inserted a FLAG tag at the N-terminus of GLUT8 while keeping both the 5'UTR and 3'UTR intact (Figure 5A). Upon examination of whole protein lysates from induced GLUT8 DR180 cells that were transduced with shGLUT8 180, we showed that the degradation-resistant construct worked to protect transgenic expression of GLUT8 (Figure 5B). Despite achieving GLUT8 expression levels that were significantly higher than endogenous GLUT8 levels, the expression of shGLUT8 180 still induced growth arrest in the newly generated inducible cell lines (Figure 5B).

To exclude the possibility that the N-terminal FLAG tag was somehow disrupting GLUT8 function, we tested an untagged version of the GLUT8 DR180 construct. Once again, we induced expression of GLUT8 with doxycycline and then transduced with the GLUT8-targeting shRNA. Expression of the untagged GLUT8 DR180 did not rescue proliferation either. Thus, there was a 70-80% reduction in cell number of shGLUT8 180-transduced cells compared to the Scrambled control shRNA-transduced cells 48 hours post-transduction (Figure 5D).

Our conclusions about levels of GLUT8 protein expression following introduction of the various rescue constructs were compromised by the lack of a reliable antibody for detection, and the fact that GLUT8 function cannot be reliably evaluated solely by investigating glucose uptake. Thus, we turned to the study of GLUT1, a much better characterized GLUT isoform. Experimentation with GLUT1 provided an advantage over GLUT8 due to the existence of reliable antibodies to monitor expression and the lack of expression of any known splice variants. Thus, we generated two inducible GLUT1 over-expressing MB-231 cell lines, GLUT1 DR500 and GLUT1 DR768, each with synonymous point mutations in the binding sequence of one of the shRNAs used for knockdown, shGLUT1 550 or shGLUT1 768. GLUT1 expression was induced with doxycycline for 24 hours, then the cells were transduced with GLUT1 shRNA. As designed, the amount of transgenic GLUT1 protein was not affected by the introduction of GLUT1 shRNA. However, the production of transgenic protein was unable to rescue growth arrest (Figure 6B, C).

Interestingly, we noticed the pattern of GLUT1 expression by the inducible constructs was higher than endogenous protein (Figure 6A and B). We suspected the

expression vector (pLVX) was directing the synthesis of incorrectly processed GLUT1, and that was contributing to the lack of rescue of GLUT1-associated function in knockdown cells. A previous study showed a Western blot of correctly processed and functional exogenous GLUT1, therefore we redesigned GLUT1 expression vectors using the same retroviral backbone, pQCXIP, that was used in the study [9]. We verified that the band for over-expressed GLUT1 in both GLUT1 DR550 and GLUT1 DR768 cell lines had the expected size (Figure 7A). We transduced the stable GLUT1 overexpression and Empty Vector cell lines with either scrambled shRNA, shGLUT1 550, or shGLUT1 768 lentivirus and examined the effect of shRNA-mediated knockdown on cell proliferation. Once again, we found that expression of degradation resistant GLUT1 was unable to rescue growth arrest (Figure 7B). GLUT1, unlike GLUT8, is a mediator of extracellular glucose uptake in MB-231 cells (Chapter 3) providing us a reliable functional test for GLUT1 expression. Thus, we examined 2-deoxyglucose uptake in stable GLUT1 550DR or GLUT1 768DR cells that expressed GLUT1 shRNA. We found both shRNA resistant forms of transgenic GLUT1 maintain 98% and 70%, respectively, the amount of glucose uptake as the Empty Vector condition when GLUT1 shRNA are expression (Figure 7C). Our rescue strategy does in fact restore glucose uptake activity but does not rescue the growth arrest phenotype. This finding suggests that the effect of the shRNAs we have tested on MB-231 cells is potentially an off-target effect that cannot be attributed to the loss of the targeted glucose transporter alone.

To address this issue, we decided to increase the number of control shRNA species used. Our knockdown studies thus far have utilized a single scrambled shRNA control while we have tested 2-4 shRNAs specific to each GLUT isoform. Control

shRNA/siRNA are sequences that are designed without a complementary mRNA in any known gene, or to target genes that are not endogenously expressed. These controls test for effects of viral infection, introduction of foreign RNA or DNA species, effects on endogenous bioprocessing of microRNA and activation of innate immune responses. We tested two additional control shRNAs, one that does not target any known mammalian genes and one that targets TurboGFP (Table 1). We then assessed cell proliferation and stained for the induction of senescence. Surprisingly, we found that expression of TurboGFP shRNA caused a reduction in cell proliferation and induced senescence, while the non-mammalian targeting shRNA had no detectable effect (Figure 8A and B). To address the possibility that the multiplicity of infection (MOI) of our control constructs was not well matched, we titered the virus supernatants and performed additional transductions at the MOI of 1 and 5. We then analyzed proliferation and stained for senescence. At both MOIs, 1 and 5, TurboGFP shRNA decreased proliferation relative to non-transduced parental MB-231 cells over 72 hours by 25% and 70%, respectively (Figure 8C). The cells treated with Non-Mammalian shRNA cells grew at nearly the same rate as the parental cells with the MOI of 5 condition having 20% more after 72 hours showing the lentiviral transduction alone does not inhibit proliferation. We found that regardless of the MOI used, TurboGFP shRNA transduction induced cell senescence (Figure 8D). We conclude that out of three scramble sequences used as controls, one induced senescence in a way that resembled specific anti-GLUT shRNAs.

DISCUSSION

In this study we sought to understand the effect of inhibition of glucose uptake inhibition on breast cancer cells and whether the expression of multiple glucose transporters allowed for compensation when individual GLUT species were inhibited. To do this we utilized multiple strategies to interrogate the reliance of MB-231 cells on glucose and glucose transport. We found that, when treated with the GLUT inhibitor WZB117, growth of MB-231 cells was inhibited and 30% of the cells became senescent within 72 hours. Unlike WZB117 treatment, when we cultured the cells in media without glucose or in media containing the glucose analog 2-DG proliferation was inhibited but senescence was not induced. The lack of proliferation without the coinciding senescence induction could be due to apoptosis or cell cycle arrest resulting from low glucose or 2-DG treatments which could be tested in the future. 2-DG is a known inducer of apoptosis in breast cancer cell lines [10]. One explanation for the difference might be by the degree to which glucose uptake and ultimately glucose metabolism is inhibited. While we found WZB117 treatment at 30μM resulted in a 40% reduction in glucose uptake it is possible both the low glucose and 2-DG treatments used have a more potent effect on glucose metabolism, low glucose by exhausting the extracellular supply and 2-DG by indirectly inhibiting glucose uptake by blocking glycolysis. Examining the effect of higher concentrations of WZB117 on senescence induction could help explain this difference in response.

Our initial genetic studies to knockdown expression of the GLUT transporters GLUT8 and GLUT1 proved promising when we were able to phenocopy treatment with WZB117. We tested multiple commercial GLUT8 antibodies for specific GLUT8 detection

and none proved to be suitable (Chapter 3); as an alternative strategy we sought to rescue the shRNA-associated growth phenotype through ectopic expression of GLUT8 mRNAs designed to be resistant to shRNA activity. Multiple iterations of the GLUT8 rescue strategy failed to relieve the shRNA phenotype. To investigate this further, we shifted our focus to the study of GLUT1 to engage the antibody and functional tools available. Once again, we were unable to rescue the growth arrested phenotype with re-expression of a degradation resistant GLUT1. However, we successfully rescued glucose uptake. This result suggested the arrest of growth and induction of senescence were occurring due to off-target shRNA effects. To further validate our suspicions, we utilized two additional control shRNA, non-mammalian shRNA and turboGFP shRNA and surprisingly turboGFP also induced senescence and disrupted proliferation.

The non-specific induction of senescence by shRNA expression in MB-231 raises important questions about the use of RNAi tools to interrogate gene function and the importance of performing control experiments in which expression of the knocked down gene is rescued by transgenic expression to allow confident attribution of shRNA-induced phenotypes to the gene of interest. Use of shRNA to study GLUT8 function has been previously reported. Multiple studies examining GLUT8 function in the liver have used the same shRNA we are reporting on here shGLUT8 180, they however do not report cell growth assays [11], [4]. GLUT8 shRNA were also used to evaluate the significance of GLUT8 expression in multiple myeloma cells and these studies do report a reduction in cell viability however they were performed using different shRNA sequences then what we describe here [12]. It is possible this effect is cell line-specific and further studies will be needed to understand this phenomenon.

The use of RNAi is known to cause unintended off-target effects. These effects fall into three categories: first being unintended mRNA silencing due to sequence complementarity[13]; second overwhelming the endogenous miRNA processing pathway [14]; and the third is activation of innate immune response due to either recognition of dsRNA or the method of RNAi introduction [15]. Studies performed to examine the off-target effects of siRNA have shown that sequence complementarity specifically within the seed sequence can be predictive of potential off-target inhibition and full-sequence blast analyses of entire 19-mer siRNA sequences are not sufficient to predict potential off-target mRNAs[13]. It is possible that our senescence-inducing shRNAs are targeting similar genes or pathways that themselves are involved in induction of senescence. Identification of these genes could be useful in understanding why MB-231 cells are sensitive to shRNA expression.

It is unlikely our shRNA effect is the result of overwhelming the endogenous miRNA processing machinery. To control for this possibility, we employed the use of two separate non-specific shRNA, scrambled shRNA and non-mammalian shRNA. Their expression did not result in any adverse phenotypes. It is possible these two controls have flaws in their design which results in them either being non-expressive or non-participatory in the endogenous bioprocessing. Additional shRNAs that target innocuous genes and could be tested to demonstrate active shRNA function would alleviate this concern.

Use of multiple shRNAs is the minimal standard for functional genetic studies with RNAi. Each shRNA should have unique seed sequences so that any observed common phenotypes from different shRNA can be confidently assigned to the target gene of

interest. The gold standard for confirmation of phenotypes is the genetic rescue, which we have performed using multiple strategies on different genes, yet we are able to rescue glucose uptake but unable to rescue senescence. Although the percentage of senescence cells decreased with the MOI used for transduction, at a MOI of 1 a significant portion (20%) of the cell population was senescent. This means, at least with this cell line, shRNA expression is likely to produce an undesired or off-target phenotype. Use of alternative expression systems such as inducible or a system containing a weaker promoter might help alleviate the undesired affects however these alternatives will have the trade-off of lower levels of target gene knockdown. Alternatively, use of siRNA or CRISPR to study gene function may be beneficial, nonetheless rescue studies are recommended to provide support for the function of that gene.

MATERIAL AND METHODS

Cell Lines and Culture

All cell lines were cultured in a humidity controlled, 37°C incubator in 5% CO_2. MB-231 (MB-231) and MDA-MB-436 (MB-436) stocks were maintained in complete media defined as follows: DMEM with 4.5g/L glucose (Gibco, cat# 11965), 5% fetal bovine serum (FBS; VWR, cat# 89510-194), and 1% penicillin/streptomycin (Gibco, cat# 15140122). T47D cells were maintained in RPMI 1640 (Gibco, cat# 11875), 10% fetal bovine serum, and 1% penicillin/streptomycin. HEK293T/17 (293T) cells were maintained in DMEM with 1.0g/L glucose, sodium pyruvate, and HEPES (Gibco cat# 12320032), 5% FBS, and 1% PenStrep. FBS was dialyzed using a 3.5k MWCO membrane in PBS overnight exchanging the PBS once during this period. After dialysis the FBS was then sterile filtered using a 0.45μM filter. Dialyzed FBS was used at a final concentration of 5% in DMEM (Gibco, cat #11966) lacking glucose.

Virus Preparation and Cell Line Transductions

Lentiviral constructs (overexpression and shRNA) were packaged in 293T cells by co-transfection with psPAX2 (Addgene cat# 12260), pMD2.G (Addgene cat# 12259), and transgene-containing plasmid using Lipofectamine LTX (Invitrogen, cat# 15338100). Supernatants were harvested and filtered using 0.45μm sterile filters. Cells were transduced by combining 0.5mL of viral supernatant with $1.0x10^5$cells and 9.6ug/mL polybrene (Sigma-Aldrich, cat# 107689). After 48hrs infected cells were selected with 1.6μg/mL puromycin (Sigma-Aldrich, cat# P9620). For inducible cells lines, sequential transduction was performed first using lentiviral supernatants containing the pLVX Tet3G-neo vector (Clontech). Clones were generated using G418 selection and screened for

doxycycline-inducible activity. Suitable clones were then transduced a second time with lentiviral supernatants containg the pLVX TRE3G-puro vector (Clontech), which included the expression cassette for the gene of interest. Finally, infected cells were selected by puromycin.

Retroviral constructs were packaged in 293T cells by transfecting pQCXIP (Clontech) with pMD.Gag-Pol [16] and pVSVG [17] packaging plasmids using Lipofectamine LTX (Invitrogen, cat# 15338100). Supernatants were harvested and filtered using 0.45μm sterile filters. Transduction by retrovirus was performed by spinoculation; briefly, 1mL of viral supernatant was combined with $2.0x10^5$ cells followed by a 2-hour centrifugation at 1200g at room temperature. The cells were then resuspended in media and plated. After 48 hours, infected cells were selected using 1.6μg/mL puromycin (Sigma-Aldrich, cat# P9620).

Lentiviral titers were determined by transducing 1.0×10^5 cells with either 100μL, 10μL, or 1μL of viral supernatant. The following day, the transduced cells from each dilution were re-plated dividing 80%, 10%, and 1% of the cells into separate 10cm dishes. 48-hours after transduction, cells were selected using puromycin. The selected cells were cultured for 7-10 days and colonies were counted to determine the number of infectious units/mL (IU/mL).

Lentiviral shRNA constructs

Human GLUT8 shRNA clones TRCN0000300122 and TRCN0000300180 and human GLUT1 clones TRCN0000418550 and TRCN0000424768 were purchased from Sigma-Aldrich. Three control non-targeting shRNAs were used, scrambled shRNA (Addgene, cat# 1864), Non-mammalian shRNA control (Sigma-Aldrich, cat# SHC202),

and TurboGFP shRNA control (Sigma-Aldrich, cat# SHC204). We designed the following two GLUT8 shRNAs to target the 3'UTR for rescue studies: shGLUT8 UTR-1 (sense sequence GCCTTATCGGGAAGGAAATTT) and shGLUT8 UTR-2 (sense sequence CCCTCCATGCGCAAGACTAAA).

Generation of GLUT8 expression constructs

GLUT8 expression constructs were generated from GLUT8 clone 4641145 (Accession#BC019043; Dharmacon, cat# MHS6278-202832055). The lentiviral construct containing GLUT8 without the 3' UTR were produced as follows. GLUT8 cDNA was amplified by PCR (Forward primer 5'-CTGCTGTCTAGAGGCGGTTCAGGCG-3' and Reverse primer 5'-CGCGGGCGCGCCTCATCGCCCCTCAAAA-3') then subcloned into pLenti-E1falpha by using XbaI and AscI restriction enzymes. The lentiviral GLUT8 expression construct containing portions of the 5' and 3'UTRs was generated by PCR amplification (Forward primer 5'-CTGCTGTCTAGAGGCGGTTCAGGCG-3' and Reverse primer 5'-CGCGGGCGCGCCGGTTTGTTTTTTTTTGCTGTTTATT-3') then subcloned into pLenti-E1falpha by using XbaI and AscI restriction enzymes. A GLUT8 version that was non-degradable by GLUT8 sh180 was generated with synonymous mutations introduced into 3 sites by performing mutagenesis using the primer 5'-CTCCCTCATGCTGCTTCTGATGTGTTTTATGCCCGAGACCCC-3'. Mutagenesis PCR reaction products were treated with DpnI and then transformed in Stbl3 *E. coli*, and clones were screened by sequencing to confirm accuracy. All cloning was performed using Q5 polymerase (NEB, cat# M0491).

The inducible GLUT8 expression construct containing portions of the 5' and 3'UTRs was generated by PCR amplification (Forward primer 5'-CTGCTGGGAT

CCGGCGGTTCAGGCG-3’ and Reverse primer 5’-CTGCTGGAATTCGGTTTGTTTTTT TTTGCTGTTTATT-3’), then digested and subcloned between the BamHI and EcoRI sites of pLVX TRE3G (Clontech). A non-degradable GLUT8 sh180 version used in this manuscript was generated as described previously using mutagenesis PCR.

The retroviral GLUT8 expression construct (pQCXIP puromycin^R backbone) containing portions of the 5’ and 3’UTRs was generated by PCR amplification (Forward Primer 5’-CTGCTGGGATCCGGCGGTTCAGGCG-3’ and Reverse Primer 5’-CTGCTGGAATTCGGTTTGTTTTTTTTTGCTGTTTATT), then digested and subcloned between the BamHI and EcoRI sites of pQCXIP. A non-degradable GLUT8 sh180 version used in this manuscript was generated as described previously.

To insert a FLAG tag into the N-terminus of GLUT8, the plasmid was amplified with the primer 5’-GGCCGCCGACATGGATTATAAAGATGATGATGATAAAACGCCCGAGG ACC-3’. Amplification was performed as described previously for mutagenesis.

Generation of GLUT1 expression constructs

GLUT1 expression constructs were generated from GLUT1 clone# 40085220 (Genbank#BC21804; Dharmacon, cat #MHS6278-211690539). The inducible GLUT1 expression construct (pLVX TRE3G, Clontech) was generated by amplifying the GLUT1 ORF using the Forward Primer 5’-CTGCTGGGATCCATGGAGCCCAGCAG-3’ and Reverse Primer 5’-CTGCTGCCCGGGTCACACTTGGGAATCAG-3’. The PCR product was then digested and subcloned between the BamHI and XmaI sites of pLVX.

The retroviral GLUT1 expression construct (pQCXIP puromycin^R backbone) was generated by amplifying the GLUT1 ORF using the Forward Primer 5’-CTGCTGGCGGCCGCATGGAGCCCAGCA-3’ and Reverse Primer 5’-

CTGCTGGGATCCTCACACTTGGGAATCAG-3'. The PCR product was then digested and subcloned between the NotI and BamHI sites of pQCXIP.

Non-degradable GLUT1 expression constructs (GLUT1 550DR and GLUT1 768DR) were generated with synonymous mutations introduced by mutagenesis using the primers 5'-TACCCCGGATGTCCTATCTTAGTATTGTTGCGATTTTCGGCTTT GTGG CCTTCTTTG-3' for shGLUT1 550 or 5'-GCCTGTGTATGCCACCATCGGTTCTG GCATTGTTAATACGGCCTTCACTGTCG-3' for shGLUT1 786. All constructs were sequenced to confirm accuracy.

Assay of Cell Number

Cell number assays were performed using FluoReporter Blue Fluorometric dsDNA quantitation kit (Molecular Probes cat# F2962). Prior to quantification, cell lines were seeded in 24-well plate at $1.5x10^4$-$2.5x10^4$ cells per well. At the experimental endpoint, the plates were washed briefly in PBS and frozen at -80^{o}C. The plates were then thawed and 200µl of water was added to each well followed by 1-hour incubation at room temperature. Cell lysis was completed by freezing the plates again at -80^{o}C. The plates where thawed and 100µl of the cell lysate was transferred to black well 96-well plates, and 100µl of Hoechst 33258 diluted in TNE buffer was added. Fluorescent values were then obtained using the ClarioStar fluorescent plate reader (UW small molecule screening facility) at Ex/Em 346nm/460nm.

To test the effect of small molecule inhibitors on proliferation, MB-231 cells were plated in triplicate and cultured overnight. The following day, the cells were washed in PBS and then cultured in either WZB117 (Sigma-Aldrich) or 2-deoxyglucose (2-DG) (Sigma-Aldrich) in complete media at the indicated concentrations for 48hrs. Low Glucose

media conditions are as follows: DMEM without glucose (Gibco, cat# 11966) and 5% FBS (FBS is the only glucose source provided). To test the requirement for either glucose or fructose for cell growth, cells were plated in triplicate cultures in complete media overnight. The following day, the cells were washed in PBS and then cultured in DMEM without glucose (Gibco, cat# 11966) containing 5% FBS with glucose or fructose added at the final concentrations indicated. 5% dialyzed FBS was used for the assay to examine growth in the presence of fructose. To assay the effect of shRNA knockdown, cells were plated in triplicate 4 days after transduction with lentiviral shRNA constructs. All assays were performed with three independent replicates unless indicated in the figure legend.

Assay of Senescence by ß-Galactosidase staining

Senescence was assayed using the Senescence ß-Galactosidase staining kit (Cell Signaling Ref 9860) according to the manufacturer's protocol. Briefly, cells were seeded ($2.5x10^4$ or $5.0x10^4$ cells/well) in chamber slides and incubated for at least 48hrs before staining. To assay the effect of inhibitors or low glucose culture on senescence, cells were plated in chamber slide in either standard culture media containing 30μM WZB117 or 5mM 2-DG; or in low Glucose media as defined previously. To assay the effect of shRNA knockdown, cells were plated 4 days after transduction with lentiviral shRNA constructs and assayed after 48 hours. Quantification was performed by counting 500 to 1000 cells per condition. All assays were performed with three independent replicates unless indicated in the figure legend.

Glucose Uptake assays

Glucose uptake was assayed using two methods as indicated in the results and figure legends. To examine the effect of WZB117 on glucose uptake, cells were assayed

using 1.0mCi/mL H^3 2-deoxy-D-glucose (Perkin Elmer, cat# NET549A). Cells were plated in triplicate at $2.5x10^4$ cells per well in 24-well plates in complete media and incubated in a 37^{o}C incubator overnight. The following day, the cells were washed in PBS, and media was replaced with DMEM (Gibco, cat# #11966) lacking glucose supplemented with 5% FBS and containing either 30μM WZB117 or DMSO (vehicle) and incubated for 10 minutes at 37^{o}C. Afterwards, 2μCi/well of H^3 2-deoxy-D-glucose was added (yielding a final concentration of 4μCi/mL of media) and then incubated for 30min. Following the 30min incubation, glucose analog uptake was halted by washing the cells in ice-cold PBS. Cells were then lysed in 400μL of 10mM Tris-Cl (pH 8.0) with 0.1% SDS. The cell lysates were then transferred into liquid scintillation vials and radioactivity was assay by liquid scintillation. Normalization of radioactivity by cell number was performed by plating an additional plate in parallel and assessing cell number by FluoReporter assay as previously described.

To examine the effect of shRNA-mediated knockdown of GLUTs and subsequent rescue of GLUT expression on glucose uptake, acute glucose uptake was also assayed using Glucose Uptake-Glo Assay (Promega, cat# J1341). Cells were plated in triplicate in 96-well plates and incubated overnight. The assay was then performed according to manufacturer's instructions. Luminescence was assessed using the PheraStar Plate reader (UW small molecule screening facility). Normalization of uptake by cell number was performed by plating an additional plate in parallel and assessing cell number by FluoReporter assay as previously described.

Western Blotting

Proteins were analyzed by SDS-PAGE with Western blotting as follows. Cells were lysed in RIPA lysis buffer (25 mM Tris-Cl pH7.4, 150 mM NaCl, 1% Triton X-100, 1% Sodium Deoxycholate, 0.1% Sodium Dodecyl Sulfate) with the addition of Halt Protease Inhibitor (Pierce, cat# 78430) and Halt Phosphatase Inhibitor (Pierce, cat# 78428) for 10 minutes at 4^{o}C on a rocker. Lysates were cleared, protein concentration assayed, and proteins separated by SDS-PAGE from 10-20μg of protein lysates. Proteins were then transferred to polyvinyl difluoride (PVDF) membranes. PVDF membrane were then blocked in 5% dry milk in tris buffered sulfate with 0.1% Tween-20. Antibodies used in this study included Flag-M2 (Sigma, cat# F3165), Vinculin (Millipore, cat# 05-386), and anti-GLUT1 (a generous gift of Dr. Steven M. Anderson, University of Colorado-Denver).

Quantitative Real-Time PCR

RNA was isolated from cultured cells using the RNeasy Mini Kit according to instructions (Qiagen, cat# 74104). cDNA was prepared using QuantiTect Reverse Transcription Kit (Qiagen, cat# 205311) and RT-qPCR was performed as previously described [18] using Sybr Select Master Mix (Applied Biosystem, cat# 4472918). Relative gene expression was determined using the comparative $\Delta\Delta$Ct method. The following primers were used: HRPT: forward, 5'-CCTCATGGACTGATTATGGACAG-3'; reverse, 5'-AATCCAGCAGGTCAGCAAAG-3'; YWHAZ: forward, 5'-AAGACAGCACGCTAATAATGC-3'; reverse, 5'-TTGGAAGGCCGGTTAATTTTC-3'; GLUT8: forward, 5'-ACGAACCAGGAGCACAGTGAAG-3'; reverse 5'-GATCTCTGACATGAGGAGCCAG-3'; GLUT1: forward, 5'-TTGCAGGCTTCTCCAACTGGAC-3'; reverse 5'-ACGAACCAGGAGCACAGTGAAG-3'.

REFERENCES

1. Vander Heiden, M.G., L.C. Cantley, and C.B. Thompson, *Understanding the Warburg effect: the metabolic requirements of cell proliferation.* Science, 2009. **324**(5930): p. 1029-33.

2. Mueckler, M. and B. Thorens, *The SLC2 (GLUT) family of membrane transporters.* Mol Aspects Med, 2013. **34**(2-3): p. 121-38.

3. Timmerman, L.A., et al., *Glutamine sensitivity analysis identifies the xCT antiporter as a common triple-negative breast tumor therapeutic target.* Cancer Cell, 2013. **24**(4): p. 450-65.

4. Debosch, B.J., et al., *Glucose transporter 8 (GLUT8) mediates fructose-induced de novo lipogenesis and macrosteatosis.* J Biol Chem, 2014. **289**(16): p. 10989-98.

5. Ibberson, M., M. Uldry, and B. Thorens, *GLUTX1, a novel mammalian glucose transporter expressed in the central nervous system and insulin-sensitive tissues.* J Biol Chem, 2000. **275**(7): p. 4607-12.

6. Corpe, C.P., et al., *Intestinal dehydroascorbic acid (DHA) transport mediated by the facilitative sugar transporters, GLUT2 and GLUT8.* J Biol Chem, 2013. **288**(13): p. 9092-101.

7. Liu, Y., et al., *A small-molecule inhibitor of glucose transporter 1 downregulates glycolysis, induces cell-cycle arrest, and inhibits cancer cell growth in vitro and in vivo.* Mol Cancer Ther, 2012. **11**(8): p. 1672-82.

8. Liu, F., et al., *Cotranslational association of mRNA encoding subunits of heteromeric ion channels.* Proc Natl Acad Sci U S A, 2016. **113**(17): p. 4859-64.

9. Young, C.D., et al., *Modulation of glucose transporter 1 (GLUT1) expression levels alters mouse mammary tumor cell growth in vitro and in vivo.* PLoS One, 2011. **6**(8): p. e23205.

10. Aft, R.L., F.W. Zhang, and D. Gius, *Evaluation of 2-deoxy-D-glucose as a chemotherapeutic agent: mechanism of cell death.* Br J Cancer, 2002. **87**(7): p. 805-12.

11. Mayer, A.L., et al., *SLC2A8 (GLUT8) is a mammalian trehalose transporter required for trehalose-induced autophagy.* Sci Rep, 2016. **6**: p. 38586.

12. McBrayer, S.K., et al., *Multiple myeloma exhibits novel dependence on GLUT4, GLUT8, and GLUT11: implications for glucose transporter-directed therapy.* Blood, 2012. **119**(20): p. 4686-97.

13. Birmingham, A., et al., *3' UTR seed matches, but not overall identity, are associated with RNAi off-targets.* Nature Methods, 2006. **3**(3): p. 199-204.

14. Jackson, A.L. and P.S. Linsley, *Recognizing and avoiding siRNA off-target effects for target identification and therapeutic application.* Nat Rev Drug Discov, 2010. **9**(1): p. 57-67.

15. Robbins, M., A. Judge, and I. MacLachlan, *siRNA and innate immunity.* Oligonucleotides, 2009. **19**(2): p. 89-102.

16. Ory, D.S., B.S. Neugeboren, and R.C. Mulligan, *A stable human-derived packaging cell line for production of high titer retrovirus/vesicular stomatitis virus G pseudotypes.* Proc. Natl. Acad. Sci. USA, 1996. **93**: p. 11400-11406.

17. Yee, J.K., et al., *A general method for the generation of high-titer, pantropic retroviral vectors: highly efficient infection of primary hepatocytes.* Proc Natl Acad Sci U S A, 1994. **91**(20): p. 9564-8.

18. Chin, E.N., et al., *Lrp5 Has a Wnt-Independent Role in Glucose Uptake and Growth for Mammary Epithelial Cells.* Mol Cell Biol, 2015. **36**(6): p. 871-85.

Table 1

shRNA name	Sense sequence (seed sequence in bold)	Source
Scrambled shRNA	CCTAAGGTTAAGTCGCCCTCG	Addgene #1864
Non-Mammalian shRNA Control	CAACAAGATGAAGAGCACCAA	Sigma Cat #SHC202
TurboGFP shRNA Control	CGTGATCTTCACCGACAAGAT	Sigma Cat #SHC204
shGLUT8 122	GCTCCTCATGTCAGAGATCTT	Sigma Clone TRCN0000300122
shGLUT8 180	GCTGCTTCTCATGTGCTTCAT	Sigma Clone TRCN0000300180
shGLUT8 UTR-1	GCCTTATCGGGAAGGAAATTT	Prepared In-house
shGLUT8 UTR-2	CCCTCCATGCGCAAGACTAAA	Prepared In-house
shGLUT1 550	TGAGCATCGTGGCCATCTTTG	Sigma Clone TRCN0000418550
shGLUT1 768	TTGGCTCCGGTATCGTCAACA	Sigma Clone TRCN0000424768

Figure 1

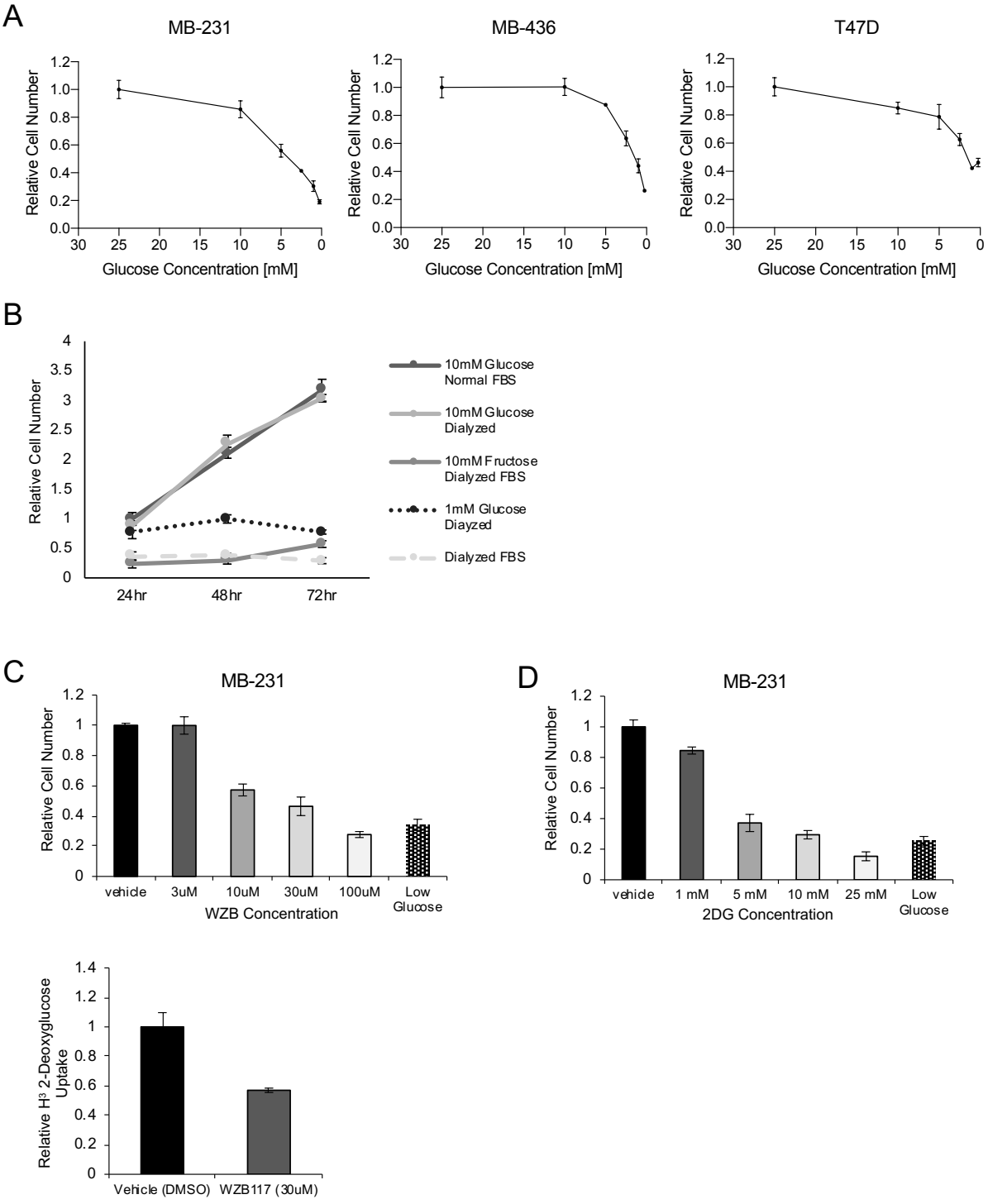
A
MB-231
MB-436
T47D
Relative Cell Number
Glucose Concentration [mM]
B
Relative Cell Number
24hr
48hr
72hr
10mM Glucose Normal FBS
10mM Glucose Dialyzed
10mM Fructose Dialyzed FBS
1mM Glucose Diayzed
Dialyzed FBS
C
MB-231
Relative Cell Number
vehicle
3uM
10uM
30uM
100uM
Low Glucose
WZB Concentration
Relative H³ 2-Deoxyglucose Uptake
Vehicle (DMSO)
WZB117 (30uM)
D
MB-231
Relative Cell Number
vehicle
1 mM
5 mM
10 mM
25 mM
Low Glucose
2DG Concentration

Figure 1. Breast cancer cell lines are dependent on glucose for growth A. Assay of cell proliferation while cultured over 72 hours in indicated amounts of glucose from 25mM to 0.25mM. The data is presented relative to the mean of the 25mM condition. **B.** Growth curve of MB-231 cells cultured in two different hexose sugars, glucose or fructose, for 72 hours. The data is presented relative to the mean of the 10mM Glucose in normal FBS at 24-hours. **C.** (top) MB-231 cells were cultured in increasing concentrations of the GLUT inhibitor WZB117 and relative the cell number was assessed after 48hrs. The data is presented relative to the mean of the vehicle condition; (bottom) the effect of WZB117(30μM) treatment on H^3 2-deoxyglucose uptake in MB-231 cells. The data is presented relative to the mean of the vehicle condition. **D.** MB-231 cells were culture in increasing concentration of the glucose metabolism inhibitor 2-deoxyglucose. The data is presented relative to the mean of the vehicle condition. Error bars indicate +/- SD

Figure 2

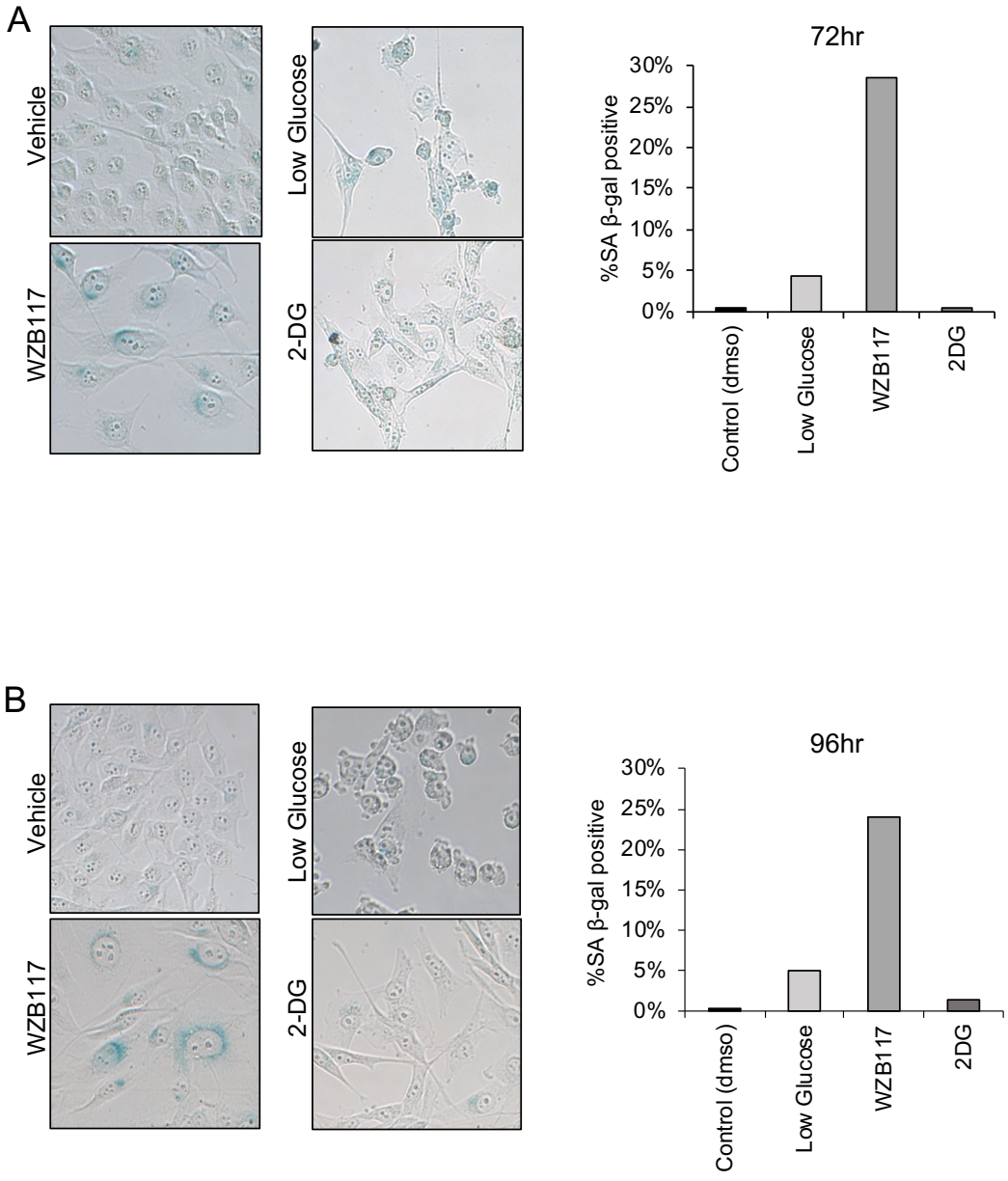

Figure 2. WZB117 induces senescence in MB-231 cells. A. Senescence-associated β-galactosidase staining of MB-231 cells cultured in reduced glucose media for 72 hours. N=1 **B.** Senescence-associated β-galactosidase staining of MB-231 cells cultured in reduced glucose media for 96 hours. N=1

Figure 3

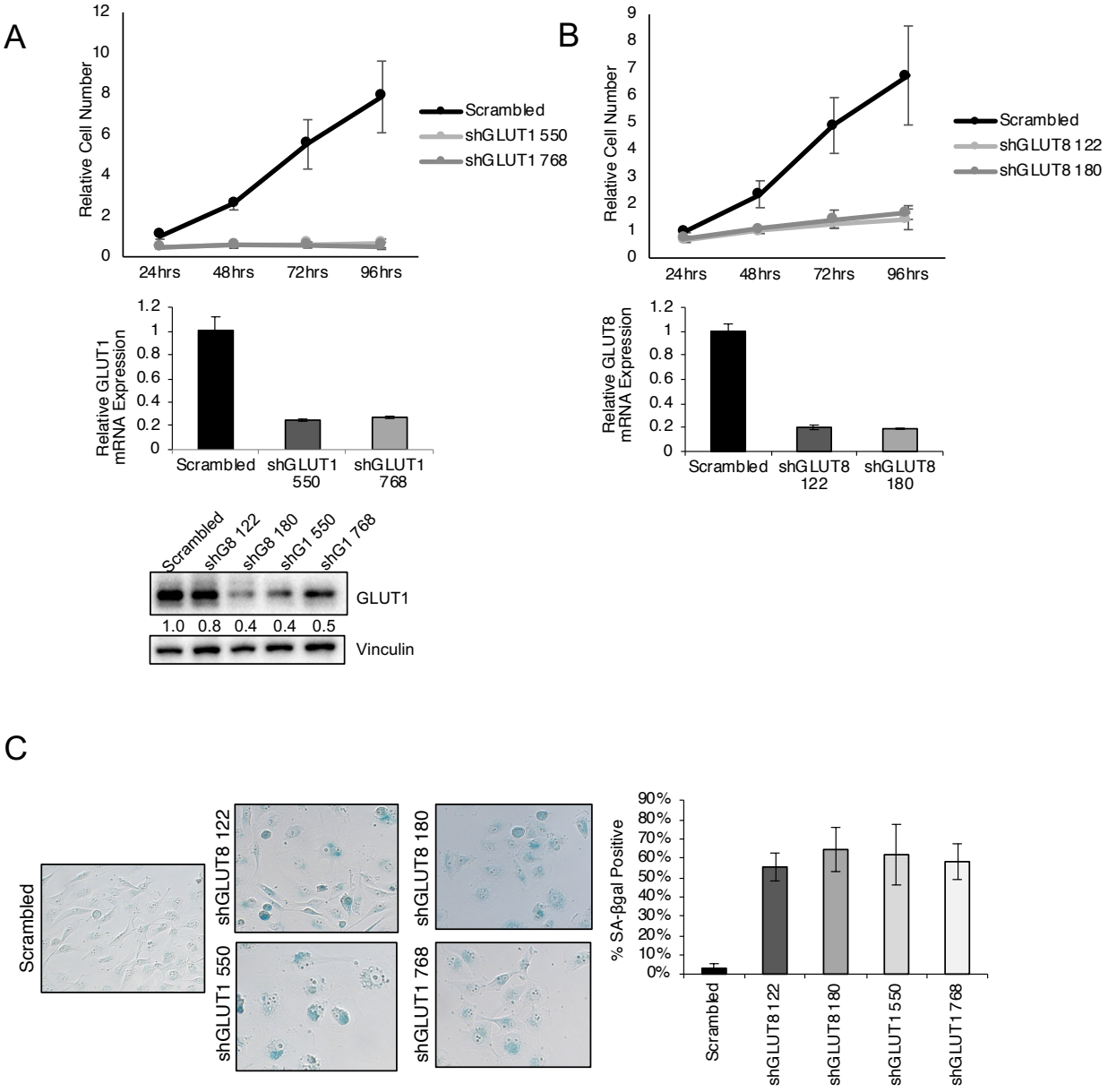
A
Relative Cell Number
12
10
8
6
4
2
0
24hrs
48hrs
72hrs
96hrs
Scrambled
shGLUT1 550
shGLUT1 768
Relative GLUT1 mRNA Expression
1.2
1
0.8
0.6
0.4
0.2
0
Scrambled
shGLUT1 550
shGLUT1 768
Scrambled
shG8 122
shG8 180
shG1 550
shG1 768
GLUT1
1.0 0.8 0.4 0.4 0.5
Vinculin
B
Relative Cell Number
9
8
7
6
5
4
3
2
1
0
24hrs
48hrs
72hrs
96hrs
Scrambled
shGLUT8 122
shGLUT8 180
Relative GLUT8 mRNA Expression
1.2
1
0.8
0.6
0.4
0.2
0
Scrambled
shGLUT8 122
shGLUT8 180
C
Scrambled
shGLUT8 122
shGLUT8 180
shGLUT1 550
shGLUT1 768
% SA-βgal Positive
90%
80%
70%
60%
50%
40%
30%
20%
10%
0%
Scrambled
shGLUT8 122
shGLUT8 180
shGLUT1 550
shGLUT1 768

Figure 3. Expression GLUT shRNA induces senescence in MB-231 cells. A. (top) Growth curve of MB-231 cells following shRNA-mediated knockdown of GLUT8. The data is presented as cell numbers relative to the mean of the scrambled condition at 24-hours (bottom) RT-qPCR analysis of GLUT8 knockdown by shRNA. Data shows GLUT8 mRNA levels following expression of GLUT8-specific shRNA versus scrambled shRNA control. **B.** (top) Growth curve of MB-231 cells after shRNA-mediated knockdown of GLUT1. The data is presented as relative to the mean of the scrambled condition at 24-hours (middle) RT-qPCR analysis of GLUT8 knockdown by shRNA to show expression of GLUT8 relative to scrambled shRNA control. (bottom) Western blot of lysates isolation from MB-231 cells to asses GLUT1 knockdown after transduction with GLUT shRNA lentivirus. **C.** Senescence-associated β-galactosidase staining of MB-231 cells after knockdown of GLUT8 or GLUT1.

Figure 4

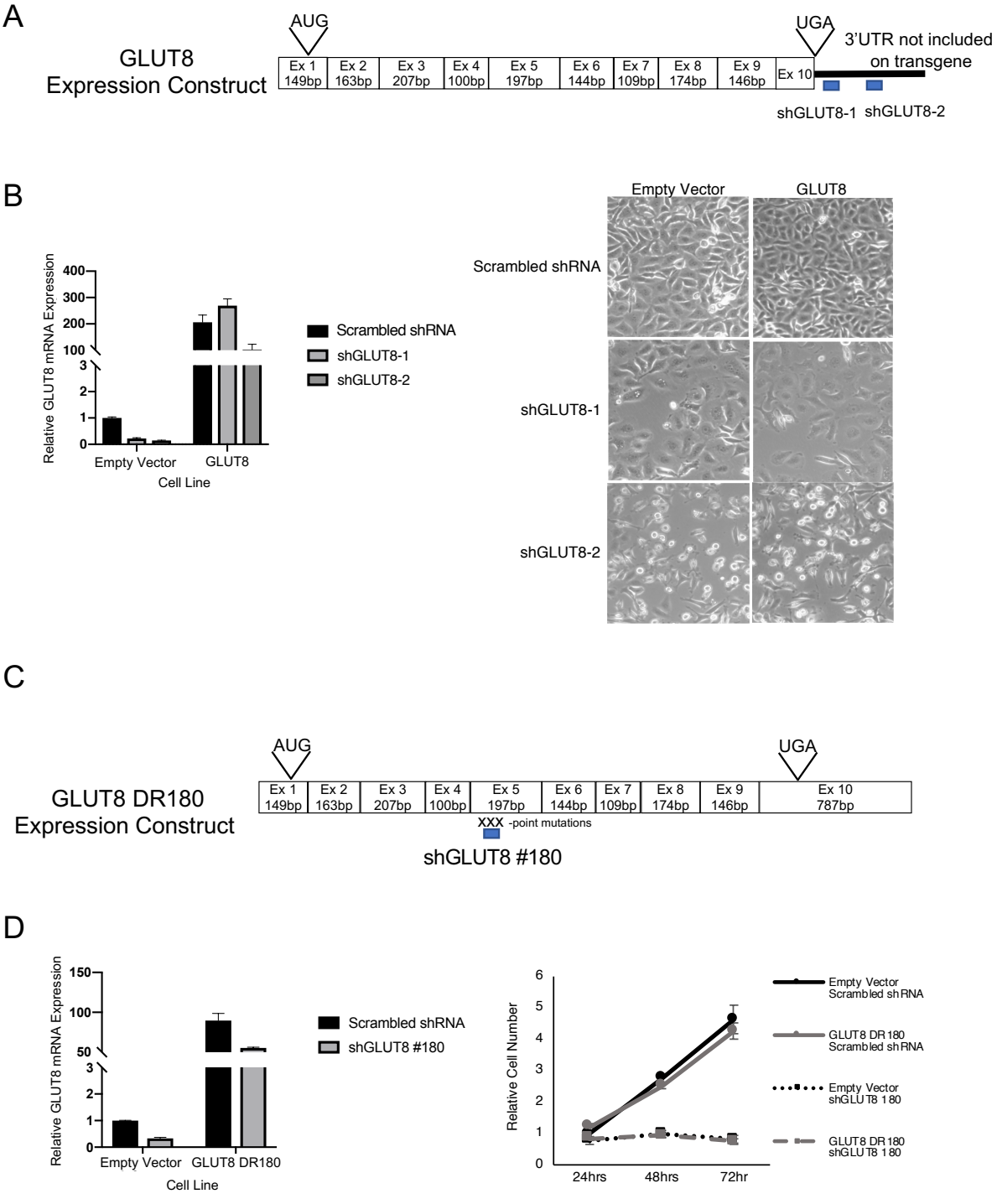
A
GLUT8
Expression Construct
AUG
UGA
3'UTR not included
on transgene
Ex 1 149bp
Ex 2 163bp
Ex 3 207bp
Ex 4 100bp
Ex 5 197bp
Ex 6 144bp
Ex 7 109bp
Ex 8 174bp
Ex 9 146bp
Ex 10
shGLUT8-1
shGLUT8-2
B
Relative GLUT8 mRNA Expression
Empty Vector
GLUT8
Cell Line
Scrambled shRNA
shGLUT8-1
shGLUT8-2
Empty Vector
GLUT8
Scrambled shRNA
shGLUT8-1
shGLUT8-2
C
GLUT8 DR180
Expression Construct
AUG
UGA
Ex 1 149bp
Ex 2 163bp
Ex 3 207bp
Ex 4 100bp
Ex 5 197bp
Ex 6 144bp
Ex 7 109bp
Ex 8 174bp
Ex 9 146bp
Ex 10 787bp
XXX -point mutations
shGLUT8 #180
D
Relative GLUT8 mRNA Expression
Empty Vector
GLUT8 DR180
Cell Line
Scrambled shRNA
shGLUT8 #180
Relative Cell Number
24hrs
48hrs
72hr
Empty Vector Scrambled shRNA
GLUT8 DR180 Scrambled shRNA
Empty Vector shGLUT8 180
GLUT8 DR180 shGLUT8 180

Figure 4. Degradation-resistant GLUT8 does not rescue proliferation. A. Schematic of GLUT8 construct to indicate region of targeting by GLUT8 shRNA **B.** (left) RT-qPCR to assess expression of GLUT8 in Empty Vector and GLUT8 overexpression MB-231 cells after transduction with control and GLUT8 targeting shRNA lentivirus. (right) Pictures of MB-231 GLUT8 overexpression cells after transduction with control and GLUT8 targeting shRNA lentivirus. **C.** Schematic of GLUT8 construct to indicate insertion of mutations in GLUT8 shRNA binding region. **D.** (left) RT-qPCR to assess expression of GLUT8 in Empty Vector and GLUT8 DR180 MB-231 cells after transduction with control and GLUT8 180 targeting shRNA lentivirus. (right) Growth curve of Empty Vector and GLUT8 DR180 overexpression MB-231 cells after transduction with scrambled and GLUT8 180 shRNA. The data is presented relative to the mean of the Empty Vector/Scrambled shRNA condition at 24-hours. N=1

Figure 5

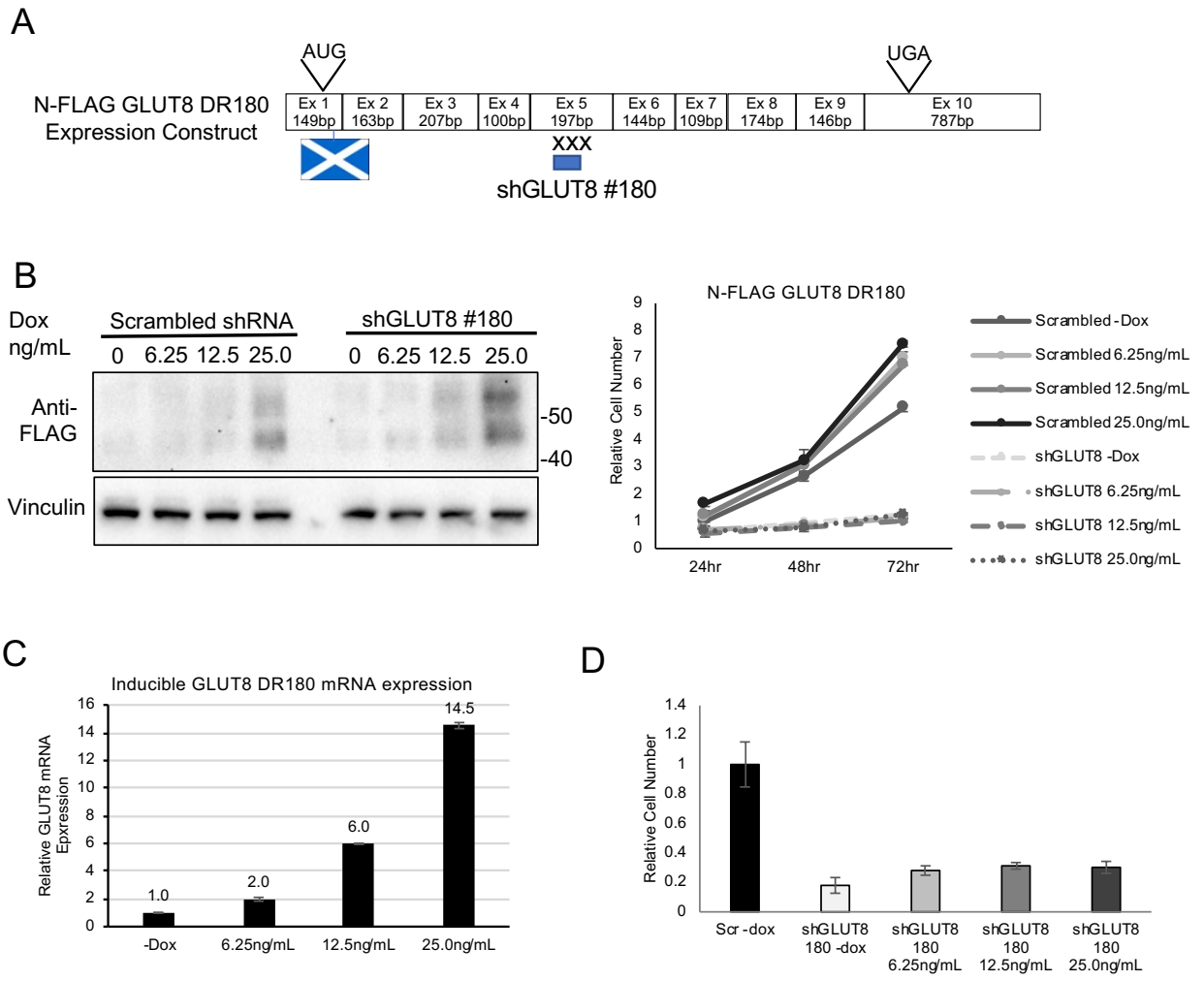
A
AUG
UGA
N-FLAG GLUT8 DR180
Expression Construct
Ex 1 149bp
Ex 2 163bp
Ex 3 207bp
Ex 4 100bp
Ex 5 197bp
Ex 6 144bp
Ex 7 109bp
Ex 8 174bp
Ex 9 146bp
Ex 10 787bp
XXX
shGLUT8 #180
B
Dox ng/mL
Scrambled shRNA
shGLUT8 #180
0 6.25 12.5 25.0
0 6.25 12.5 25.0
Anti-FLAG
Vinculin
-50
-40
N-FLAG GLUT8 DR180
Relative Cell Number
24hr
48hr
72hr
Scrambled -Dox
Scrambled 6.25ng/mL
Scrambled 12.5ng/mL
Scrambled 25.0ng/mL
shGLUT8 -Dox
shGLUT8 6.25ng/mL
shGLUT8 12.5ng/mL
shGLUT8 25.0ng/mL
C
Inducible GLUT8 DR180 mRNA expression
Relative GLUT8 mRNA Epxression
1.0
2.0
6.0
14.5
-Dox
6.25ng/mL
12.5ng/mL
25.0ng/mL
D
Relative Cell Number
Scr -dox
shGLUT8 180 -dox
shGLUT8 180 6.25ng/mL
shGLUT8 180 12.5ng/mL
shGLUT8 180 25.0ng/mL

Figure 5. Inducible expression of degradation resistant GLUT8 does not rescue proliferation. A. Schematic of GLUT8 construct to indicate insertion of mutations in GLUT8 shRNA binding region. **B.** (left) Western blot of N-FLAG tag GLUT8 DR180 to confirm that mRNA is resistant to shGLUT8 180 expression and is being translated. (right) Growth curve of inducible GLUT8 DR180 MB-231 cells after transduction with scrambled control or shGLUT8 180. The data is presented relative to the Scramble shRNA -Dox (no doxycycline) condition at 24-hours N=1 **C.** RT-qPCR to confirm inducible expression of GLUT8 DR180 when treated with doxycycline. **D.** Proliferation of inducible untagged GLUT8 DR180 after transduction with scrambled control or shGLUT8 180**.** The data is presented relative to the Scrambled shRNA -Dox (no doxycycline) condition at 48-hours N=1.

Figure 6

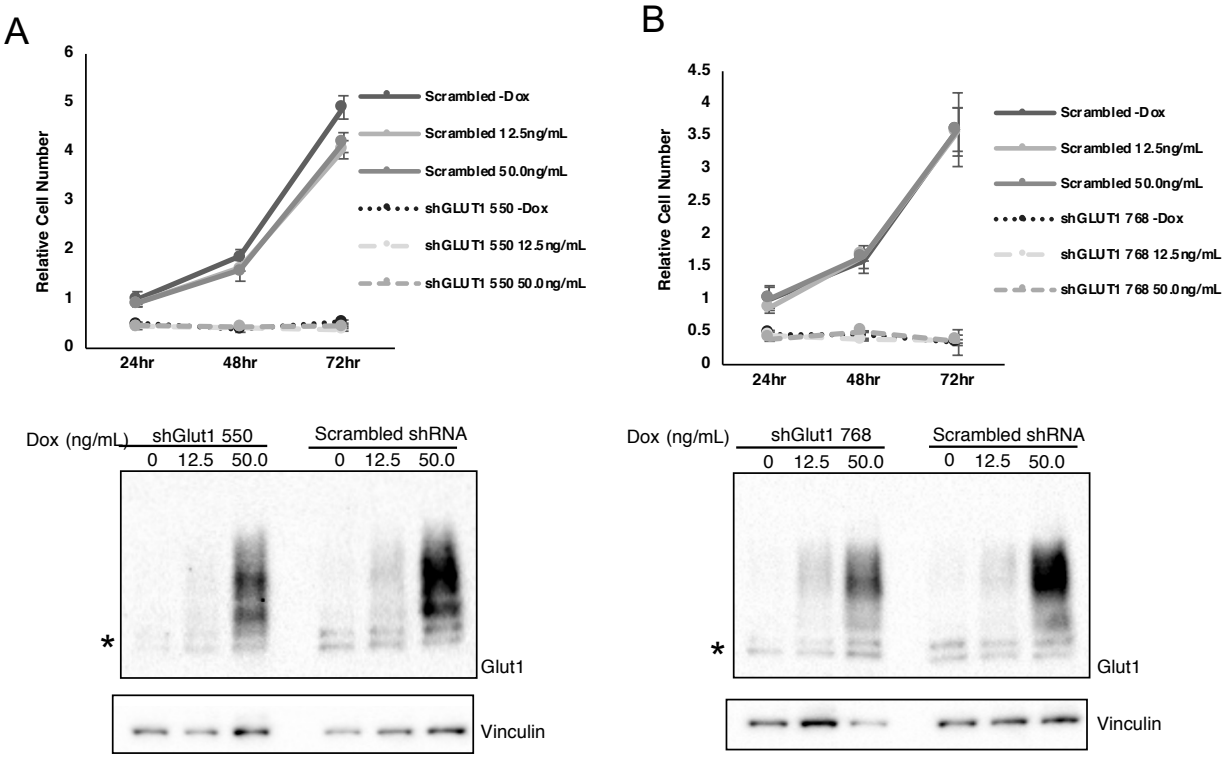
A
Relative Cell Number
Scrambled -Dox
Scrambled 12.5ng/mL
Scrambled 50.0ng/mL
shGLUT1 550 -Dox
shGLUT1 550 12.5ng/mL
shGLUT1 550 50.0ng/mL
24hr
48hr
72hr
Dox (ng/mL)
shGlut1 550
Scrambled shRNA
0 12.5 50.0
0 12.5 50.0
*
Glut1
Vinculin
B
Relative Cell Number
Scrambled -Dox
Scrambled 12.5ng/mL
Scrambled 50.0ng/mL
shGLUT1 768 -Dox
shGLUT1 768 12.5ng/mL
shGLUT1 768 50.0ng/mL
24hr
48hr
72hr
Dox (ng/mL)
shGlut1 768
Scrambled shRNA
0 12.5 50.0
0 12.5 50.0
*
Glut1
Vinculin

Figure 6. Inducible expression of degradation-resistant GLUT1 does not rescue proliferation. A. (top) Proliferation of doxycycline inducible MB-231 cells expressing a shRNA resistant GLUT1 were transduced with lentivirus containing either Scrambled shRNA control or GLUT1 shRNA 550. The data is presented relative to the Scrambled shRNA -Dox (no doxycycline) condition at 48-hours N=1. (bottom) Western blot examination of shRNA resistance of inducible GLUT1 expression. The asterisks * indicate endogenous GLUT1 band. **B**. (top) Proliferation of doxycycline inducible MB-231 cells expressing a shRNA resistant GLUT1 were transduced with lentivirus containing either Scrambled shRNA control or GLUT1 shRNA 768. The data is presented relative to the Scrambled shRNA -Dox (no doxycycline) condition at 48-hours N=1. (bottom) Western blot examination of shRNA resistance of inducible GLUT1 expression. The asterisks * indicate the endogenous GLUT1 band

Figure 7

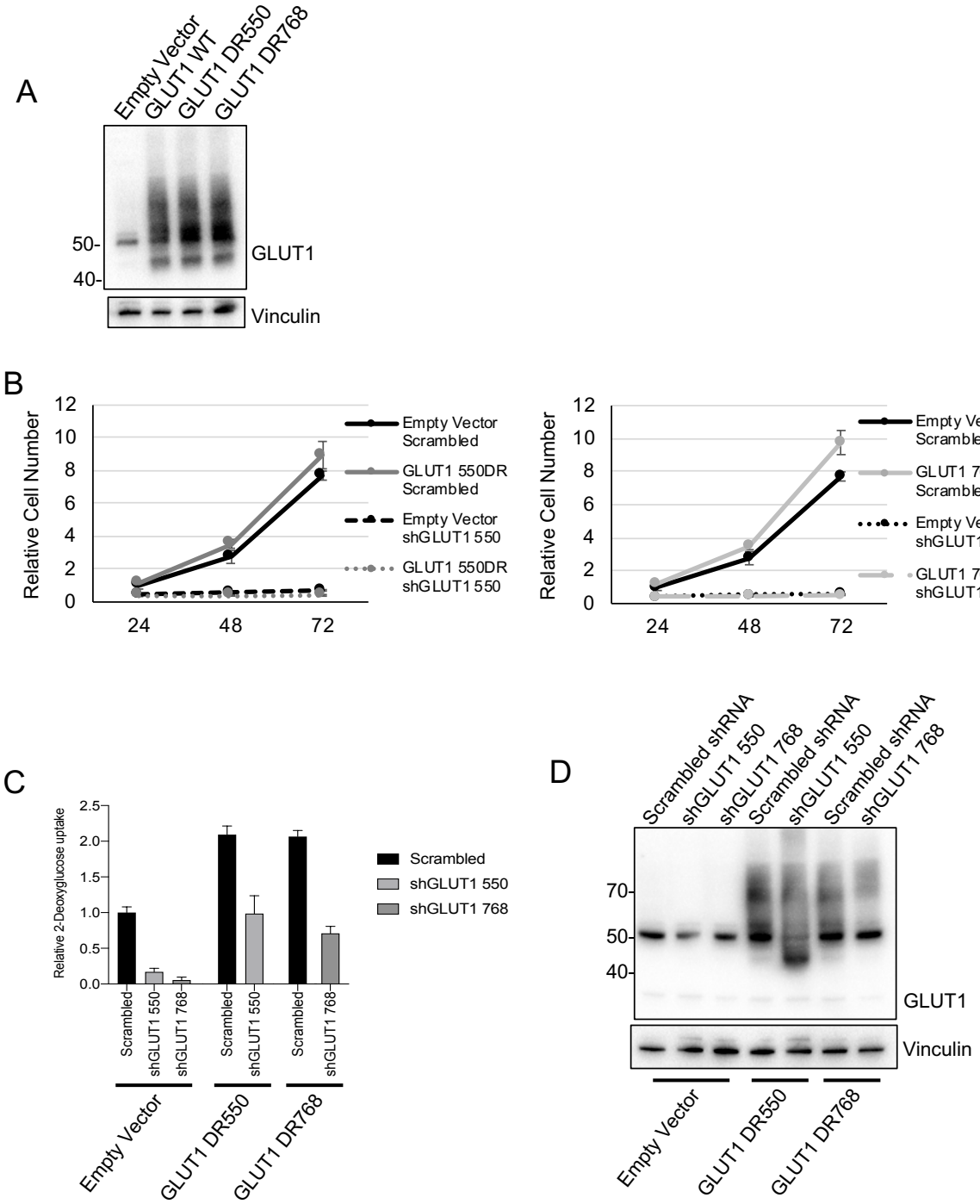
A
Empty Vector
GLUT1 WT
GLUT1 DR550
GLUT1 DR768
50-
40-
GLUT1
Vinculin
B
Relative Cell Number
Empty Vector Scrambled
GLUT1 550DR Scrambled
Empty Vector shGLUT1 550
GLUT1 550DR shGLUT1 550
Empty Vector Scrambled
GLUT1 768DR Scrambled
Empty Vector shGLUT1 768
GLUT1 768DR shGLUT1 768
24
48
72
C
Relative 2-Deoxyglucose uptake
Scrambled
shGLUT1 550
shGLUT1 768
Empty Vector
GLUT1 DR550
GLUT1 DR768
D
Scrambled shRNA
shGLUT1 550
shGLUT1 768
70-
50-
40-
GLUT1
Vinculin
Empty Vector
GLUT1 DR550
GLUT1 DR768

Figure 7. **Retroviral expression of GLUT1 does not rescue proliferation but does rescue glucose uptake. A.** Western blots of lysates isolated from pQCXIP retroviral GLUT1 overexpression cell lines. **B.** (left) Growth curve of Empty Vector and GLUT1 DR550 overexpression MB-231 cells after transduction with scrambled shRNA control and shGLUT1 550. The data is presented relative to the mean of Empty Vector/Scrambled shRNA condition N=1. (right) Growth curve of Empty Vector and GLUT1 DR768 overexpression MB-231 cells after transduction with scrambled shRNA control and shGLUT1 768. The data is presented relative to the mean of Empty Vector/Scrambled shRNA condition N=1. **C.** 2-deoxyglucose uptake assay (luminescence) of Empty Vector and GLUT1 DR overexpression MB-231 cells after transduction with scrambled shRNA control and shGLUT1 N=1 **D.** Western blots of lysates isolated from pQCXIP retroviral GLUT1 overexpression cell lines after transduction with scrambled shRNA control and shGLUT1

Figure 8

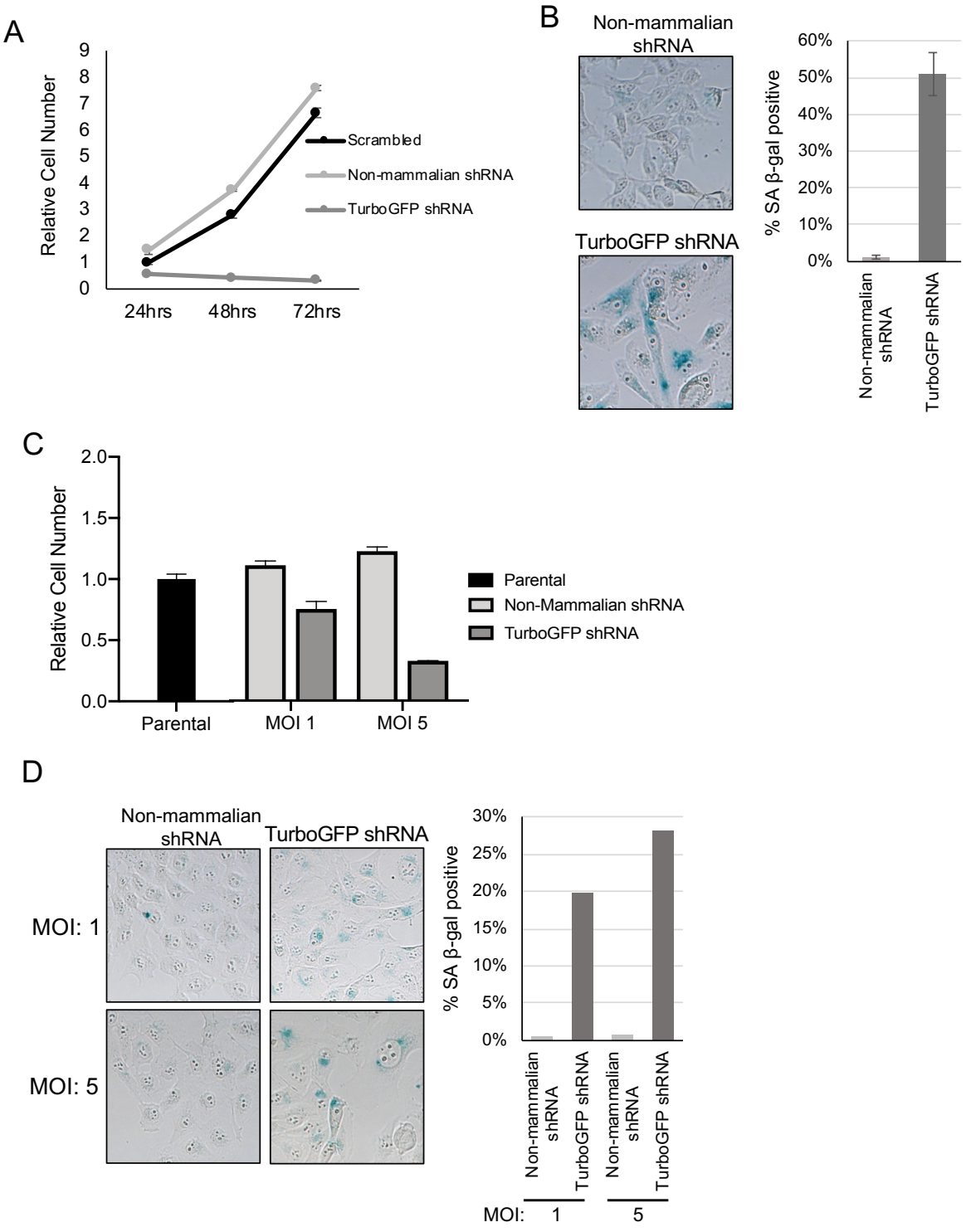
A
Relative Cell Number
9
8
7
6
5
4
3
2
1
0
24hrs
48hrs
72hrs
Scrambled
Non-mammalian shRNA
TurboGFP shRNA
B
Non-mammalian shRNA
TurboGFP shRNA
% SA β-gal positive
60%
50%
40%
30%
20%
10%
0%
Non-mammalian shRNA
TurboGFP shRNA
C
Relative Cell Number
2.0
1.5
1.0
0.5
0.0
Parental
MOI 1
MOI 5
Parental
Non-Mammalian shRNA
TurboGFP shRNA
D
Non-mammalian shRNA
TurboGFP shRNA
MOI: 1
MOI: 5
% SA β-gal positive
30%
25%
20%
15%
10%
5%
0%
Non-mammalian shRNA
TurboGFP shRNA
Non-mammalian shRNA
TurboGFP shRNA
MOI:
1
5

Figure 8. Control shRNA also induces growth arrest and senescence in MB-231 cells. A. Growth curve of Scrambled shRNA, Non-mammalian shRNA and TurboGFP shRNA MB-231 cells after transduction. The data is presented relative to the mean of the Scrambled shRNA condition N=1. **B.** Senescence associated β-galactosidase staining of MB-231 Non-mammalian shRNA and TurboGFP shRNA N=2. **C.** Growth of Non-mammalian shRNA and TurboGFP shRNA MB-231 cells after transduction at indicated MOI. The data is presented relative to the mean of the Parental (not transduced) MB-231 cells N=1. **D.** Senescence associated β-galactosidase staining of MB-231 Non-mammalian shRNA and TurboGFP shRNA after transduction at indicated MOI N=1.

Chapter V

Discussion & Future Perspectives

DISCUSSION

Expression and functional regulation of GLUT8 in breast cancer cells

The aim of this thesis was to increase our understanding of GLUT8 regulation and determine whether GLUT8 is an active contributor to growth of breast cancer cells. GLUT8 has proven to be enigmatic as work thus far has failed to decipher its precise function. Multiple studies have found GLUT8 localized to intracellular vesicles which calls into question whether it acts as a canonical glucose transporter [1-3]. Of course, one of the most well understood GLUTs, GLUT4, primarily resides in intracellular vesicles in order to tightly regulate its glucose transport activity [4]. GLUT4 is primarily expressed in muscle and adipose tissue and its translocation is induced by insulin secreted from the pancreas in response to high levels of glucose in the circulating blood. One study has shown GLUT8 translocation in response to insulin in pre-implantation blastocysts [5]. Others have tried to replicate regulated translocation in primary adipocytes, Cos-7, and N2A cells, but GLUT8 remained intracellular when treated with insulin. Thus, the stimulus for translocation of GLUT8, if any exists, has yet to be identified [6, 7]. It appears in most circumstances GLUT8 will only accumulate at the cell surface when its N-terminal di-leucine retention motif is mutated [2, 6-8]. We have also shown, when expressed in MDA-MB-231 (MB-231) breast cancer cells, GLUT8 is localized intracellularly within LAMP1-positive vesicles. Functionally, we found GLUT8 overexpression does not increase cellular uptake of the glucose analog 2-deoxyglucose (2-DG), while overexpression of GLUT1 robustly increases uptake of 2-DG. These results suggest GLUT8 is unlikely to be a cell surface glucose transporter in MB-231 cells.

We also identified a previously undescribed cleavage of GLUT8 that produces an approximately 10kDa peptide from the C-terminal end. We estimate, based upon the molecular weight of the deglycosylated full-length as well as the N-terminal and C-terminal domains, the cleavage of GLUT8 likely occurs in the 10th transmembrane domain. Interestingly, the 10th transmembrane domain is 100% conserved between humans, mouse, and rat GLUT8 protein sequences pointing to a possible evolutionary significance of this domain of the protein. Interestingly, membrane-bound, nutrient-sensing proteins are known to undergo cleavage as part of their activity. One of the most well-studied nutrient-sensing proteins, SREBP, is responsible for maintaining cholesterol homeostasis [9]. This protein requires a two-step cleavage in response to cholesterol deprivation. The cleavage event results in the release of the N-terminal domain, which enters the nucleus to drive expression of genes responsible for sterol synthesis. The intracellular localization and cleavage of GLUT8 might reflect its activity as a nutrient sensor.

Additionally, we have also confirmed the existence of multiple splice variants of the human GLUT8 mRNA. The full-length, variant 1, GLUT8 mRNA contains ten exons and is translated into the complete GLUT8 transporter. Analysis of GLUT8 expression in breast cancer data from The Cancer Genome Atlas (TCGA) revealed the presence of an alternative exon 1 to exon 4 junction that leads to the expression of shortened variant 3 mRNA. This analysis also predicted the existence of, albeit rare, a splice variant which lacks exon 9 referred to as variant 2. The putative proteins from, variant 2 and variant 3, would have alternative C- and N-termini respectively. We were able to perform quantitative analysis of full-length GLUT8 variant 1 and the alternative variant 3, in normal

human tissues and human cancer cell lines. This analysis showed the full-length variant 1 was the predominant species within most of the normal tissues, and was most expressed in the testis and liver, in line with previously published northern blot data [5, 8, 10]. Interestingly, the ratio of variant 1 to variant 3 approached one to one in the cell lines we analyzed, which contrasted with the normal tissues in which variant 1 was the predominantly expressed form. One study identified splice variants of GLUT8 in mouse tissues as well [11]. Specifically, the authors identified and functionally tested four variants of GLUT8 that they cloned from the intestine of the mouse and found overexpression of the alternatively spliced variants did not alter glucose consumption rates. Although both human and mouse GLUT8 contain 10 exons, the splice variants identified in the aforementioned study do not correspond to those expressed in the human samples we tested. This difference could reflect tissue- or species-specific splicing patterns since they examined splicing of GLUT8 exclusively in mouse intestine while we examined human cell lines and other non-intestine human tissues. We further tested the function of three of the variants we identified and found that only full-length variant 1 and variant 2 produce a protein product, while variant 3 does not produce a stable protein. The lack of translational product of variant 3 could be due to multiple factors: (i) The loss of exons 2 and 3 produce an in-frame shift in the original open-reading frame resulting in a premature stop codon within the 4th exon. This premature stop codon overlaps with the alternative translation start site that is predicted to produce the variant 3 protein product. Thus, it is possible that ribosomes carrying out translation from the initial start codon block the initiation of translation from the downstream start codon. (ii) Analysis of the Kozak sequence of variant 3 suggests that translation from the second start codon is weak. (iii)

The location of the start codon for the predicted variant 3 protein is in a transmembrane domain, and the projected topology of the protein may preclude this molecule from being translated. Overexpression of variants 1 or 3 does not alter proliferation or glucose uptake. Variant 2 has yet to be tested but its predicted protein product will lack multiple transmembrane domains and may not be functional as a transporter.

Two approaches for inducing senescence in MB-231 cells

We set out to determine the roles of GLUT8 and GLUT1 in breast cancer cell lines. We utilized both genetic inhibition of GLUT8 and GLUT1 by shRNA and pharmacologic inhibition by WZB117. WZB117 treatment induced senescence, a phenotype that was not observed following application of two other conditions designed to test glucose inhibition, glucose restriction and treatment with 2-deoxyglucose. Our initial studies demonstrated that disruption of glucose uptake either by WZB117 or by shRNA targeting GLUT8 or GLUT1 results in cell senescence. To verify the effect of the GLUT-targeting shRNAs, we made multiple attempts to rescue shRNA-induced growth arrest and senescence using expression of shRNA-resistant transgenes. Despite being functionally effective, for example GLUT1 expression rescued glucose uptake, our strategies were unable to rescue the growth-related phenotypes. This failure led us to test additional shRNA controls to determine if senescence was being induced by off-target shRNA effects. Surprisingly, one of the three control shRNA also induced senescence within the same timeline as the GLUT-targeting shRNA suggesting that MB-231 cells are sensitive to shRNA expression. Off-target effects of RNAi are a known hazard of the technique, which complicates interpretation of data. There are three common types of off-target effects associated with the use of RNAi: (i) off-target mRNA silencing due to unaccounted for

sequence complementarity; (ii) activation of the innate immune response either due to recognition of dsRNA or the method of RNAi introduction; (iii) overwhelming the endogenous miRNA processing pathway [12] (Figure 1). Further exploration is required to understand the causes of the off-target shRNA-induced phenotype. Alternatively, more modern methods of gene silencing, such as CRISPR, can be employed bearing in mind that they may also be burdened with off-target effects.

Wnt receptor Lrp5 regulates glucose uptake

Our lab has previously shown the Wnt receptor Lrp5 is required for Wnt-induced mammary tumorigenesis despite the fact that, in its absence, the sister protein, Lrp6, is still capable of initiating the Wnt signaling pathway [13]. To determine a molecular basis for this requirement, we performed loss-of-function studies of Lrp5 and Lrp6 in mouse mammary epithelial cells (MMECs). Using shRNA to stably knockdown Lrp5 or Lrp6 in MMECs, we found that only Lrp5 knockdown cells exhibited a decrease in proliferation. This observed phenotype was unique to Lrp5 as cells without Lrp6 expression proliferated at the same rate as cells treated with a scrambled shRNA control. Additionally, we found that proliferation off MMECs is sensitive to restriction of glucose in the media. This finding led us to identify Lrp5 as mediator of glucose metabolism. Importantly, we observed that depletion of Lrp5 alone resulted in decreased glucose consumption. This identified Lrp5, not the sister receptor Lrp6, as the principle mediator of proliferation and glucose consumption in MMECs. Next, we tested whether this effect applied to human breast cancer cell lines as well as MMECs. Thus, we examined the effect of stable knockdown of Lrp5 on MB-231 cells and found that Lrp5 knockdown results in decreased proliferation of this cell type. Interestingly, Lrp5 has also been identified as a determinant of glucose

uptake and glycolysis in differentiating osteoblasts [14]. This study found that Wnt signaling-induced glycolysis is mediated by Lrp5 and is independent of both Lrp6 and the canonical Wnt signaling effector β-catenin. Interestingly, mutations in LRP5 lead to alterations in bone mass, where gain-of-function and loss-of-function mutations in LRP5 cause high or low-bone mass phenotypes in humans, respectively [15, 16].

Future Perspectives

Identification of the protease regulating GLUT8 cleavage

To determine whether the C-terminal peptide could be the product of an alternative translational start site, we evaluated potential open reading frames within the GLUT8 cDNA. There are no open reading frames capable of generating the GLUT8 C-terminal fragment with the C-terminal FLAG translated in-frame, ruling out the possibility of the C-terminal fragment being produced from an alternative translational start site.

Proteolytic cleavage of membrane proteins is a crucial regulatory step of cellular metabolic processes, as is the case for the tightly regulated production of cholesterol mediated by SREBP cleavage. Identifying the sequence of the N-terminal and C-terminal domains along with the potential cleavage site will allow interrogation of GLUT8 activity. To identify the GLUT8 cleavage site, the uncleaved full-length protein and the N-terminal domain could be immunoprecipitated using the N-terminal FLAG-tagged GLUT8 construct expressed in MB-231 cells and the precipitate analyzed by mass spectrometry to identify the protein sequence. An *in-silico* protease prediction tool (PROSPER, Monash University) revealed at least 9 potential protease cleavage sites near the 10^{th} transmembrane domain. Identification of the protein fragments of GLUT8 and putative cleavage site will facilitate further testing into the regulation of GLUT8 cleavage. Any

putative proteases that cleave GLUT8 could be verified using available inhibitors. The cleavage site could also be mutated to identify a cleavage-resistant form of GLUT8. These studies could be followed up with immunofluorescent microscopy analyses to examine the effect of GLUT8 cleavage on its subcellular localization. The results from these experiments will lead us towards understanding how GLUT8 cleavage is regulated, and what the biological role of the putative intracellular GLUT may be.

The anti-GLUT8 BB1A antibody we use can detect overexpression of GLUT8 in MB-231 cells, however it failed to detect endogenous levels of GLUT8 in total protein lysates harvested from MB-231 and HepG2 cells. HepG2 cells have previously been used in studies examining the role of endogenous GLUT8 in *de-novo* lipogenesis [17]. It is possible that the anti-GLUT8 BB1A antibody we use has a lower affinity for GLUT8 than the GLUT8 C-term antibody used in the lipogenesis study. Since cleavage of GLUT8 could be an artifact of its overexpression in MB-231 cells, it is important to show that the phenomenon is observed even with endogenous GLUT8. Membrane fractionation of MB-231 lysates could be used to enrich GLUT8-containing membranes and potentially eliminate the need for utilizing overexpression systems for exploring GLUT8 function *in-vitro*.

Investigating the mechanism of GLUT8 cleavage

The phenotypes of GLUT-knockout mouse models differ in their severity, with only GLUT1 and GLUT3 knockout in mice resulting in embryonic lethality [4, 18, 19]. GLUT8-related phenotypes are much more subtle. GLUT8-knockout mice fed normal chow have no overt phenotypes and there are conflicting reports on whether GLUT8-knockout results in smaller litter sizes [20, 21]. Sperm from GLUT8 knockout mice have decreased motility

with abnormal mitochondria formation [22]. When female GLUT8-knockout mice are maintained on a high fructose diet, they are resistant to diet-induced macrosteotosis and *de-novo* lipogenesis [17]. The same study showed that wild type mice display an increase in both hepatic cholesterol and triglycerides when fed a high fructose diet while GLUT8-knockout mice show significantly decreased hepatic lipogenesis when fed a high fructose diet. Thus, GLUT8 could be serving as a fructose sensor in the liver, providing a signal for fatty acid production accordingly. Testing whether cleavage of GLUT8 is crucial for this activity would shed light on the biological function of GLUT8, which has been difficult to identify thus far. Examining GLUT8 cleavage in liver tissue of mice on a high fructose diet or primary hepatocytes when cultured with or without fructose or glucose would test if cleavage is regulated by exposure to sugars. Examination of other tissues from mice on high fructose diets with high expression of GLUT8 (Chapter 3) such as the testis or intestine could determine whether GLUT8 cleavage is regulated this way in other tissues as well or if the observed phenomenon is tissue-specific [23].

Determining the cause of shRNA-induced growth arrest and senescence

The use of RNAi to study gene function is widespread and, when properly applied, can contribute to functional characterization of a gene of interest. shRNA-mediated knockdown of GLUT8 or GLUT1 in MB-231 cells was used to examine functionality of these two proteins within this cellular context. Results showed that knockdown of GLUT8 or GLUT1 caused the cells to senesce as detected by senescence associated ß-galactosidase staining. Interestingly, attempts to rescue the knockdown-induced senescent phenotype by over-expression of the knocked down gene failed to reduce senescence. This result, combined with the induction of senescence by one out of three

non-targeting control shRNAs, suggested that senescence was induced by an off-target effect of RNAi in MB-231 cells. A recent study of siRNA off-target effects identified the seed-sequence of siRNAs and the complementation to the 3'UTRs of off-target mRNAs to be predictive of unintended gene suppression [24]. The authors designed an online tool to help inform siRNA design. Using this tool to perform an *in-silico* analysis, I identified 20 potential genes that each contain two or more 3'UTR binding sites for the seed sequences of all five shRNAs that induce senescence (shGLUT8 122, shGLUT8 180, shGLUT1 550, shGLUT1 768, and shTurboGFP). These 20 genes uniquely share sequences to these five shRNAs and lack complementary 3'UTR sequences to the two non-targeting control shRNAs that did not cause a phenotype. In order to identify possible off-target genes that are being disrupted by our shRNA, changes in genes expression could be assessed by RNA-seq to provide an unbiased screen of potential non-specific targets. Once these genes are identified, any known functional associations between these gene and the induction of senescence can be pinpointed. These genes could also be compared to those identified using the *in-silico* analysis platform. Such a comparison would validate the utility of this tool for the design of RNAi constructs including shRNA and siRNA.

Another potential off-target effect of RNAi is the activation of the innate immune response (Figure 1). Detection of foreign RNA by the innate immune response serves to protect cells from infection by potentially pathogenic agents by detecting, for example, viral genomes. RNAi constructs have also been shown to be detected by the RNA-sensing apparatus of the cell, resulting in cytotoxic effects [12, 25, 26]. Cell lines can have defective interferon responses, but a number of studies have identified shRNA expression

as a source of interferon-stimulated gene (ISG) activation resulting in undesired phenotypes [25-27]. RNA-seq data could also be mined to assess activation/expression of interferon stimulated genes (ISG), which could indicate that expression of the GLUT-targeting and control (turboGFP) shRNAs leads to activation of the innate immune response in MB-231 cells.

In addition to non-specific mRNA suppression, RNAi can cause undesired off-target effects through the saturation of the endogenous RNAi machinery (Figure 1). Expression of shRNA utilizes the same nuclear export machinery as immature miRNAs and can disrupt expression of endogenous miRNAs. It has been shown that exportin-5 overexpression can increase the knockdown activity of both endogenous miRNA and exogenous shRNA against target mRNAs, and can rescue the activity of endogenous miRNAs when shRNAs are expressed [28]. To identify whether endogenous miRNAs are being disrupted, RNA-seq data from cells expressing GLUT-targeting and turboGFP shRNAs could be analyzed to identify genes that are upregulated following administration of the constructs. If a common set of mRNAs are shown to be upregulated when the shRNAs are expressed, then that would be indicative of disruption of endogenous miRNA expression. A miRNA array can then be performed to analyze the expression of miRNAs and identify which are downregulated following administration of exogenous shRNA constructs. These miRNAs could be correlated with RNA-seq mRNA data to identify native miRNA:mRNA interactions that are disrupted due to exogenous shRNA expression. Two of the non-targeting control shRNAs did not affect cell growth following expression in MB-231. These shRNAs can be used as controls for saturation of endogenous RNAi machinery. The lack of phenotype following expression of these

control shRNAs suggests that saturation of the endogenous miRNA machinery is an unlikely mechanism for the off-target effects observed following administration of other shRNAs. If it appears that endogenous miRNAs are being disrupted, then the two non-targeting control shRNAs need to be subjected to more thorough functional testing since their failure to induce a growth phenotype suggests that it is possible, they are not being processed by endogenous RNAi enzymes to produce mature shRNA. A luciferase-based assay commonly used to verify miRNA targeting of 3'UTRs from target mRNAs could be adapted to contain sequences complementary to the control shRNAs and suppression of luciferase activity could be tested in the presence of control shRNA expression. This would confirm whether the control shRNAs are functioning as intended and producing mature functional shRNA.

Only one of the three control shRNA sequences, the turboGFP shRNA, induced senescence. One explanation for the lack of phenotype from the other control shRNAs is that they are not participating in the RNAi biogenesis pathway and thus are not functional controls, I addressed one way to examine this possibility previously in the discussion. Another possibility we considered was that the lentiviral titer for the turboGFP shRNA was higher than the others. We tested turboGFP and non-mammalian control shRNAs by matching the multiplicity of infection (MOI) and determined that only the turboGFP shRNA induced senescence and an abnormally high MOI (Chapter 4). We have also shown that decreasing the MOI results in a corresponding decrease in the level of senescence induced by the turboGFP shRNA. It seems plausible that the level of shRNA expression could be decreased further to limit of the off-target effects while maintaining a sufficient level of knockdown to test a gene-specific phenotype. Using an inducible-shRNA system

to maintain low levels of shRNA expression could possibly eliminate negative off-target effects while maintaining sufficient knockdown of the target gene for functional analysis. However, for some gene-shRNA combinations, sufficient knockdown of target genes might not be achievable without off-target effects.

There is preliminary data that shows expression of GLUT8 shRNAs is growth inhibitory in other breast cancer cell lines. Transduction of these cell lines with the turboGFP shRNA and examination of the effect on proliferation and senescence would identify whether the off-target effects we identified in MB-231 are more broadly observed in other cell lines.

Mapping the functional domains of Lrp5

We have identified a glucose uptake function of the Wnt coreceptor Lrp5 in mammary epithelial cells. The novel function is unique to Lrp5 and is unrelated to its activity in the canonical Wnt pathway. Structural studies of Lrp6 have identified a unique region in the cytoplasmic domain. This region, which is lacking in Lrp5, is required for efficient phosphorylation in response to Wnt ligand binding and transduction of a downstream signal [29]. The domain within Lrp5 that mediates glucose uptake can be identified by analyzing the activity of various mutants. Doing so will allow for mapping of the glucose uptake regulatory domain within Lrp5 (Figure 2). In conjunction with this approach, characterization of Lrp5-associated proteins could be performed by mass-spectrometry. Proteins in complex with Lrp5 could be compared to those associated with Lrp6 to identify unique partners of Lrp5 which could represent candidate protein(s) mechanistically and functionally involved in Lrp5-mediated glucose uptake. Depending on the outcome of the domain mapping studies, more precise mapping of Lrp5 function

through mutagenesis would be aimed at disrupting interactions with putative binding partners.

In summary, we identified previously undescribed alternative splice variants of GLUT8 in human tissue and cell lines. We have also, for the first time, shown that GLUT8 is cleaved when expressed in breast cancer cell lines, and a fraction of the C-terminal peptide generated is localized separately from the N-terminal domain. The functional significance of this cleavage, and the overall function of GLUT8 in general, remain to be uncovered as attempts to elucidate these functions in the context of MB-231 cells by RNAi were complicated by off-target effects. Given the intracellular localization and the now known cleavage of GLUT8, we propose that this transporter may serve a sensory role for intracellular metabolites. We also advise that, when utilizing RNAi for functional studies, it is important to establish the specificity of the relevant shRNA or siRNA through rescue studies. Specifically, it is essential to verify that expression of a functional shRNA does not result in adverse effects in the cell line of interest prior to pursuing gene-specific knockdown studies using common controls such as turboGFP shRNA.

REFERENCES

1. Augustin, R., J. Riley, and K.H. Moley, *GLUT8 contains a [DE]XXXL[LI] sorting motif and localizes to a late endosomal/lysosomal compartment.* Traffic, 2005. **6**(12): p. 1196-212.

2. Diril, M.K., et al., *Lysosomal localization of GLUT8 in the testis--the EXXXLL motif of GLUT8 is sufficient for its intracellular sorting via AP1- and AP2-mediated interaction.* FEBS J, 2009. **276**(14): p. 3729-43.

3. Schmidt, U., et al., *Endocytosis of the glucose transporter GLUT8 is mediated by interaction of a dileucine motif with the beta2-adaptin subunit of the AP-2 adaptor complex.* J Cell Sci, 2006. **119**(Pt 11): p. 2321-31.

4. Augustin, R., *The protein family of glucose transport facilitators: It's not only about glucose after all.* IUBMB Life, 2010. **62**(5): p. 315-33.

5. Carayannopoulos, M.O., et al., *GLUT8 is a glucose transporter responsible for insulin-stimulated glucose uptake in the blastocyst.* Proc Natl Acad Sci U S A, 2000. **97**(13): p. 7313-8.

6. Lisinski, I., et al., *Targeting of GLUT6 (formerly GLUT9) and GLUT8 in rat adipose cells.* Biochem J, 2001. **358**(Pt 2): p. 517-22.

7. Shin, B.C., R.A. McKnight, and S.U. Devaskar, *Glucose transporter GLUT8 translocation in neurons is not insulin responsive.* J Neurosci Res, 2004. **75**(6): p. 835-44.

8. Ibberson, M., M. Uldry, and B. Thorens, *GLUTX1, a novel mammalian glucose transporter expressed in the central nervous system and insulin-sensitive tissues.* J Biol Chem, 2000. **275**(7): p. 4607-12.

9. Brown, M.S. and J.L. Goldstein, *The SREBP pathway: regulation of cholesterol metabolism by proteolysis of a membrane-bound transcription factor.* Cell, 1997. **89**(3): p. 331-40.

10. Doege, H., et al., *GLUT8, a novel member of the sugar transport facilitator family with glucose transport activity.* J Biol Chem, 2000. **275**(21): p. 16275-80.

11. Romero, A., et al., *Expression of GLUT8 in mouse intestine: identification of alternative spliced variants.* J Cell Biochem, 2009. **106**(6): p. 1068-78.

12. Jackson, A.L. and P.S. Linsley, *Recognizing and avoiding siRNA off-target effects for target identification and therapeutic application.* Nat Rev Drug Discov, 2010. **9**(1): p. 57-67.

13. Lindvall, C., et al., *The Wnt signaling receptor Lrp5 is required for mammary ductal stem cell activity and Wnt1-induced tumorigenesis.* J Biol Chem, 2006. **281**(46): p. 35081-7.

14. Esen, E., et al., *WNT-LRP5 signaling induces Warburg effect through mTORC2 activation during osteoblast differentiation.* Cell Metab, 2013. **17**(5): p. 745-55.

15. Gong, Y., et al., *LDL receptor-related protein 5 (LRP5) affects bone accrual and eye development.* Cell, 2001. **107**(4): p. 513-23.

16. Van Wesenbeeck, L., et al., *Six novel missense mutations in the LDL receptor-related protein 5 (LRP5) gene in different conditions with an increased bone density.* Am J Hum Genet, 2003. **72**(3): p. 763-71.

17. Debosch, B.J., et al., *Glucose transporter 8 (GLUT8) mediates fructose-induced de novo lipogenesis and macrosteatosis.* J Biol Chem, 2014. **289**(16): p. 10989-98.

18. Wang, D., et al., *A mouse model for Glut-1 haploinsufficiency.* Hum Mol Genet, 2006. **15**(7): p. 1169-79.

19. Schmidt, S., et al., *Essential role of glucose transporter GLUT3 for post-implantation embryonic development.* J Endocrinol, 2009. **200**(1): p. 23-33.

20. Adastra, K.L., et al., *Slc2a8 deficiency in mice results in reproductive and growth impairments.* Biol Reprod, 2012. **87**(2): p. 49.

21. Schmidt, S., et al., *Deletion of glucose transporter GLUT8 in mice increases locomotor activity.* Behav Genet, 2008. **38**(4): p. 396-406.

22. Gawlik, V., et al., *Targeted disruption of Slc2a8 (GLUT8) reduces motility and mitochondrial potential of spermatozoa.* Mol Membr Biol, 2008. **25**(3): p. 224-35.

23. DeBosch, B.J., M. Chi, and K.H. Moley, *Glucose transporter 8 (GLUT8) regulates enterocyte fructose transport and global mammalian fructose utilization.* Endocrinology, 2012. **153**(9): p. 4181-91.

24. Birmingham, A., et al., *3' UTR seed matches, but not overall identity, are associated with RNAi off-targets.* Nature Methods, 2006. **3**(3): p. 199-204.

25. Bridge, A.J., et al., *Induction of an interferon response by RNAi vectors in mammalian cells.* Nat Genet, 2003. **34**(3): p. 263-4.

26. Fish, R.J. and E.K. Kruithof, *Short-term cytotoxic effects and long-term instability of RNAi delivered using lentiviral vectors.* BMC Mol Biol, 2004. **5**: p. 9.

27. Sledz, C.A., et al., *Activation of the interferon system by short-interfering RNAs.* Nat Cell Biol, 2003. **5**(9): p. 834-9.

28. Yi, R., et al., *Overexpression of exportin 5 enhances RNA interference mediated by short hairpin RNAs and microRNAs.* RNA, 2005. **11**(2): p. 220-6.

29. MacDonald, B.T., et al., *Dissecting molecular differences between Wnt coreceptors LRP5 and LRP6.* PLoS One, 2011. **6**(8): p. e23537.

Table 1

NCBI Accession ID	Transcript Name
NM_006581	fucosyltransferase 9 (FUT9), mRNA
NM_207406	BEN domain containing 4 (BEND4), transcript variant 1, mRNA
NM_001159547	BEN domain containing 4 (BEND4), transcript variant 2, mRNA
NM_005504	branched chain amino acid transaminase 1 (BCAT1), transcript variant 1, mRNA
NM_001178091	branched chain amino acid transaminase 1 (BCAT1), transcript variant 2, mRNA
NM_001178092	branched chain amino acid transaminase 1 (BCAT1), transcript variant 3, mRNA
NM_001178093	branched chain amino acid transaminase 1 (BCAT1), transcript variant 4, mRNA
NM_001178094	branched chain amino acid transaminase 1 (BCAT1), transcript variant 5, mRNA
NM_006609	mitogen-activated protein kinase kinase kinase 2 (MAP3K2), transcript variant 1, mRNA
NM_001173484	nebulette (NEBL), transcript variant 3, mRNA
NM_002655	PLAG1 zinc finger (PLAG1), transcript variant 1, mRNA
NM_001114634	PLAG1 zinc finger (PLAG1), transcript variant 2, mRNA
NM_001114635	PLAG1 zinc finger (PLAG1), transcript variant 3, mRNA
NR_038265	PTPRF interacting protein alpha 2 (PPFIA2), transcript variant 8, mRNA
NM_002867	RAB3B, member RAS oncogene family (RAB3B), mRNA
NM_015071	Rho GTPase activating protein 26 (ARHGAP26), transcript variant 1, mRNA
NM_001135608	Rho GTPase activating protein 26 (ARHGAP26), transcript variant 2, mRNA
NM_004815	Rho GTPase activating protein 29 (ARHGAP29), transcript variant 1, mRNA
NR_045628	sodium voltage-gated channel alpha subunit 7 (SCN7A), transcript variant 2, non-coding RNA
NM_174909	transmembrane protein 167A (TMEM167A), mRNA

Figure 1

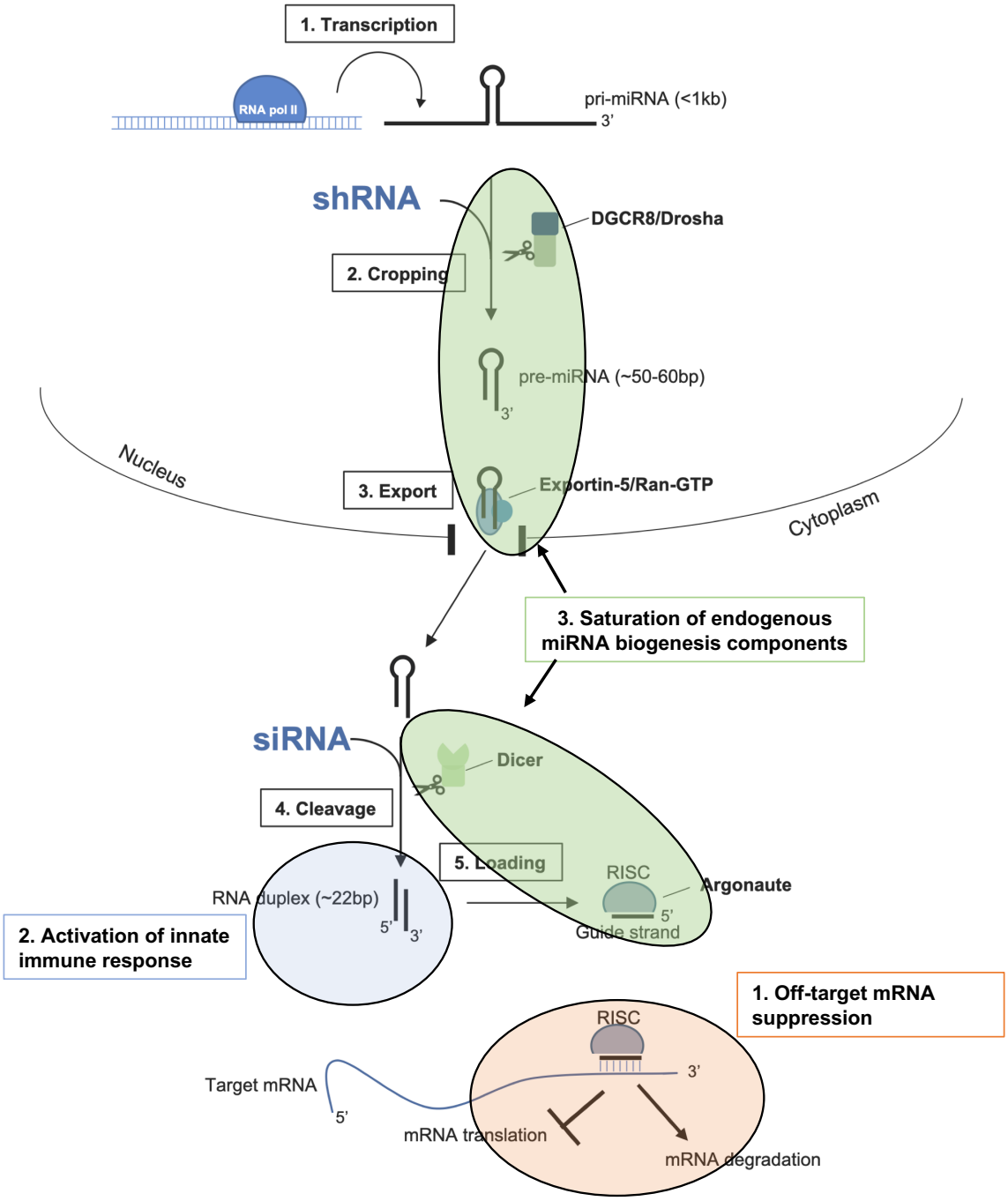
1. Transcription
RNA pol II
pri-miRNA (<1kb)
3'
shRNA
DGCR8/Drosha
2. Cropping
pre-miRNA (~50-60bp)
3'
Nucleus
3. Export
Exportin-5/Ran-GTP
Cytoplasm
3. Saturation of endogenous miRNA biogenesis components
siRNA
Dicer
4. Cleavage
5. Loading
RISC
Argonaute
RNA duplex (~22bp)
5'
3'
5'
Guide strand
2. Activation of innate immune response
1. Off-target mRNA suppression
RISC
3'
Target mRNA
5'
mRNA translation
mRNA degradation

Figure 1. Schematic depicting potential sources of off-target shRNA effects which could be pursued in future studies. There are three types of off-target effects that could be interrogated through gene expression analysis that could identify the mechanism of the shRNA activity described in this thesis. **1**. Off-target mRNA suppression **2.** Activation of innate immune response through recognition of short RNAs by RNA-sensing apparatus **3.** Saturation of endogenous RNAi biogenesis disrupting the function of endogenous miRNAs

Figure 2

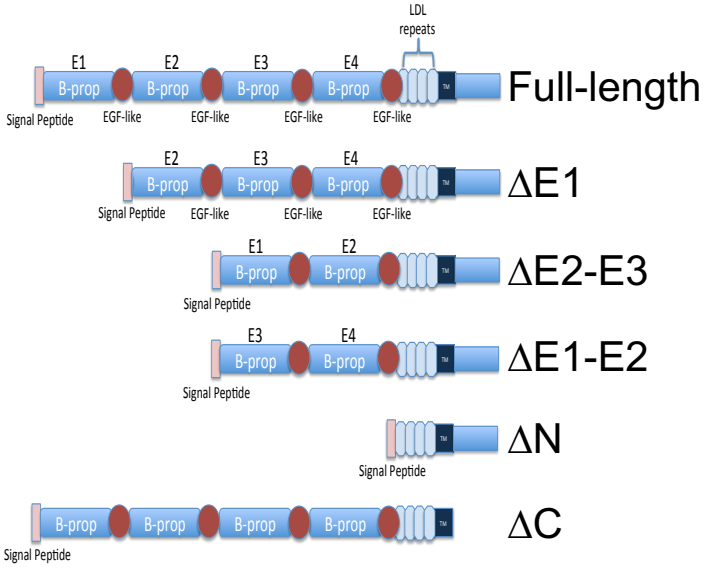

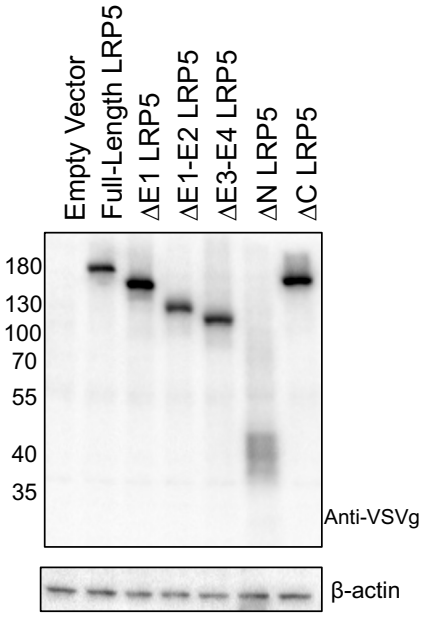

LRP5 construct	Predicted Size
Full-Length	177 kDa
ΔE1	146 kDa
ΔE1-E2	115 kDa
ΔE3-E4	106 kDa
ΔN	33 kDa
ΔC	161 kDA

Figure 2 Schematic depicting Lrp5 deletion mutants and western blot confirming the expression of mutant construct in HEK293T cells. Future studies of Lrp5 regulated glucose uptake could focus on mapping the glucose regulating domain using Lrp5 deletion mutants.